Synthetic Biology Guidelines for Diffusion Based Molecular Communication

Simon Sassine Assaf

Nanonetworking Center in Catalunya

Universitat Politècnica de Catalunya

Advisors:

Dr. Eduard Alarcón

Dr. Josep Solé-Pareta

A thesis submitted for the degree of

Doctor of Philosophy in Computer Architecture

April 2019

To my parents, for their faith in my capabilities, for their endless love, encouragement, and support

Acknowledgement

I would like to express my sincere gratitude to my advisers Prof. Eduard Alarcón, and Prof. Josep Solé-Pareta for the continuous support of my Ph.D study and related research, for their patience, motivation, and immense knowledge. I would like to thank you for encouraging my research and for allowing me to grow as a research scientist. Their guidance helped me in all the time of research and writing of this thesis. I could not have imagined having a better advisers and mentors for my Ph.D study. I also want to thank you for letting my defense be an enjoyable moment, and for your brilliant comments and suggestions, thanks to you.

Above all, I want to show my endless love and gratitude to the people who have given me the strength and motivation to undertake the great journey of my Ph.D. Last but not the least, I cannot find the words to express my gratitude to my parents and my sisters. This achievement would not have been possible without their encouragement, support and love.

Contents

English Summary

Nanotechnology is widely seen as having huge potential to bring benefits to many areas of research and application. Nowadays, research studies are focusing on realizing nano-machines on the order of nanometers in size. A nano-machine is capable of performing simple tasks such as computing, data storing, sensing, and actuation. The capability for such nano-machine to communicate with each other would considerably expand their potential. Thereby, in order to fulfill more complex tasks nano-networks are needed. Indeed, nano-networks are the connection and cooperation of millions of nano-machines. However, the traditional mechanisms used in traditional communication networks have been found inappropriate at the nano-scale. Thus, to enable this cooperation between nano-machines, several communication mechanisms have been proposed. Among the different methods for interconnecting nano-machines, Molecular Communications (MC) system is considered one of the most promising mechanisms, which is biologically plausible and occurs in living beings.

MC uses physical molecules as information carriers. By employing molecules as information carriers, MC has quickly emerged as a bio-inspired approach. The exchange of information between the transmitter and an intended receiver is carried out via the transmission, propagation, and reception of molecules. The communication range of molecular communications can range from short-range to long-range.

The focus of this Ph.D. thesis is on the most fundamental type of molecular communication, namely, Diffusion-based Molecular Communication (DMC) where the propagation of information molecules between a transmitter and a receiver is realized through free diffusion in a fluid environment. It begins by investigating and modeling the neuronal physical layer (layer 1) to understand better through simulation, and then to derive the appropriate performance metrics imposed by a point-to-point neuron neighboring receivers link, as well as by the Single Input Multiple Output (SIMO) network. Following that, the aim is to characterize the physical channel of the neuron-to-neuron communication system, and to analyze the effect of the toxic proteins aggregation on the brain since this accumulation turns out to be the main reason behind chronic neurodegenerative disorder as in Alzheimer's disease, then ultimately to come up with a complete sense-actuation closed-loop system vision for fighting this neurodegenerative disorder. Lastly, the goal is to build a mathematical model to track the movement of spermatozoa during the process of chemotaxis, to describe better through simulation, to understand by quantifying the communication problem, then to investigate the effect of varying the appropriate metrics on the

arrival time of the spermatozoa and then to propose new treatments which are more reliable, and less expensive than the existing one.

It is concluded that the proposed study will provide to synthetic biology design oriented guidelines. In addition, this study presents new solutions for treating diseases which establish a new vision of dealing with them, as well as serve as guidelines for the medical committee.

Catalan Summary

Des de fa un cert temps, s'està veien que la nanotecnologia té un gran potencial per a la seva aplicació en molts camps de recerca . En l'actualitat els temes de recerca d'aquests camps se centren en la realització de nano-màquines i xarxes de nano-màquines. Essent una nano-màquina, aquell giny capaç de realitzar tasques senzilles de computació, d'emmagatzematge de dades, de detecció (actuant com a sensors) i l'actuació d'altres dispositiu, que quan tenen la possibilitat de poder-se comunicar entre elles augmenten considerablement el seu potencial. D'aquesta manera, per a realitzar tasques més complexes és oportú utilitzar nano-xarxes, entenent per nano-xarxes la interconnexió de milions de nano-màquinessón per cooperar entre elles. En aquest sentit, però, els mecanismes tradicionals utilitzats en les xarxes de computadors s'han trobat inadequats a escala nanomètrica, de manera que per poder portar a terme la cooperació entre nano-màquines, s'estan proposant mecanismes de comunicació alternatius. D'entre les xarxes de nano-màquines que es considera més prometedores són els sistemes de Comunicacions Moleculars (CM) que són biològicament plausible i es produeix en els éssers vius.

En les Comunicacions Moleculars s'utilitzen molècules físiques com a portadores d'informació, per la qual cosa les MolCom es consideren bio-inspirades. Així, l'intercanvi de portadores d'informació entre un transmissor i un receptor es realitza via transmissió, propagació i recepció de molècules. Essent els possible abast de les comunicacions moleculars de tres rangs possibles, curt, mitjà i llarg abast.

Aquesta tesi doctoral se centre en els sistemes bàsics de comunicació molecular, és a dir, en la Comunicació Molecular basada en la difusió (DMC), on la propagació de molècules d'informació entre un transmissor i un receptor es realitza mitjançant la seva lliure difusió en medi fluid. En primer lloc, per comprendre-la millor, s'investiga i es modela la capa física neuronal (capa 1) a través de la simulació, i es deriven les mètriques de rendiment apropiades per a dos casos diferents, un enllaç punt a punt amb els receptors veïns i una xarxa d'un sol transmissor i múltiples receptors. A continuació, es caracteritza el canal físic d'un sistema de comunicació entre neurones i s'analitza l'efecte de l'agregació de les proteïnes tòxiques al cervell, ja que aquesta acumulació resulta ser la raó principal de trastorns neurodegeneratius crònics com ara la malaltia de l'Alzheimer. Finalment, proposem una actuació sensorial completa, basada en un sistema de circuit tancat, per combatre aquest desordre neurodegeneratiu.

La tesi conclou amb la construcció d'un model matemàtic molt preliminar que permeti fer un seguiment del moviment d'espermatozoides durant el procés de quimiotaxis. L'objectiu és obrir

el tema per a la comunitat científica, ajudar a descriure millor el problema mitjançant un primer conjunt de simulacions per, a continuació, investigar l'efecte de variar els intervals d'arribada dels espermatozoides a les cèl·lules mare i després proposar nous tractaments, més fiables i menys costosos que els existents, per millorar la fertilitat.

En resum, aquest treball vol proporciona directrius orientades al disseny de biologia sintètica, presenta noves solucions per al tractament de malalties, establint una nova visió de tractar-les i vol servir de guia per al comitè mèdic.

French Summary

La Nanotechnologie est désormais largement reconnue comme ayant un énorme potentiel pouvant apporter de considérables avancées dans de nombreux domaines d'investigation et application. De nos jours, les principales études et recherches se concentrent sur la réalisation de Nano-Machines ou machines moléculaires à l'échelle du nanomètre. Une nano-machine est capable de réaliser de simples tâches telles que des calculs, du stockage de données, détection ou activation de mouvement. On imagine donc que la capacité qu'auraient de telles machines à communiquer entres elles augmenterait considérablement leur potentiel. Il est alors indispensable de passer par la création de nanoréseaux afin de pouvoir enfin voir la complexité et diversité de leurs tâches effectuées s'améliorer. Un nanoréseau n'est autre que la connexion et coopération de milliers de nano-machines entres elles, cependant, aucun des mécanismes traditionnels précédemment utilisés dans la science des réseaux ne s'est avéré adapté à l'échelle du nanomètre. Par conséquent, afin de pouvoir avancer sur la recherche, de nombreux systèmes de communication ont déjà été proposés, parmi lesquels la Communication Moléculaire (CM) ou Communication Cellulaire qui reste encore aujourd'hui considérée comme le système d'intercommunication le plus prometteur, ce qui est biologiquement plausible et est présent chez les êtres vivants.

La Communication Moléculaires (CM) utilise nos propres molécules comme directs porteurs d'information. Cette approche inédite de la CM sur le sujet a vite été mise en avant pour son inspiration biologique (bio-inspiration). L'échange d'information des porteurs de données avec les transmetteurs et les récepteurs est réalisé entre la transmission, la propagation et la réception des molécules, tout en sachant que la portée de ces connexions entre molécules se situe entre courte, moyenne et longue distance.

Cette thèse finale de Doctorat est axée sur le principal type de la Communication Moléculaire, c'est à dire plus précisément sur la diffusion basique de la CM où la propagation de l'information des molécules entre transmetteurs et récepteurs passe par sa libre diffusion via un fluide.

C'est en vue de réussir à mieux comprendre le processus lors de simulations et de pouvoir ensuite trouver la dérivation des indicateurs métriques imposés par, d'une part le lien établi point par point des neurones récepteurs voisins, et d'autre part le réseau SIMO (Single Input Multiple Output - Entrée unique/Multiples Sorties) qu'il est nécessaire de passer par l'étude et la modélisation du premier niveau physique du neurone (niveau 1). L'objectif est donc de caractériser le cheminement physique complet du système de communication liant un neurone à un autre, pour ensuite analyser l'effet des groupes de protéines toxiques trouvés dans le

cerveau tout en sachant que ces accumulations s'avèrent être la principale cause des maladies neurodégénératives chroniques telle qu'Alzheimer. À terme, cela permet de reproduire le schéma complet de ce circuit fermé complexe et ainsi d'avoir la possibilité de combattre ces problèmes neurodégénératifs. Dans un second point, l'objectif est de réussir à créer un schéma mathématique capable de suivre la progression des mouvements des spermatozoïdes au cours de la chemotaxis. Cela donnera tout d'abord une vision précise lors des simulations, et de comprendre et chiffrer les problèmes de communication rencontrés pour finalement pourvoir étudier l'effet des variables métriques adéquates à l'arrivée des spermatozoïdes jusqu'à leur destination. La finalité de cette étude est ainsi de réussir à créer de nouveaux traitements plus fiables et abordables que ceux déjà proposés.

En conclusion, cette étude se veut de proposer de nouvelles lignes directives et recommandations aux conceptions biologiques synthétiques. Elle permet de présenter des solutions innovantes pour traiter certaines maladies en proposant une vision actuelle et moderne. Un tel projet et point de vue inédit met à disposition un éventail de nouveaux moyens au traitement de certaines maladies, mais aussi un nouvel outil et de nombreuses possibilités pour le monde médical.

Chapter 1

Introduction

Nanotechnology is a very promising research field. The concept in nanotechnology was first introduced by Richard Feynman in his speech entitled "There's plenty of room at the bottom" in 1959 where he is giving rise to devices and systems in a scale ranging from one to a few hundred nanometers. Therefore, nanotechnology enables the miniaturization and fabrication of devices on a scale ranging from 1 to 100 nanometers [1]. In other words, it is manipulation of matter on an atomic and molecular scale.

Nowadays, research studies are focusing on realizing nano-scale machines or nano-machines which are defined as mechanical devices that have the potential to perform functions by using components of nanometer scale. Thereby, a nano-machine is composed of nano-scale components which are capable of performing simple tasks such as computing, data storing, sensing, and actuation [2].

There are three different perspectives targeted for the development of nano-machines which are top-down, bottom-up, and bio-hybrid. In the top-down approach nano-machines are down-scaled the current microelectronic and microelectromechanical technologies lacking the atomic level control. In the bottom-up approach, the design of nano-machines is done from molecular components. These two approaches are showed in Fig. 1.1. Finally, the bio-hybrid approach is established of existing biological nano-machines such as neuronal nano-network in the human body.

Since the capability and functionality of one nano-machine alone is limited, nano-networks are needed. Nano-network is a term that refers to the connection and cooperation of millions of nano-machines. In a nano-network, nano-machines communicate and share their information to overcome their individual limitation in size, energy and so computational capabilities.

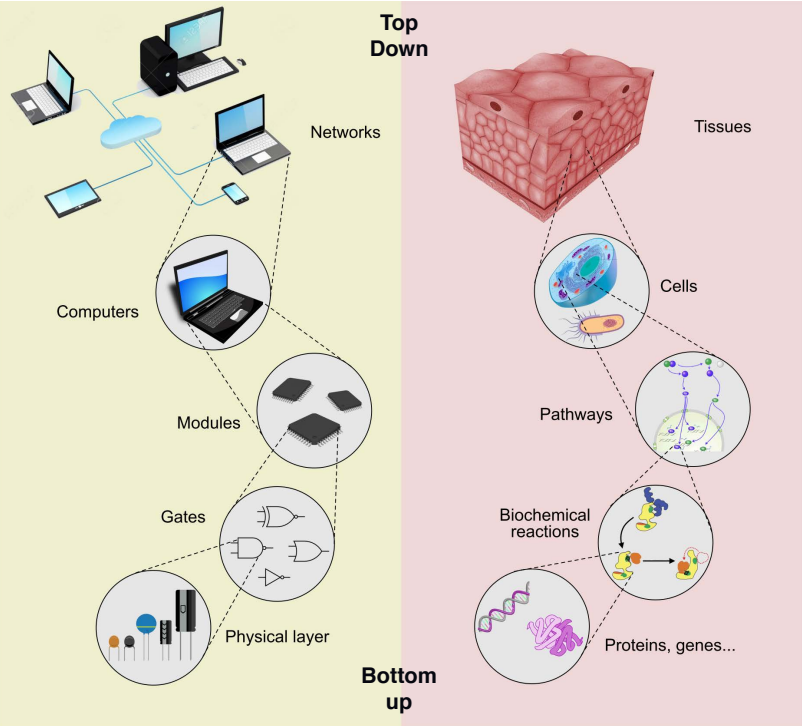

Figure 1.1: Top-down and Bottom-up approaches.

Accordingly, nano-network allows expanding the capabilities of a single nano-machine.

The physical communication channels in nano-networks differ from the conventional wired or wireless channels due to the small size of nano-machines. Hence, the traditional mechanisms used in traditional communication networks have been found inappropriate at the nanoscale, due to the difficulty of scaling down current transceivers. To enable this cooperation between nano-machines, several communication mechanisms have been suggested and examined by this time, including nano-mechanical communication, acoustic communication, molecular communication [3–7], and nano-electromagnetic communication [8–14]. In nano-mechanical communication, the information is sent through nano machines that are linked physically. In acoustic communication, the communication is realized by the transmission of ultrasonic waves through nano-machine integrated transducers. Moreover, nano-electromagnetic communication uses electromagnetic waves as information bearers. Lastly, Molecular Communications (MC) is a molecule based communication paradigm.

Among these different alternative methods for interconnecting nano-machines, the nano-electromagnetic communication and the MC system are considered the most promising mechanisms. An overview of nano-electromagnetic communication, and molecular communication, follows.

Nano-electromagnetic communication is defined as the transmission and reception of electro-

magnetic radiation from nano-scale components. Unfortunately, in nano-electromagnetic communication the channel characteristics are different from those in the conventional electromagnetic communication [15]. Nano-electromagnetic communication is based on communication using electromagnetic waves and wireless technology. Hence, nano-electromagnetic communication uses electromagnetic waves as information carriers.

The traditional transceiver of classical wireless communication is not feasible for nano-scale communication, however novel graphene based nano-materials have shown potential to overcome this limitation [9, 16]. Graphene is a one atom thick planar sheet that consists of carbon atoms arranged on a honeycomb crystal lattice. Two of the known derivatives of graphene are carbon nanotubes and graphene nanoribbon. Therefore, in the field of wireless communications, graphene and its derivatives have been proposed to implement miniaturized radio frequency antennas, namely, graphene radio frequency plasmonic antennas, or graphennas [17]. The miniaturization of classical metallic antennas with a size of a few micrometers, to satisfy the size constraints of a nano-machine, allow them to radiate electromagnetic waves. In the case of graphene antennas the electromagnetic waves radiate in the terahertz band between 0.1 THz and 10 THz [8, 18]. The use of this frequency band between 0.1 and 10 THz becomes extremely attractive due to the abundance of bandwidth and the potential for low area and power footprints, yet challenging given the large propagation losses and the lack of mature devices and circuits for terahertz operation [11]. In the latter, it is important to mention here that the electromagnetic waves propagation in graphene-based antennas have a lower propagation speed than in metallic antennas.

MC is a bio-inspired paradigm where the exchange of information is realized through the transmission, propagation, and reception of molecules. Accordingly we can define MC as transmission and reception of information by means of molecules [19].

Research working on MC has been inspired by investigating the information exchange at the cellular level of biological systems, where in such paradigm, transmitter nano-machines use molecules as message carrying for encoding and transmitting information to the receiver's nano-machines side.

The general phases of MC are similar to traditional communication systems: First, information encoding, where the transmitter encodes information using molecules that can be modulated in frequency modulation or amplitude modulation. Second, information propagation, where the transmitter initiates the signaling process by propagating information molecules into the

medium. Third, information receiving which is performed by the receiver, where the receptors of the receiver detect the received information molecules. The different information molecules can be detected by different receptors. Lastly, decoding of the information which is done by the receiver, where after receiving the information molecules the receiver decodes it, and according to the information molecules the receiver selects a desired reaction.

MC employs passive and active transport methods to exchange information molecules. In the passive method, information particles are randomly moved without using chemical energy. While in active transport, the information particles are actively transported from a transmitter to a receiver using special proteins. Thus, two main types of MC are defined, namely, the walkway based [20, 21], and the diffusion-based [22, 23]. In the walkway based molecular communication, the molecules are propagated by active carriers which transport them through predefined pathways. Specifically, the molecules use molecular motors in order to transport information, where the molecular motors move along predefined paths which are deployed between the transmitter(s) and the receiver(s) [14]. Molecular motors are biological nano-machine for transporting particles among living organisms by transforming chemical energy to motion [24–26]. However, in the Diffusion-based Molecular Communication (DMC), the molecules diffuse randomly through the medium from regions of high concentration to those of low concentration to reach the receiver. These molecules cover the distance between the transmitter and the receivers by following spontaneous diffusion in a fluid medium.

In addition, in respect to the communication range, molecular communications are classified as follows: short-range, medium-range, and long-range. The communication scale for the short-range MC is from nm to μm such as intra-cell and inter-cell. There are two approaches for short-range communication, namely, the molecular motors [27] which is an active transport, and the calcium signaling [28] which is a passive transport. As for the medium-range MC the propagation of molecules is done from μm to mm such in flagellated bacteria, and catalytic nano-motors [29]. Finally, the communication scale for the long-range MC is from mm to m. This type of communication is seen in nature where for example many species diffuse pheromones that only the same species can recognize them [30].

The focus of this Ph.D. thesis is on ***Molecular Communications (MC) where the propagation of molecules employs passive transport, namely, Diffusion-based Molecular Communication (DMC)***. In DMC the propagation of information molecules between a transmitter and a receiver is realized through free diffusion in a fluid. This class of communication takes inspiration

from existing communication mechanisms between biological entities.

Therefore, in this Ph.D. thesis:

- First we investigate and model the neuronal physical layer (layer 1) to understand better through simulation, and then to derive the appropriate performance metrics imposed by a point-to-point neuron neighboring absorbing receivers link, as well as by the Single Input Multiple Output (SIMO) network while taking into consideration two types of receivers, namely, absorbing receivers and Adsorption and Desorption (A&D).

- Second, we address two cases studies: the neurodegenerative disease and the fertility problems. The aim to address the neurodegenerative disease is to characterize the physical channel of the glutamatergic synapses between glutamate vesicles and AMPA receptors, and to analyze the effect of the toxic proteins aggregation on the brain. However, the goal to address the fertility problems is to build a mathematical model to track the movement of spermatozoa during the process of chemotaxis, to describe better through simulation, to understand by quantifying the communication problem, then to investigate the effect of varying the appropriate metrics on the system.

Hence, while investigating the case studies mentioned above we can provide to synthetic biology design oriented guidelines, as well as we can provide guidelines for the medical committee to come up with new solutions for the diseases that have no treatment as well as to create new treatments which are more reliable and less expensive than the existing one.

1.1 Neurodegenerative Disease

Alzheimer's and Parkinson's diseases are the most common chronic neurodegenerative disorders that affect individuals in their sixties or seventies. Parkinson's Disease (PD) is a progressive disorder of the central nervous system that mainly affects the motor system, hence, shaking, rigidity, slowness of movement, and difficulty with walking are the PD symptoms; while Alzheimer's Disease (AD) causes progressive brain disorder which slowly destroys thinking, memory capabilities and the ability to execute even the simplest tasks.

As was mentioned, PD is a progressive neurodegenerative disease. It is progressive since it grows and gets worse with time. It is neurodegenerative disease because during the disease there is actually a loss, a degeneration of particular kind of neurons called dopamine neurons.

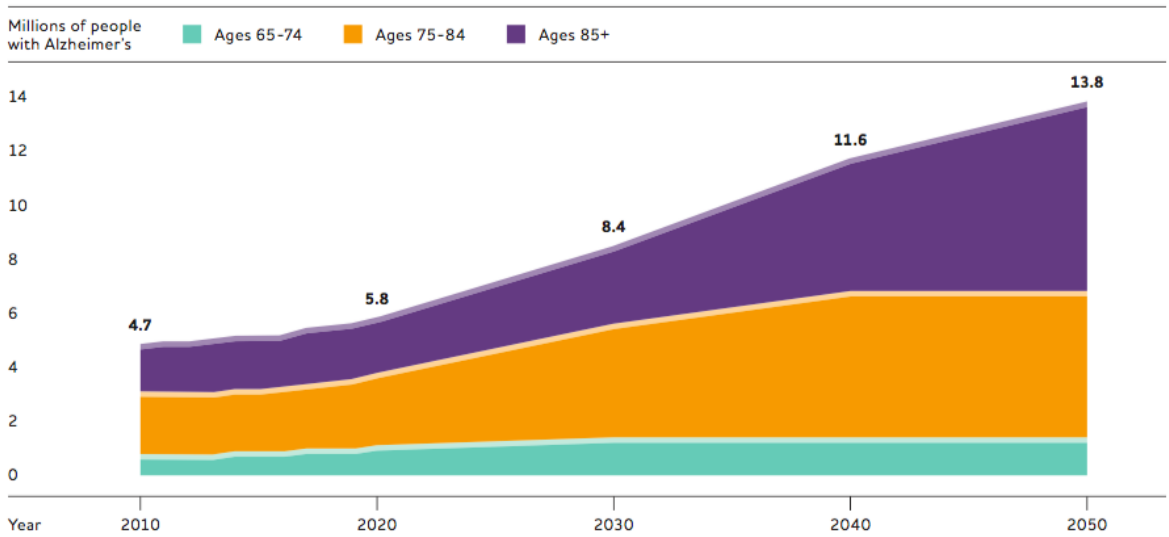

Figure 1.2: Projected number of people aged 65 and above (total and by age group) in the U.S. population with Alzheimer's Disease (AD), 2010 to 2050. [32]

Dopamine neurons are really important for allowing humans to make normal movements and since these neurons are used to produce dopamine, hence when they are lost the amount of dopamine in the brain will be reduced which will lead to Parkinson's symptom namely shaking at rest, muscle rigidity, slowed movements and impaired coordination. With regard to Parkinson's the US National Institute of Neurological Disorders and Stroke (NINDS) estimates that 1 million Americans living with PD and more than 10 million people worldwide [31].

Concerning Alzheimer's Disease (AD), in 2017, Alzheimer's Association estimated that 5.3 million people in the US had AD [32]. Due to the advance in medicine and medical technology, social and environment conditions, a large part of the American population has begun to reach the age of 65 and older. Thus, since 85 percent of people age 75 and above will be affected by Alzheimer's [32], therefore the number of cases with this disease will dramatically increase by years as shown in Fig. 1.2. This figure shows that by 2025, the number of people aged 65 and above is estimated to reach 7.1 million which is a 35 percent increase from 2017. However, by 2050 it is estimated that the number of people with AD will reach 13.8 million people age 65 and above. Moreover, Alzheimer's Disease International (ADI), in its 2016 report [33] indicates that there are worldwide 47 million people that live with AD or a related dementia disease, and estimates that the number of people affected by this disease will grow up worldwide to 131 million people by 2050.

Both Parkinson's and Alzheimer's Diseases are a progressive neurodegenerative disease where the area which is critical for learning and memory in the brain is affected. Therefore,

the neurotransmitters called acetylcholine are progressively diminished over the course of the disease which will lead to the loss of memory.

Nowadays, the drug treatments are the only solution for neurodegenerative diseases, where the aim of these treatments is to increase the amount of dopamine in the case of Parkinson's disease, where in the case of Alzheimer's disease the goal of these treatments is to maintain the neurotransmitter acetylcholine. Unfortunately with time the advantages of these drug treatments decrease and start to be useless.

1.2 Fertility Problems

World Health Organization defines Infertility as a disease of the reproductive system when the pregnancy is not achieved after 12 months or more of regular and unprotected sexual intercourse. In order for pregnancy to happen a sperm needs to meet up with an egg. Pregnancy officially starts when a fertilized egg implants in the lining of the uterus. However, both men and women can contribute to fertility problems. About 12% of married women aged between 15 to 44 years in the United States have trouble getting pregnant or sustaining a pregnancy [34]. Moreover, according to U.S Centers of Disease Control and Prevention infertility has risen 20% from 6.1 million individuals in 1995 to 7.3 million in 2002, hence today one in every eight couples of child-bearing age is infertile.

At this time, treatment for infertility tends to follow a hierarchical progression. The first stage of treatment is a diagnostic workup, involving a thorough examination of each partner's reproductive organs. Couples who initiate treatment begin at Level one, which involves initial ovarian stimulation with clomiphene citrate. Level two involves the use of exogenous gonadotrophins (another drug used to stimulate ovulation), with or without Intrauterine insemination (IUI) where in this procedure specially prepared sperms are inserted into the woman's uterus. Lastly, level three involves assisted reproductive technologies such as In Vitro Fertilization (IVF) where both the egg and the sperms are handled in a lab.

Approximately 44% of women with infertility have sought medical assistance, but of those who seek medical intervention approximately 65% give birth [35]. Fertility treatments help many women to get pregnant, yet these treatments can lead to health issues as getting pregnant with multiple babies which cause health problems for the pregnant woman and her babies. Additionally, infertility treatments can be unreliable, and quite expensive.

1.3 Motivation of this Thesis

1.3.1 Alzheimer's Disease (AD)

The facts that are mentioned in section 1.1 about the numbers of affected people, which are estimated to increase dramatically and the fact that there are no efficient treatments to treat these neurodegenerative diseases lead us to the necessity of a novel solution to this problem. What if we can fight the disorders of the nervous system as Parkinson's and Alzheimer's disease in an efficient way by using artificial neuron nano-networks so we can compensate for the loss and degeneration of neurons? What if we can fight Alzheimer's disease by suggesting a new vision for treating it? Our study aims to answer these questions by focusing on neuron based MC that exploits neurons as a communication component, and then analyzing the effect of the toxic proteins aggregation on the brain since this accumulation turns out to be the main reason behind AD, then ultimately to come up with a complete sense-actuation closed-loop system vision for fighting this neurodegenerative disorder.

1.3.2 Fertility Problems

As we saw in section 1.2 the 35% of treatment failure, the expensive cost, and the side effects of the multiple level of treatments lead us to propose new techniques to treat the fertility problems. What if we can fight fertility problems by understanding it as a communication problem? What if we add more density of spermatozoa? What if we can change the medium to make it more viscous? What if we can modify the chemo-attractant concentration released by the egg? Another purpose of this thesis is to answer these questions by building a mathematical model to track the movement of spermatozoa during the process of chemotaxis, to describe better through simulation, to understand by quantifying the communication problem, then to investigate the effect of varying the appropriate metrics to propose new treatments which are more reliable, and less expensive then the existence one.

Briefly, these analyses are carried out since synthetic biology is an emerging area of research that can be described as the design and construction of novel artificial biological pathways, organisms or devices, as well as the redesign of existing natural biological systems for useful purpose, hence the proposed analysis can provide design oriented guidelines. In addition, these studies present new solutions for treating diseases which establish a new vision of dealing with them, as well as serve as guidelines for the medical committee.

Consequently, the rest of this Ph.D. thesis is organized as follows. Chapter 2 contains the literature review of neuron-to-neuron communication network which also includes a survey of the results from previous works along with the open problems pertinent to the neuron-to-neuron communication network, and neuron-to-neuron Diffusion-based Molecular Communication (DMC). Furthermore, the anatomy of the sperm, and the anatomy of the female reproductive system is presented. In addition, the movement of spermatozoa during the process of chemotaxis is explained, and the previous works done in this field as well as the open problems are stated.

The objective and the methodology relevant to this Ph.D. thesis are provided in Chapter 3. Additionally, the list of the main simulators that have been recently proposed for Molecular Communications (MC) system are shown.

In chapter 4, the MolCom Markup Language (MolComML) is defined. The main objectives as well as the architecture of the MolComML are shown. Moreover, the N3Sim simulator is validated by comparing the N3Sim output results first with BiNS2 simulator, and second with the theoretical assumptions. Lastly, the MolComML portability, and the possibility of combining different platforms by using the MolComML are shown.

In Chapter 5, the point-to-point neuron neighboring absorbing receivers communication link, and the SIMO networks of a neuron-to-neuron DMC are analyzed. The adequate metrics performance of the systems mentioned above are derived, and the influence of neighboring receivers upon the Inter-Symbol Interference (ISI) are studied. Lastly, for the SIMO networks the effect of a SIMO adsorption and desorption neighboring receivers, and the SIMO absorbing neighboring receivers is investigated by comparing their achievable throughput (the rate of message that successfully delivered over the communication channel).

In Chapter 6, the physical channel of a Molecular Communications (MC) between glutamate vesicles and AMPA receptors, as well as the effect of increasing the number of the toxic Amyloid Beta ($A\beta eta$) on this channel are characterized. In addition, we introduce and develop a new closed-loop system vision which leverages such characterization to infer $A\beta eta$ concentration for fighting Alzheimer's Disease (AD) while using serotonin.

A 3-dimensional (3D) model of sperm movement in the reproductive female tract is modeled in Chapter 7. Moreover, the effect of varying the dose of spermatozoa released, modifying the viscosity of the medium, and releasing higher concentration of chemo-attractant on the channel are examined.

In Chapter 8, the research contributions are summarized and future research directions are

identified. In $Appendix A$ the MolCom Markup Language (MolComML) configuration file that describes a point-to-point communication link between a Platelet and a T-Cell, using CD40L as communication molecules is illustrated. In addition, in $Appendix\ B$ a short tutorial section on how to simulate SIMO MC scenarios in N3Sim is shown. Finally, the publications emerged from the research presented in this Ph.D. thesis are listed in $Appendix\ C$.

Chapter 2

State of the Art

In section 2.1 the literature of neuron-to-neuron communication network is explained in details. The anatomy of the sperm, and the anatomy of the female reproductive system are shown in section 2.2. Moreover, in this section the movement of spermatozoa during the process of chemotaxis is described. Lastly, in section 2.3 the results from the literature and the open problems focused on the neuron-to-neuron communication network, the neuron-to-neuron Diffusion-based Molecular Communication (DMC), Alzheimer's Disease (AD), and the movement of the human spermatozoa in the reproductive female tract are presented and analyzed.

2.1 Neuron-to-Neuron Communication

Neurons are fundamental components of the nervous system as the brain and the spinal cord. The structure of a neuron is composed of three major parts which are the soma, the axon, and the dendrites as shown in Fig. 2.1. The soma is the central part of a neuron which is responsible for spike generation in a response to a stimulus. Dendrites arise from the soma and play a role in the reception of the excitation. Axon is a cellular extension from the soma which is responsible for guiding the impulses to the axon terminals [36].

Neurons are connected to form networks, as a result neuron-to-neuron communication network occurs between two neurons where two types of phenomena are involved in processing the nerve impulse from one neuron to another, namely, electrical and chemical. Electrical events propagate a signal within a neuron, and chemical processes transmit the signal from one neuron to another. Hence, neuron-to-neuron DMC occurs between two neurons where the transmission of information is done by chemical substances called neurotransmitters.

Fig. 2.2 illustrates the neuron-to-neuron communication network which can be divided into

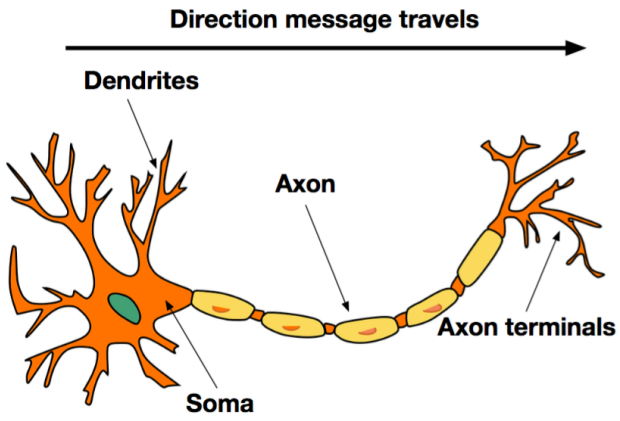

Figure 2.1: Structure of a neuron.

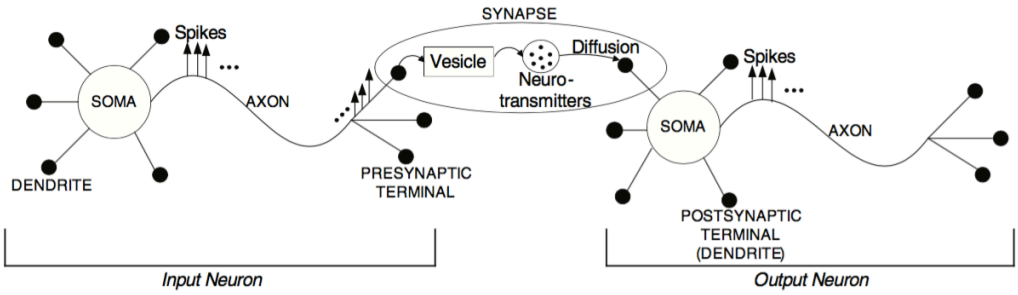

Figure 2.2: Neuron-to-Neuron network. [37]

three parts: the axonal transmission, the synaptic transmission, and the spike generation [37]. An overview of the axonal transmission, the synaptic transmission, and the spike generation, follows.

2.1.1 Axonal Transmission

The axonal transmission is the propagation of the spikes along the axon as we can see from Fig. 2.2. At long last of the axon reside the presynaptic terminals or the axon terminals whose release neurotransmitters to the synaptic cleft. Specifically, there are two general classes of neurotransmitters, namely, large neuropeptides or smaller amines/amino acids. The large peptides are synthesized in the cell body of the neuron and are transported to the synaptic terminal through the axon. However, the smaller amines/amino acids can generally be synthesized at the presynaptic terminal itself. Once the neurotransmitters are synthesized, they will be collected into vesicles and will be ready to be diffused over the synaptic cleft [38].

2.1.2 Synaptic Transmission

The synaptic transmission is defined as neuron-to-neuron DMC, and is considered as a short-range molecular communications (from nm to mm) because of the synaptic cleft which is defined as a gap between the presynaptic and postsynaptic cells that is about 20 nm wide [39]. The synaptic transmission is divided into two parts, namely, the neurotransmitters release, and the short-range diffusion. An explanation of the neurotransmitters release, and the short-range diffusion follows.

1. Neurotransmitters release: When the electrical signal (action potential) gets to the presynaptic terminal, some of the voltage gated Ca^{2+} channels in the membrane get open. Once these channels are open, calcium ions from the surrounding extra-cellular environment rush into the presynaptic terminal [38]. As the calcium ions encounter the vesicles, the membrane of the vesicles fuse with the membrane of the presynaptic terminal, right at the synaptic cleft. Finally, as the vesicles fuse with the membrane, the neurotransmitters are diffused into the synaptic cleft. Briefly, the neurotransmitters that are released in the synaptic cleft are caused by action potential generated at the presynaptic neuron, which are forced to exocytosis from special containers called synaptic vesicles. This phase of MC is known as information encoding where the number of neurotransmitters that should be released depend on the action potential.

2. Short-range diffusion: Transmission of information between neurons takes place in specialized sites called synapse or synaptic cleft as displayed in Fig. 2.2. In other words, the neuron-to-neuron DMC is confined to the synaptic transmission of neurotransmitters between the two neurons, where the exchange of these neurotransmitters is done through the propagation in the synaptic cleft depending only on the Fick's laws of diffusion. Particularly the presynaptic terminal emits neurotransmitters which propagate and spread in the synaptic cleft through diffusion process [37]. Then, the receptors node in the output neuron act as receivers which sense these neurotransmitters and collect them.

   By cause of neglecting the interaction among the emitted molecules [40], the dynamics of these neurotransmitters are described by the Brownian motion [40], which in mathematics are described by Wiener process as a continuous-time stochastic process. The flow of these released molecules goes from the regions with high concentration located next to the input neuron to the regions with lower concentration located next to the output neuron. This

flow is governed by the Fick's second law of diffusion, which describes the macroscopic behavior of molecules, and estimates the concentration of molecules at any position in the medium. The solution to Fick's second law in three dimensional environment for the free diffusion equation, without considering the reception model (i.e., the receiver is assumed to be transparent) is given by [41]:

$$C\left(D,t\right)=\frac{Q}{\left(4\pi D_f\ t\right)^{3/2}}e^{-D^2/4D_f\ t} \tag{2.1}$$

where Q represent the number of neurotransmitters released by the vesicles, D_f denotes the diffusion coefficient, D is the distance between the vesicles and the dendrites, and t the time. This phase of MC is known as information propagation.

2.1.3 Spike Generation

The neurotransmitters that diffuse in the synaptic cleft affect the output neuron through the receptors that lay on the postsynaptic terminal (Dendrite) [36]. There are two major types of receptors specifically, the ionotropic receptors and metabotropic receptor. The contrast between these two kinds of receptors is that the inotropic receptors immediately excite the neurons whereas the metabotropic receptors have an indirect effect. When these neurotransmitters hitch on the receptors they will lead to ions movement. The ion movements will contribute excitation of the membrane potential (the difference in electric potential between the output neuron and the exterior) of the output neuron and conduct to the spike generation. Note that neurons have a threshold value to depolarize so the excitation requirements should be beyond this threshold. Likewise, a neuron will typically generate a spike only if its membrane potential represented by Vm reaches a variable threshold value of about -50 to 50 mV [42]. However, spiking is controlled by a refectory period, which is the time period during which a cell is incapable of sending a new spike. In other words, during this refectory period, the neuron will not be able to process any other incoming signals from other neurons, until this period is completed so the action potential cannot be invoked immediately because of the absolute refectory period that is needed. Briefly, this phase of MC is the last two phases, namely, information receiving, and information decoding.

Briefly, neurotransmitters make possible the nerve impulses of one neuron to influence the nerve impulses of another by diffusing in the synaptic cleft, and then by attaching themselves to chemical receptors in the membrane of the postsynaptic neuron where they promote excitatory

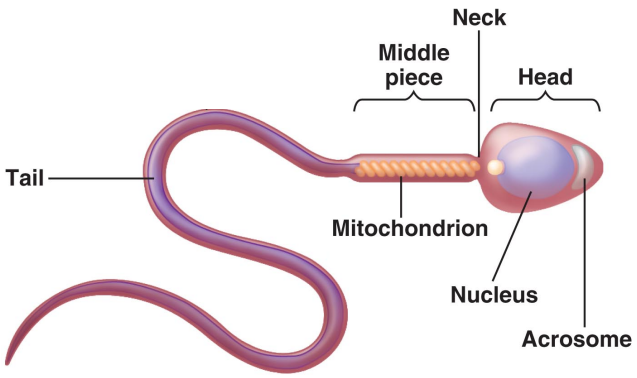

Figure 2.3: Anatomy of the Sperm.

or inhibitory changes in its membrane [43]. Excitatory changes in the postsynaptic neuron increase the probability of an action potential; however, inhibitory changes in the postsynaptic neuron decrease the probability of an action potential. As a consequence, the free diffusion of neurotransmitters allow the brain cells to communicate.

2.2 Spermatozoa and Egg Communication

A human has only one of two gametes, the mature male sex cell (spermatozoa or sperm) or the female sex cell (egg cell or oocyte). The sperm cells are developed in the testes which are part of the male reproductive system, while the egg cells are produced in the female reproductive system. Every single gamete is genetically distinctive; it contains a unique copy of half the genes of the parent source. Each spermatozoa and oocyte contains twenty-three chromosomes. Thus, when a spermatozoon reaches and joins an oocyte they form a diploid cell of forty-six chromosomes.

2.2.1 Anatomy of the Sperm

The scientist Antonie van Leeuwenhoek was the first person who described in detail the structure of a sperm cell in 1677. As Fig. 2.3 shows, the spermatozoa anatomy is made up of three basic parts: the head, the neck along with the middle-piece, and the tail, with an average total length of 50 μm [44]. First, the head is an oval shaped anatomy, with a size ranging from 5 to 8 µm. It consists of two parts: acrosome, and nucleus. The acrosome is located at one end of the sperm cell which contains proteolytic enzymes that help to impair the outer layer of the oocyte. However, The only part of the sperm cell that enters into the egg cell is the nucleus, which contains the twenty-three chromosomes of the sperm cell. Second, the neck

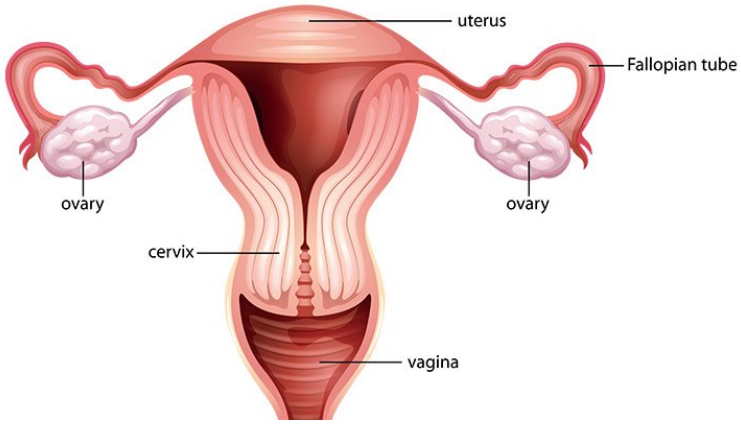

Figure 2.4: Anatomy the female reproductive system.

along with the middle-piece are the parts that can be found between the head and the tail. Their task is to attach both ends of the sperm cell. Moreover, the neck contains millions of spirally arranged mitochondria which provide the tail all the energy required to propel in the female reproductive tract. Lastly, the tail or the flagellum whose main function is to ensure sperm motility. Specifically, the motor proteins in the flagellum of the sperm generate a regular beat of the flagellum, which propels the sperm in a fluid. In addition, the flagellum of sperm serves both as a propeller and antenna that detects chemical. Therefore, sperm tail defects can lead to male fertility problems.

2.2.2 Anatomy of the Female Reproductive System

The structure of the female reproductive organs can be divided into five parts as in Fig. 2.4. First, the vagina is a muscular part whose function is to connect the uterus with the exterior. Second, the cervix is the lower part of the uterus and it bridges it with the vagina. Third, the uterus which consists mostly of a smooth muscle, and is the place where the pregnancy along with the development of the baby occurs. Forth, the Fallopian tubes which connect the ovaries with the uterus, and where the sperm meets the fertilized egg. There are two Fallopian tubes, also called the uterine tubes or the oviducts. Lastly, the ovaries which produce egg cells and release one during the fertile days of the woman's menstrual cycle [45].

2.2.3 Motion of Sperm Toward Eggs

A key process in human fertilization is bringing the two gametes together, namely, the sperm and the egg. Indeed, for fertilization to occur, the spermatozoa must reach the egg which moved after

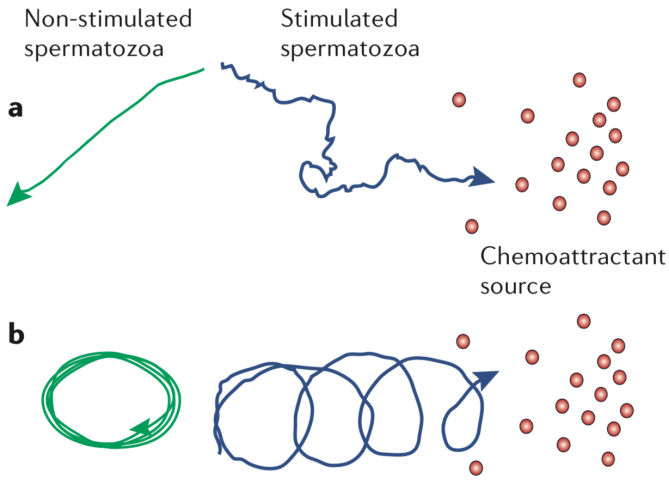

Figure 2.5: Two categories of sperm reaction to chemo-attractants. [48]

ovulation from the ovary into the Fallopian tube. The spermatozoa travel a disturbing path toward the egg after its deposition in the vagina. Some of the obstacles that the sperms face include: first the vaginal pH where not every sperm is able to survive due to the acidic pH. Second, the cervical mucous which should be liquid and less dense to facilitate the passage of the sperm. Lastly, the response of the immune system where the female's white blood cells detect the sperm cells as bacteria, and try to destroy them. Hence, one of every million spermatozoa succeed in entering the Fallopian tubes [46, 47].

2.2.3.1 Behavioural Mechanisms of Chemotaxis

Once the sperms overcome the vaginal, cervical, uterine barriers, and hit the Fallopian tubes they start to feel the concentration of certain chemicals via chemo-reception which are released by the egg. The chemicals that are released by the egg and which exist in the fluid are able to bind to specific receptors on the membrane of the sperm [48–50]. The chemo-attractants that bind to receptors on the sperms act as a chemical communication system between the egg and the sperm, causing the sperm to adapt its moving direction in order to reach the egg. Chemotaxis is the process where sperm cells are guided to the egg by chemo-attractants.

Fig. 2.5 a) and b) shows two categories of sperm response to chemo-attractants. The first type is shown in Fig. 2.5 a), where the non-stimulated spermatozoa swim in almost straight or curved lines, however, when the spermatozoa sense the chemo-attractant released by the egg they become stimulated, then there is a sudden alter in the direction of the sperm swimming towards the chemo-attractant source. In this category we can find the human spermatozoa [51,52], as well as the spermatozoa of hydrozoa (Campanularia flexuosa and Gonionemus vertens). The second

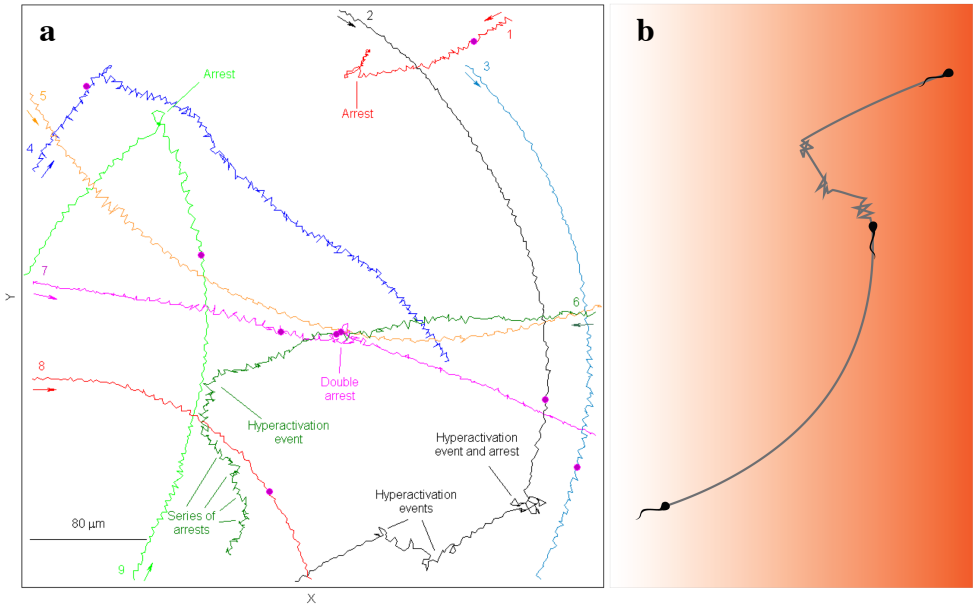

Figure 2.6: Track of human spermatozoa. a) Tracks of human spermatozoa in a controlled experiment. b) Model of the sperm human track in a gradient of chemo-attractant. [58]

type is presented in Fig. 2.5 b), where the non-stimulated spermatozoa swim in circles, but, when the spermatozoa sense the chemo-attractant released by the egg they become stimulated, then the circles movement of the sperm become a biased movement, which result in a spiral movement in the direction of the chemo-attractant source. This category includes the spermatozoa of the sea-urchin, the starfish, the hydromedusa, and the ascidian [53–55].

Moreover, Fig. 2.6 displays the track movement of human spermatozoa. Fig. 2.6 a) shows the different behaviors of the human spermatozoa in response to the progesterone chemo-attractant [56, 57] in a controlled experiment [58]. As we can see when no progesterone is released the sperms swim straight or in a curved lines with random tumbles, however, when progesterone is released the sperms start to swim in tight circles rather than a straight line towards where the chemo-attractant is diffused in the fluid. Fig. 2.6 b), illustrates the model of the sperm human track in a gradient of chemo-attractant. The intensity of the background color represents the chemo-attractant concentration. As long as the sperm cell senses an increase in the chemo-attractant concentration, the sperm cell swims in a roughly straight line. However, when the sperm cell senses a decrease in the chemo-attractant concentration, the sperm cells picks a random direction by swimming in tight circles trying to replace the current one.

Concisely, when the spermatozoa sense that the surrounding concentration of chemo-attractant is increasing (they are moving in the correct direction and approaching from where the egg reside), they will keep swimming in a straight line for a longer time before they turn.

Though, when the spermatozoa sense that the surrounding concentration of chemo-attractant is decreasing (they are moving away from where the egg reside), turns and hyper-activation events take over, hence, they pick a random direction by swimming in tight circles trying to replace the current one. Not to mention that human spermatozoa swim more in straight lines since the fraction of hyper-activated spermatozoa is low [59]. In addition, the flow of the released chemo-attractant by the egg is governed by the Fick's second law of diffusion explained before in equation 2.1, where the chemo-attractant molecules diffuse freely in the medium from the regions with high concentration to the regions with lower concentration. In our work, we will focus on the movement of human spermatozoa during the process of chemotaxis.

2.3 Previous Work and Open Problems

2.3.1 Neuronal physical layer

A few works evaluate a higher level approach such as in [60], where the authors consider an optimistic research direction where they suggest the implementation of DMC networks inside the human body. Moreover, in [61], the first step toward designing a Mobile Ad hoc Molecular Nano-network (MAMNET) with electrochemical communication is considered. MAMNET consists of mobile nano-machines and infostations. Nano-machines and infostations are assumed as genetically modified cells with additional capabilities. Nano-machines are assumed to sense the environment and gather some environmental information to deliver infostations. Based on the collected information coming from nano-machines, infostations are assumed to make decision for an appropriate action. The authors presented an analytical framework that incorporates the effect of mobility into the performance of electrochemical communication among nano-machines.

However, the other researchers consider particular application scenarios of DMC. In [37], the neuronal physical layer is studied based on a probability of error and delay in spike detection at the output. In addition, the physical neuron-to-neuron communication channel is treated in [62] as a preliminary step in defining the stages of communication among neurons. The work presents an input/output relationship at each communication block in terms of transfer functions with the purpose of nano-machine to neuron communication. In [63], the authors analyze the mechanisms underlying the initiation of spikes and they suggest a strategy to control the intercellular calcium concentration through the changes in membrane voltage. Furthermore, in [64] the ergodic capacity of the synaptic Multiple Input Multiple Output (MIMO) communication channel is

investigated by using the statical properties of neuronal communication without taking into consideration the effect of neighboring receivers on the channel behavior. Finally, in [65] they studied the synaptic interference channels in a Single Input Single Output (SIMO) and Multiple Input Single Output (MISO) by modifying the synaptic conductances (channel weights).

Moreover, the two system that are modeled in [66] and [67] assume that molecules are removed from the environment after hitting the receivers. This can be modeled as the first-hitting process, where in this process each molecule can contribute to the signal only once. On the other hand, for instance in [68] and [69] the models used omit the first-hitting process, where the molecules can go inside and out of the receivers many times without any alternation on the dynamic movement of the molecules.

In the literature of DMC, first ISI has not been taken into account as in [70–74], and [75]. Then, in [76], and [77] the authors considered that the transmitters should not release molecules before making sure that the receivers received the intended molecules, and this is inefficient in terms of transmission rate since symbol duration will be infinite. Afterwards, some literature took into consideration the ISI effect, for example, they suggested to use incorporating ISI mitigation techniques in [78–81], multiple molecules in [78], and enzymes in [69, 82, 83] to reduce the ISI.

Hence, it is found that in particular application scenarios there is no research that has been conducted to analyze and to derive the achievable throughput, the Bit Error Rate, the Inter-symbol Interference with a closed-form analytic model of the neuron-to-neuron DMC in a point-to-point neighboring receivers, and in a SIMO perspective while taking into consideration the effect of the neighboring receivers in the channel.

2.3.2 Alzheimer's Disease

The only work that considers the neurodegenerative diseases as a MC problem is in [84]. In this paper, a theoretical investigation about the reason of abnormal gliotransmitters concentration is presented. In addition, a Ca^{2+}-signalling-based molecular communications framework is proposed to control the abnormal gliotransmitters concentration.

Therefore, as far as we know there is no study that has been presented to understand, to model, and to characterize through simulation the neuron-to-neuron DMC physical channel, nor to propose a new vision which can provide a new and more efficient solution to treat AD.

2.3.3 Movement of the Human Spermatozoa in the Reproductive Female Tract

The chemotaxis models have been developed for many organisms in [85–87]. In these works, complete models are developed by using differential equations which characterize the curvature paths, as well as the random biased walks.

In [88], the authors developed a theoretical description of sperm chemotaxis by regulating the curvature and torsion of the swimming path. In this work, the model draws circles as the sperm approaches the egg, however, hyper-activated motility is not identified. In addition, a two dimensional model was described in [89], where the trajectory of the sperm is controlled by curvature paths. In this work, the trajectory is fixed once we know the concentration distribution and the starting position of the sperm. In [90], a deterministic model is proposed where the path curvature is controlled by the concentration of Ca2+.

Moreover, in [91] the authors developed a three-dimensional model of the spermatozoa movement. In this work, the authors build a model based on Brownian motion, rather than calculating the trajectory from the curvature.

Hence, to the best of our knowledge, modeling the movement of the human spermatozoa in the reproductive female tract and considering it as a MC problem is missing. Therefore, understanding and describing better from simulation to provide guidelines for improvement oriented to come up with new treatments are needed.

Chapter 3

Objectives, Methodology, and Molecular Communication Simulators

The literature, the previous works, and the open problems of these systems mentioned in Chapter 2 are listed to motivate the study proposed in this thesis, hence, the objective and the methodology is mentioned in section 3.1. Lastly, section 3.2 shows some of the main simulators that have been developed to characterize the broad set of Molecular Communications (MC) systems.

3.1 Objectives and Methodology

First, as we mentioned in section 2.3.1 there is no specific research that has been conducted to investigate the neuronal physical layer (layer 1), and to derive the appropriate performance metrics imposed by a point-to-point neuron neighboring absorbing receivers communication link, as well as by the Single Input Multiple Output (SIMO) networks. Therefore, we aim to fulfill the following tasks:

1. In the Point-to-Point neuron neighboring absorbing receivers communication link:

    a) Analyzing the influence of neighboring absorbing receivers on the maximum amplitude and pulse energy of the impulse response. This is done by investigating the impact of three scalars (distance from the transmitter, and the distance between the receivers, and their radius) on the impulse response.

    b) Investigating the impact of the neighboring absorbing receivers on the tail of the impulse response and to model the Inter-Symbol Interference (ISI) of this system. Evaluate the system and derive the adequate metrics performance.

2. In the SIMO networks:

    a) Modeling the synaptic SIMO channel with absorbing receivers.

    b) Modeling the synaptic SIMO channel with Adsorption and Desorption (A&D) receivers.

    c) Studying how these two systems will influence the pulse amplitude, width, energy, and tail with the objective of deriving optimum guidelines.

    d) Modeling the Inter-Symbol Interference (ISI) of the two systems while deriving and comparing the achievable throughput of each system.

    e) Checking how the numbers of receivers and the distance between the receivers will affect the performance of the two systems.

Second, as we saw in Section 1.1 the number of people affected by disorders of the nervous system as Parkinson's and Alzheimer's disease is expanding in a dramatic way. Drug treatments have not provided an effective solution since their effect diminishes with the time. In addition, Section 2.3.2 reveals that, in the literature, few investigation have been attained on neurodegenerative disease. Hence, based on these facts we aim to model the neuron-to-neuron DMC network to provide guidelines for medical community. These guidelines will help this committee to fight against the disorders in the nervous system in an efficient way by establishing again the communication that has been lost from the degeneration of neurons. Thus, we achieve the following tasks:

1. Characterizing the physical channel of a DMC between glutamate vesicles and AMPA receptors.

2. Analyzing the effect of glutamatergic neurons on each other.

3. Investigating the effect of increasing the number of the toxic Amyloid Beta on this channel.

4. Introducing and proposing a complete sense-actuation closed-loop system vision which leverages such characterization to infer the toxic Amyloid Beta concentration for fighting AD while using serotonin which, as is widely accepted, can reduce the production of Amyloid Beta proteins.

Lastly, in Section 1.3.2 we reported that guidelines for improvement oriented to come up with new treatments are needed for the case of fertility. In addition, in section 2.3.3 we saw

that considering the movement of human spermatozoa in the reproductive female tract as a communication problems is missing. Therefore, in this work, we focus on the part where the spermatozoa enter the Fallopian tube and how they alter their movement to reach the oocyte. Accordingly, we perform the following tasks:

1. Building a mathematical model to track the movement of spermatozoa during the process of chemotaxis by using MATLAB software [92].

2. Understanding the movement of spermatozoa during the process of chemotaxis, and describing better through simulation.

3. Understanding by quantifying the communication problem. Hence, investigating the effect of varying the dose of spermatozoa released, modifying the viscosity of the medium, and releasing higher concentration of chemo-attractant on the channel.

3.2 Molecular Communication Simulators

In this section, we describe the main simulation platforms that have been recently developed to characterize the broad set of MC systems:

- N3Sim: is a complete simulation framework for DMC, which allows the evaluation of the communication performance of molecular networks with several transmitters and receivers mimicking an infinite space with a given concentration of molecules [93,94]. The transmitters encode the information by releasing particles into the medium, thus varying the concentration rate in their vicinity. The diffusion of particles through the medium is modeled as Brownian motion, taking into account particle inertia and collisions among particles. Finally, the receivers decode the information by sensing the local concentration in their neighborhood. The benefits of such a simulator are multiple: the validation of existing channel models for molecular communications and the evaluation of novel modulation schemes are just two examples. It implements a three-layer architecture. The user interface layer interacts with the user to read the input data for the simulation, while the data layer writes the simulation results to files. The domain layer contains the MC model. N3Sim is a Java-based simulator; therefore, it can be used in different operating systems with the appropriate Java virtual machine. The simulation parameters are determined by means of a text configuration file editable by the user, which defines the values of all possible

variables in the simulation. These are separated into four groups of variables for clarity: simulation, space, transmitters and receivers. In addition, N3Sim allows automating the execution of multiple simulations in a simple manner by means of user-defined scripts.

- BiNS2: Biological and Nano-Scale Communication Simulator v.2 is a multi-threaded simulator of MC systems [95]. BiNS2 is implemented in Java, and includes a generic type of software object, named Nano Object. It is a simulation multi-threaded package for MC systems. Its customized design provides a set of tools for creating objects and for modeling the behavior of biological entities. it includes different algorithms for handling particle collision, that allow modeling both diffusion based and flow-based propagation models into both constrained and open space environments.

- NCSim - Bacteria nano-networks: is a comprehensive simulation framework for molecular communications, utilizing flagellated bacteria for information delivery [96]. The major focus of the framework is on different message encoding techniques. NCSim supports typical deployment policies, such as grid and random, as well as custom deployment policies. It can simulate several simultaneous links between the nano-machines. NCSim incorporates the stochastic model for bacteria mobility, and the plasmid/chromosome transfer between bacteria through the conjugation process. The tool also has an adjustable vibration generator to model different levels of stability in the environment. Currently, only the 2-dimensional configuration is supported. The accuracy of the produced metrics in major scenarios has been confirmed via comparison with analytically results in simplified scenarios. NCSim is composed of three modules: (i) physical (PHY) layer of bacterial nano-networks, including deployment, bacteria mobility and conjugation, plus messages encoding/decoding; (ii) scenarios generator and simulation monitor; and (iii) plotting tool, intended to post-processing of raw simulation data and plots generation. The PHY module, as the most computational intensive, is implemented in C++ with a number of technical enhancements to speed up the bacteria mobility and conjugation simulations. The two latter modules are written in Python for maintenance and extension simplicity.

- BNSim: is a multi-threaded Java simulator for bacteria networks [97]. These networks interconnect engineered bacteria that communicate at nano-scales. BNSim integrates three simulation methods: (i) the Gillespie stochastic simulation algorithm; (ii) stochastic

differential equations, used to model large-scale chemical system with a controlled level of approximation; (iii) a hybrid algorithm which integrates the above methods.

- COMSOL Multiphysics: is a commercial multipurpose platform designed for simulating physics-based problems [98]. It processes through a unified work flow for electrical, mechanical, fluid, and chemical applications. Hence, it implements finite element analysis, for different physics and engineering applications. In [98], they use the COMSOL Multiphysics simulator for simulating a MC drug delivery system.

- CalComSim: is a simulator based on calcium signaling. It is designed for simulating both synthetic and natural cell communications in human tissues [99]. An integration of the biological models for the signaling process governed by stochastic solvers is used to handle multiple and parallel reactions in each cell of the tissue. The biological models that are incorporated into the simulator are based on real experimental data. The simulator can be used not only by telecommunication engineers and biological scientists, but also pharmaceutical researcher that can design new drugs and treatments for diseases that emerge from impaired calcium signaling.

- NS-2 and NS-3 Based Simulators: are discrete-event network simulators, which were not originally developed for modeling Molecular Communication [100, 101]. However, their flexible structure has allowed implementing some basic Molecular Communications (MC) systems.

- HLA Simulator: is a simulator that focuses on scalability, and adopting the High Level Architecture (HLA) model [102]. The scalability options are used to comprise processing power, hence, to reduce the execution time. Therefore, this simulator allows the design of large systems.

However, to assess the objectives mentioned in section 3.1 for the neuron-to-neuron DMC network we will base our study on the java open source simulation framework N3Sim. Therefore, in Chapter 4 we validate the N3Sim simulator by comparing it to the BiNS2 simulator, and we show that the results of both simulators are similar to the theoretical assumptions. Note that The cooperation between these two simulator is done through the MolCom Markup Language (MolComML) [103, 104].

Chapter 4

MolCom Markup Language (MolComML)

This Chapter defines the MolCom Markup Language (MolComML) and overviews its objectives, elements, and functionality. In addition, in this Chapter we validate the N3Sim simulator, and we show how MolComML can be used to integrate simulators and make them interoperable.

The remainder of this chapter is organized as follows. Section 4.1 defines, and identifies the main objectives the MolComML. In addition, it illustrates the architecture of the MolComML, with a special focus on its main elements and peculiarities that allow describing MC systems. Section 4.2 validates the N3Sim simulator by comparing it to the BiNS2 simulator, and shows that the results of both simulators are similar to the theoretical assumptions. Section 4.3 evaluates the performance of the neuron MC systems by using two different simulation packages namely N3Sim and BiNS2, configured by using the MolComML, in order to demonstrate both its portability and the possibility of combining different platforms for creating complex simulation tools. Finally, the summary and the concluding remarks are shown in Section 4.4.

4.1 MolCom Markup Language (MolComML)

A new MolComML is necessary for bridging the areas of interest for molecular communications [103, 104]. Accordingly, this needs to be flexible and generic, such that it can be understood by any software and simulation platforms for MC. It also needs to be capable of providing a large level of detail by providing all governing equations, parameter values and necessary conditions, such that it can entirely describe a MC environment in either a simulation or experimental

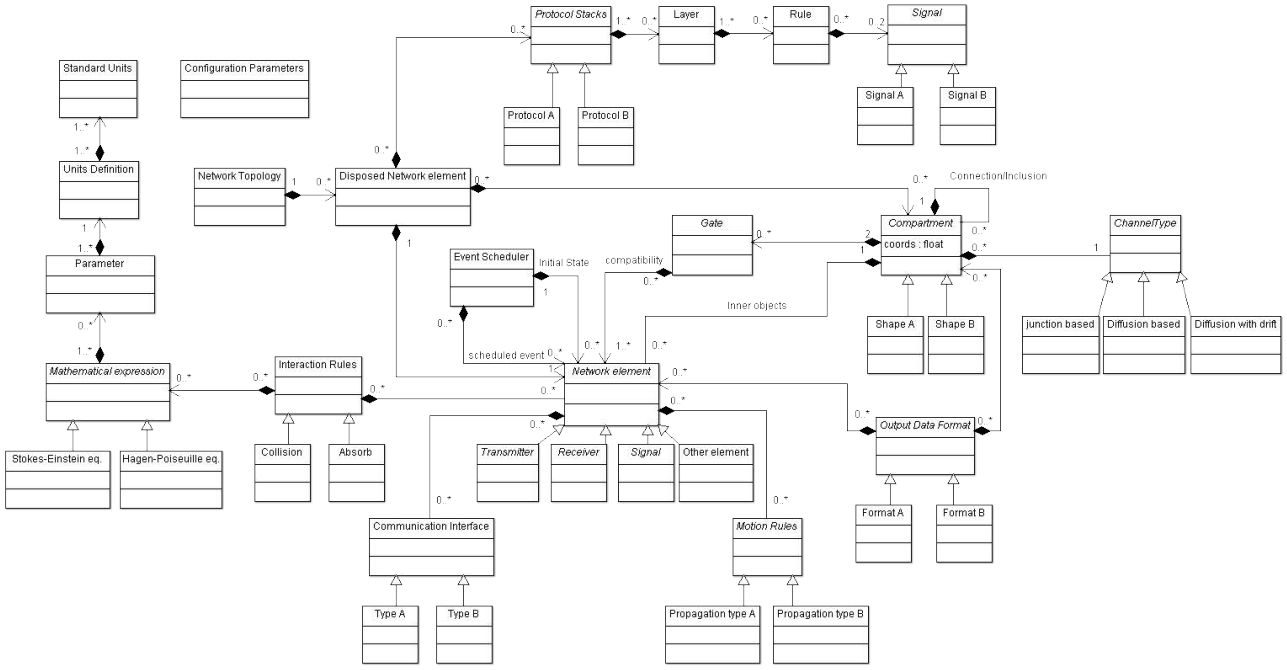

Figure 4.1: General UML diagram of the MolComML

test-bed. The MolComML is introduced as an XML-based language that reunite both numerical analysis and experimental synthesis by ensuring a flexible markup language [105]. Therefore, this tool allows cross-validation of experiments with the theoretical results, and this tool reduces significant researcher time in interfacing different software tools. In the following subsections we present the main objectives, elements and functions of the MolComML, as well as its structure

.

4.1.1 Objectives

The main objectives of the MolComML format can be summarized as follows: First the MolComML represents the different classes of MC scenarios, at all levels of abstraction. Second the MolComML enables the use of multiple software tools without having to rewrite models to conform to different file formats. Third the MolComML should guarantee the survival of models beyond the lifetime of the software used to create them. Fourth the MolComML uses a single language in order to analyze the considered scenarios through software tools, as well as to synthesize actual lab experiments. This ensures repeat-ability and cross-validation of results. Fifth the MolComML allows models to be shared and published in a form that any researcher can use in different software packages. Lastly, the MolComML should consider future extension due to the rapid expansion of the MC area.

4.1.2 Elements and Functionality

MolComML basic structure consists of several blocks reflecting the main components of a general molecular communication case. Each block is composed of a set of required and custom parameters that could be defined each time according to the MC needs. Fig. 4.1 illustrates the general UML diagram of the MolComML showing the interconnections and dependencies among different blocks. An overview of the basic elements and functionality are describes as follow:

- Network Elements: The network elements are considered as the main building blocks of the MolComML architecture. They are created and interconnected to define the simulation or experimental set-up. Each element may be defined by different levels of abstraction. For instance, it can be an entirely conceptual entity; it can have some real physical interpretation, or both. Each network element has a set of standard attributes that could be extended by the introduction of custom ones. The most important attributes describe the shape and size of the element, its mass and time to live properties, the accepted and transmitted signals and, finally, the motion rules. The main network elements can be defined as follow: First the transmitters where we need to include all the related parameters, such as the rate of creation of molecules, the rate of emission, and the molecule release mechanism. Second the receivers which assume multiple configurations, such as absorbing receivers and receivers with absorbing receptors. lastly, the signals which convey the signal carries towards the receivers.

- Communication Interface: The network elements defined above can exchange information by using the communication interface element, that characterizes the external interfaces of each network element. Such interfaces have many properties that describe the type of transmitted and received signals, their affinity and communication direction. Moreover, a subset of custom parameters can be defined in order to detail the properties of each interface. The custom parameters are identified by the <param> tag and the new attributes are defined after the <param> tag. This approach allows a high customization capability, extending the predefined attributes or introducing completely new ones.

- Compartment: The compartments are characterized by particular type and shape where species may be located. A model may contain multiple compartments organized in a hierarchical architecture or close to each other. In both cases, connections between

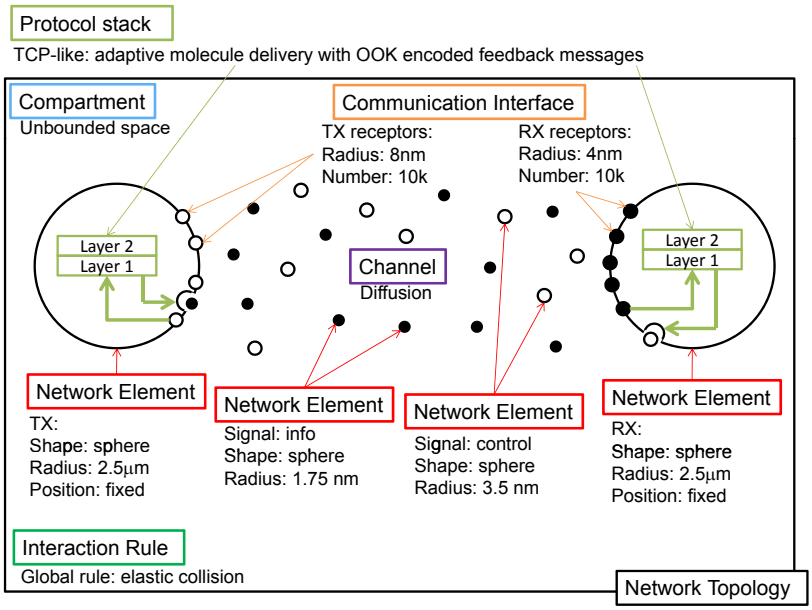

Figure 4.2: Graphical description of the MolComML

different compartments are represented by gates, that define the crossing rules. Each gate is identified by a unique name, a position, size, shape and orientation. Each network element in a simulation scenario is located within a compartment.

- Interaction Rules: Rules are defined by mathematical expressions imported from an external model (e.g. MathML [106]). Each rule could be a global rule which is valid everywhere, or specific rule which is only valid for a subset of network elements.

- Communication Channels: In MC many channel types exist as Junction-based, diffusion, and diffusion-with-drift. A channel element has to be defined and connected to each compartment placed in the communication environment. Each channel definition could be shared between two or more Compartments. The association channel-compartment is defined in the compartment section.

- Network Topology: The network topology section is used to describe the relative displacement (initial position and orientation) of network elements in the simulation environments.

- Protocol Stack: The protocol stack is associated with the internal state of the network element. Each protocol layer could either map the known protocol stacks of telecommunication systems or completely define new layers. The layers are defined by a set of rule and each one is composed of two signals, the first is for the forward communication and the

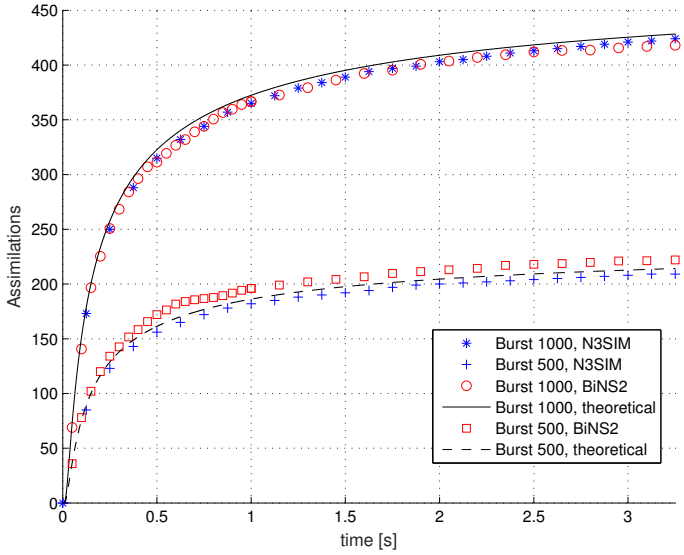

Figure 4.3: Simulation results obtained with N3Sim and BiNS2 configured with the same MolComML input file.

last is for the backward communication. For each signal, the type of carrier that will be transmitted and the modulation type are defined.

- Event Scheduler: The Event Schedulers define the initial state for each network element, and specific events that cause a state transition on a target node consequent to an event or at scheduled times.

- Output Element: The output data format is fixed for all simulations and numerical results. The defined output scheme allows it to specify which elements have to be exported. It is possible to define the list of Network Elements, of the Compartments and of their attributes, by specifying also the time interval for their monitoring. You can define a rule for each attribute of interest through the <param> tag.

Fig. 4.2 shows the matching between the main elements of the MolComML explained above and the MC scenario of a point-to-point communication link between a Platelet and a T-Cell, using CD40L as communication molecules illustrated in [107]. In addition, refer to $Appendix A$ for the MolComML configuration file that describes the same example mentioned previously.

4.2 Validation of N3Sim

To validate the N3Sim simulator we perform the following case where the simulation includes a point transmitter (T_x) with a radius 50 nm, able to release a burst of molecules (the radius of the molecules is equal to 1.75 nm), and a spherical absorbing receiver (R_x) with a radius 5 μm. The distance between T_x and R_x is equal to 5 μm. We run the simulation with two different burst sizes 500 and 1000 molecules, in order to verify possible dysfunctions with signal size. In addition, we develop an intermediate parser able to translate the MolComML specifications into the original configuration files of each simulation tool, namely, N3sim and BiNs2. This will allow a fast integration of the MolComML specification rules without any changes on the simulator source code.

The results are shown in Fig. 4.3. The black lines are relevant to the theoretical model, used to validate the results of both simulators. The black solid and dashed lines refers to a burst size of 1000 and 500 molecules, respectively. The blue markers refer to BiNS2, whereas the red ones to N3Sim. The agreement between simulation curves and theoretical ones is excellent. Hence, we demonstrate that the same MolComML data file will generate comparable simulation results between the two simulators as well as the theoretical one.

4.3 Combined Use of N3Sim and BiNS2 Simulators

In this section we show how the two simulators BiNS2 and N3Sim can cooperate by means of the MolComML. The goal of this cooperation is to simulate this scenario by N3Sim, since it is a simple but very fast simulator.

The analyzed scenario is focused on the communication via diffusion of neurotransmitters, from the axon terminal to the dendrite. This communications happens by means of messenger molecules with a radius equal to 0.2 nm. The distance of the synaptic cleft is equal to 20 nm. The radius of transmitters is 20 nm, whereas that of receivers is 1 nm. Four different simulation cases have been compared; they differ for the total amount of transmitter and receiver nodes (i.e. N = 1, 20, 50 and 100 for each type of node). At the simulation start, each transmitter node releases 1000 molecules that diffuse in the synaptic cleft. The simulation time step is set to 0.1 ns.

N3Sim simulator can simulate just absorbing receivers, without implementing the functions associated with individual receptors. Differently, this is a key function of BiNS2. Thus, the idea

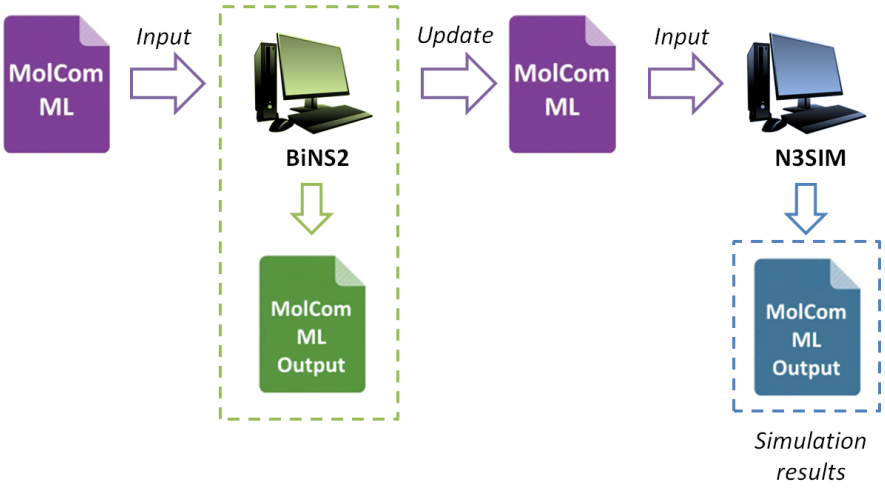

Figure 4.4: Combined use of two simulators for simulating neuronal communications leveraging MolComML.

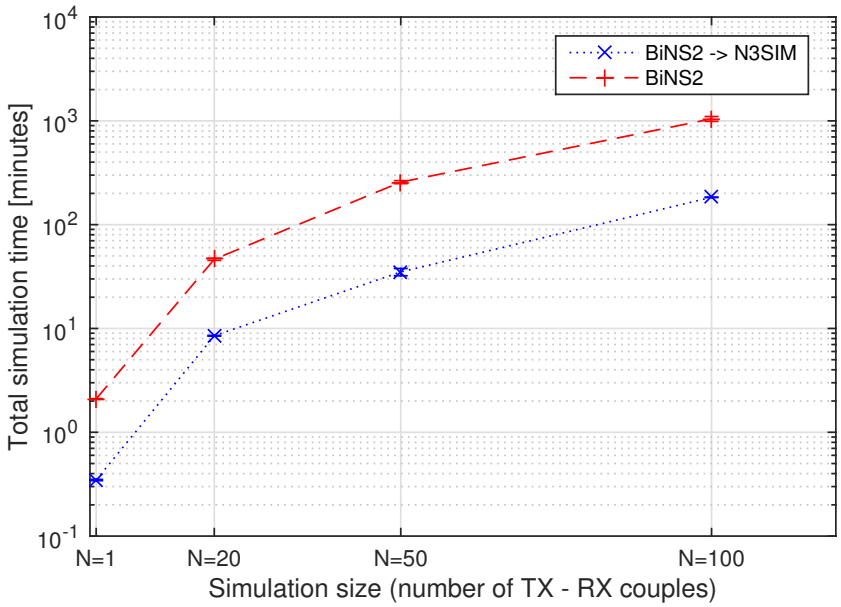

Figure 4.5: Total simulation time comparison.

is to model the overall scenario with receptors as very small absorbing receivers. The missing step is the capability of placing these receptors on specific positions over the reception surface, which can be easily done by using BiNS2.

The simulation settings are specified by MolComML, as a common simulation description language. The simulation is started in BiNS2, which easily places nodes according to the geometry of the considered scenario. This simulation ends by producing a simulation status report, encoded again by MolComML, which is the configuration input file for the N3SIM simulator, as sketched in Fig. 4.4. N3Sim runs the simulation by implementing the release of molecules by multiple nodes (neurotransmitter transporters) and the reception by multiple

adsorbing receivers (receptors on the dendrite), thus implementing a sort of Multiple Input Multiple Output (MIMO) simulation. We have uploaded as data-set the MolComML file generated by the BiNS2 simulator, where the position of each node is passed to the N3Sim in the MolComML configuration file used to set up the N3Sim simulation as a list of coordinates. The positions of both transmitter and receiver nodes are calculated by an algorithm implemented in BiNS2 and defined by a specific math rule in the section dedicated to network topology in the BiNS2 MolComML configuration file.

Fig. 4.5 shows that the simulation times obtained by the combined use of BiNS2 and N3Sim simulators are about 6 times shorter than those obtained by using only BiNS2 since the simulation times of N3Sim is faster then the simulation times of BiNS2. In addition, this difference is nearly constant with the simulation size. Lastly, the main advantage of such architecture lies in the feasibility of combining the features of both simulators, such as the customizable nano objects placement performed by BiNS2 and the reduced execution times of N3SIM.

4.4 Summary and Concluding Remarks

Briefly, first we define the MolComML, and we overview its objectives, elements, and functionality. In addition, we validate the N3Sim simulator by comparing its outcome with the BiNS2 simulator, as well as the theoretical one. We configured this simulation not only to prove that both simulators can execute it and generate the same results, but also that these results are homogeneous with the theoretical assumptions [67]. Therefore, we can base the neuron-to-neuron DMC network on the N3Sim simulator. Finally, we demonstrate the possibility of combining simulators, which may interact by means of intermediate MolComML files, and leverage their peculiarities for realizing an effective joint simulation.

Chapter 5

Characterize the Physical Influence of Neighboring Receivers

A Diffusion-based Molecular Communication (DMC) system is based on the free diffusion of particles that carry the message between the transmitter and the receivers. One of the main problems which lead to decreased data rates in such network is the Inter-Symbol Interference (ISI) caused by the heavy tail of the impulse response. In addition, the performance of a DMC system is crucially impacted by the reception process of the molecules.

Hence, in section 5.1, we study the influence of neighboring absorbing receivers upon the Inter-Symbol Interference (ISI) of a DMC point-to-point neuron link. However, in section 5.2, we study the influence of neighboring Adsorption and Desorption (A&D) receivers upon the achievable throughput of a DMC SIMO neuron link, and then we compare the results to a DMC SIMO neuron absorbing receivers. Lastly, the summary and the concluding remarks are shown in Section 5.3.

5.1 Influence of Neighboring Absorbing Receivers in a Point-to-Point Neuron Link

In this section, we focus on understanding the influence of neighboring absorbing receivers in the Inter Symbol Interference of a DMC point-to-point neuron link. Therefore, we first model the ISI point-to-point neighboring receivers communication link, then we perform a thorough analysis by evaluating the system performance as a function of Bit Error Rate (BER) as well as achievable throughput.

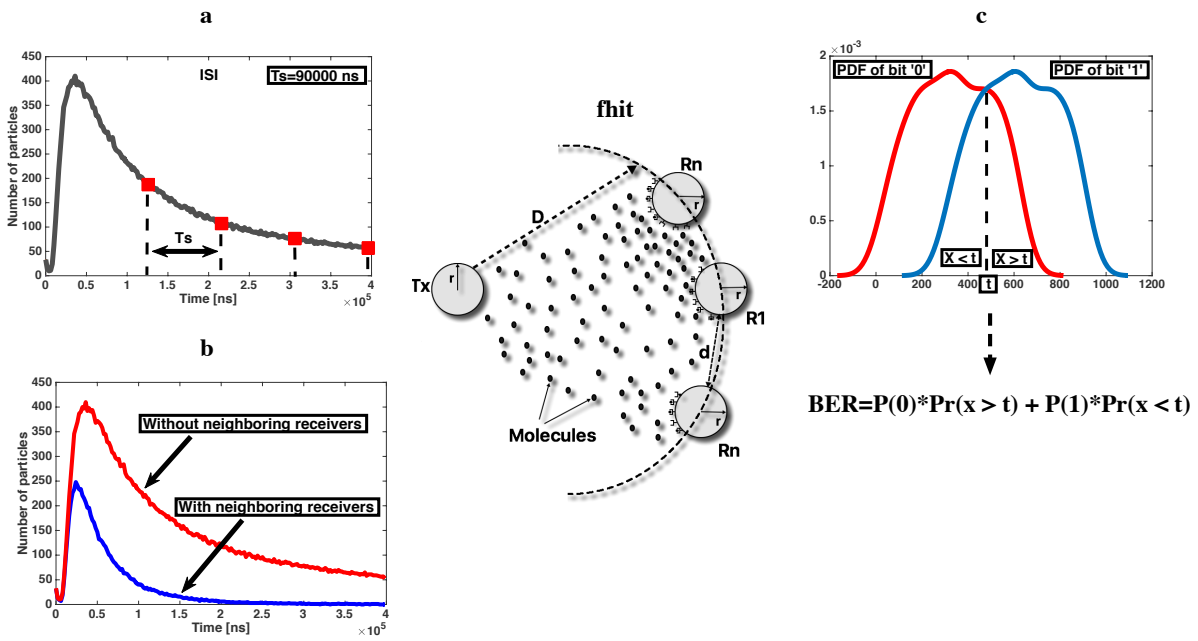

Figure 5.1: Considered point-to-point neuron Diffusion-based Molecular Communication (DMC) link with interfering neighboring absorbing receivers. (a) Shows the Inter-Symbol Interference (ISI) effect. (b) Shows the difference between the impulse responses in both cases with and without neighboring receivers. (c) Shows the Probability Density Function (PDF) of bit "0" and "1".

5.1.1 System Model

5.1.1.1 Emission and Diffusion

The MC system considered in this section is a closed system in a fluid environment (such as in human body) with one transmitter and many spherical receivers disposed on the same arc circumference, as depicted in Fig. 5.1. Molecules are used as information carriers between the transmitter and the receiver. The receivers are located at the same distance D from the transmitter and conserve a distance d between them. The radius of the receivers is expressed as r. In addition, Fig. 5.1 a) shows the effect of ISI, which will be discussed in section 5.1.1.3, Fig. 5.1 b) displays the difference in the impulse response between the two cases, which will be elaborated in section 5.1.2.1, and finally, Fig. 5.1 c) shows the Probability Density Function (PDF) of bit zero and one which will be used to calculate the achievable throughput and the BER in section 5.1.2.3.

We consider a pulse shape modulation. In DMC the digital information is modulated in a burst of molecules if the bit is "1". Otherwise, if the bit is "0" the digital information is modulated by not releasing any molecules. Therefore, the transmitter either modulates the

molecules according to an input symbol and releases a certain number of molecules at once over a time period in the medium, or it remains silent in such case the transmitter does not release any molecules. We assume that the emitted molecules are identical and indistinguishable between each other.

The molecules released by the transmitter diffuse into the medium. By neglecting the interaction among the emitted molecules [40], the dynamics of these molecules are described by Brownian motion [40] which in mathematics is described by a Wiener process as a continuous-time stochastic process. The flow of these molecules into the medium is governed by the Fick's law of diffusion. Fick's law of diffusion describes the macroscopic behavior of molecules where the concentration of molecules at any position in the medium it is given by [41]:

$$C\left(D,t\right)=\frac{Q}{\left(4\pi D_f\ t\right)^{3/2}}e^{-D^2/4D_f\ t} \tag{5.1}$$

where D_f is the diffusion coefficient of the medium, t is time, and D is the distance from the transmitter location.

5.1.1.2 Reception Process

In nature, a molecule is received by a receiver when it binds to one of the receptors on its surface. At this moment, the receiver immediately absorbs and removes the molecule from the medium through ligand-binding mechanisms [108]. Hence, after the absorption mechanism the hitting molecule cannot diffuse further and hence it contributes to the signal just once.

In this work we consider absorbing receivers that are capable of counting the number of absorbed molecules at the surface of the receivers. The number of absorbed molecules over a bit interval is then demodulated as the received signal for that bit interval, where the concentration of information molecules is interpreted as the amplitude of the signal over time.

The fraction of molecules absorbed by a molecular receiver until a time t has been derived in [79] by solving the Fick's law of diffusion with two initial boundaries while taking into consideration the absorbing process.

The hitting rate of molecules f_{hit} is calculated as

$$f_{hit}(t)=4\pi r^2 R_r p(w,t|D)=\frac{r}{D}\frac{1}{4\pi D_f t}\frac{D-r}{t}e^{-}\frac{(D-r)^2}{(4D_f t)} \tag{5.2}$$

where $p(w,t|D)$ is the molecule distribution function, t is time, w is the distance of molecules from their initial location, D is the distance between the receivers and the transmitter with radius r, and R_r is the rate of reaction.

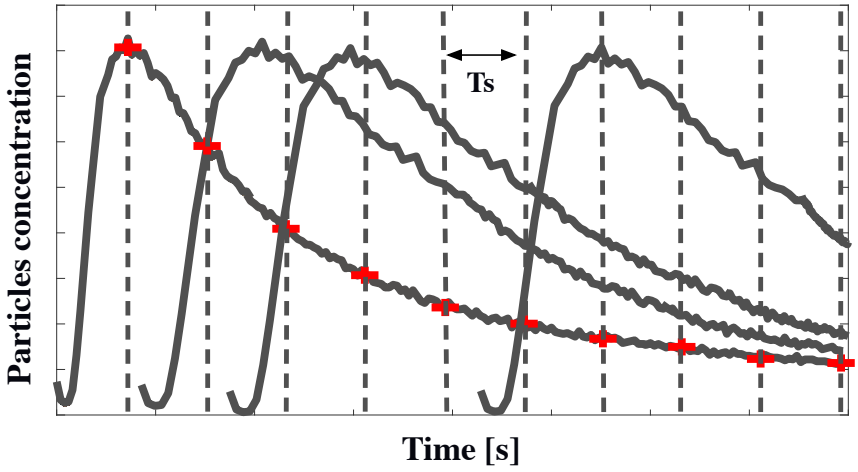

Figure 5.2: Effect of ISI encoded sequence.

Consequently, the fraction of molecules absorbed by the receiver F_{hit} until a given time t can be derived by integrating f_{hit}

$$F_{hit}(t) = \int_0^t f_{hit}(x)dx = \frac{r}{D} ercf[\frac{D-r}{\sqrt{4D_f t}}] \tag{5.3}$$

5.1.1.3 Inter-Symbol Interference (ISI)

The Inter-Symbol Interference (ISI) is calculated as the time integral of the product of two output information signals which derive from two input information signals sent from a transmitter n:

$$\int_{-\infty}^{\infty} s^i_{n,out}(t) * s^{i+1}_{n,out}(t)dt \tag{5.4}$$

where $s^i_{n,out}(t)$ is the output information signal of the MC system when the input information signal $s^i_n(t)$ is sent by the transmitter n, where i = 1, 2, ... is a sequential index.

Each number of molecules which represents one symbol sent by the transmitter is detected by the receivers in a time slot (T_s) called symbol duration. The molecules reaching the receivers in the following time slots present an interference source and lead to inaccurate decoding. Hence, ISI will increase when transmitting continuously molecules caused by the residual molecules from the previous symbols. Fig. 5.2 shows the effect of ISI across each time slot when the following binary message sequence {1,1,1,0,0,1,0,0} is used. Note that in the case of bit "1" the transmitter will diffuse molecules and in the case of bit "0" the transmitter will remain silent (no molecules will be released). Briefly, in DMC the tail of the impulse response cause the ISI even if one the signal is zero (e.g. on-off keying), since most of the molecules diffused previously into the medium take time to reach the receivers.

5.1.2 Performance Evaluation and Results

To assess the influence of the receivers upon the ISI we apply our point-to-point neuron DMC link with neighboring receivers model on the open source java simulation framework N3Sim. Therefore, we evaluate the performance of the communication via diffusion system by using neurotransmitters as the messenger molecules which diffuse in the chemical synaptic cleft to exchange information between two neurons [39]. Hence, the performance evaluation is carried out using GABA particles as the messenger molecule and, as the receiver, a device whose parameters are similar to a $GABA_A$ receptor with a fixed radius r equal to 4 nm [109]. D represents the distance of the chemical synaptic cleft and it is equal to 20 nm [39]. By disposing the receivers on the same arc circumference, the number of receivers varies from three to nineteen where d equals 1 nm. For d equals to 20 nm the number of receivers varies from three to fifteen, however, for d equals to 60 nm the number of receivers varies from three to seven. The simulation time is set to 40 μs, with a time-step of 0.2 μs. The number of released molecules is fixed to 500000 molecules. Note that the choice of the simulation parameters is in nano-metre range since the Diffusion-based Molecular Communication (DMC) is expected to be suitable for covering short distances from nanometer to micrometer (nm - μm).

Please refer to the $AppendixB$ for a short tutorial section on how to simulate SIMO Molecular Communications (MC) scenarios in N3Sim.

5.1.2.1 Impulse Response

Fig. 5.3 shows the set of the impulse responses at receiver one (R_1) with a different number of neighboring receivers (3, 7, 11, 15, and 19 receivers) where d equals to 1 nm in Fig. 5.3 a), in Fig. 5.3 b) d is equal to 20 nm and the number of neighboring receivers is equal to 3, 7, 11, and 15 receivers, lastly in Fig. 5.3 c) d is equal to 60 nm and the number of neighboring receivers is equal to 3, and 7 receivers. This set of impulse responses is compared to the ideal pulse-shape where receiver one (R_1) resides alone without any neighboring receivers. The influence of the neighboring receivers upon the pulse-shape affects first the maximum amplitude reached by the ideal case, by decreasing as the number of receiver increase. Second, the amplitude of the tail shows a significant reduction, as the number of neighboring receivers increases till it reaches zero as T_s increase. The increase of d leads to a decrease of the number of relevant receivers, hence, the amplitude of the tail as well as the maximum amplitude, thereby approaching that of the ideal impulse response case.

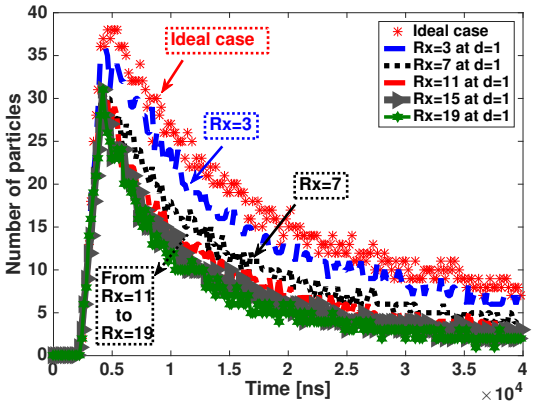

(a) d equals to 1 nm.

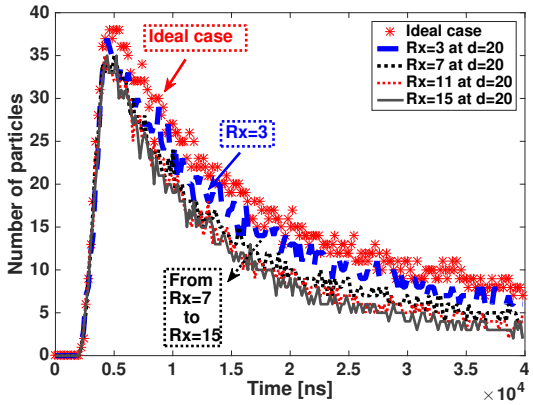

(b) d equals to 20 nm.

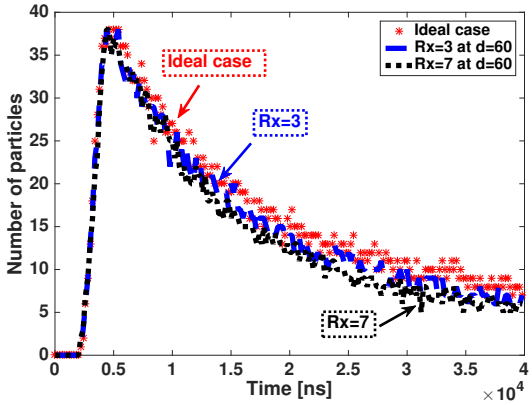

(c) d equals to 60 nm.

Figure 5.3: Set of impulse responses at receiver one R1 for different numbers of neighboring receivers where d equals to 1, 20, and 60 nm and D is fixed to 20 nm.

5.1.2.2 Normalized Amplitude, Pulse Energy and Pulse Width

In Fig. 5.4 we show the impact of the neighboring receivers as a function of amplitude, pulse energy, and pulse width on the impulse response of receiver one (R_1).

As we can see, the pulse energy and the pulse width of the detected pulse-shape decrease as the number of receivers increase for the different values of d. In particular, the pulse width and the pulse energy decrease approximately 45 % and 43 % respectively from three to nineteen receivers for the cases where d equals to 1 nm. However, the pulse width and the pulse energy decrease approximately 29 % and 22 % respectively from three to fifteen receivers for the cases where d equals to 20 nm. On the other hand, when d equals to 60 nm, the pulse width and the pulse energy decrease approximately 10 % and 6 % respectively from three to seven receivers. Besides, in the case where d equals to 1 nm, and 20 nm the amplitude of the impulse response at receiver one R_1 reaches its steady state after nine receivers even if we increase the number of receivers, since only receiver two (R_2) to receiver nine (R_9) have an impact on the maximum

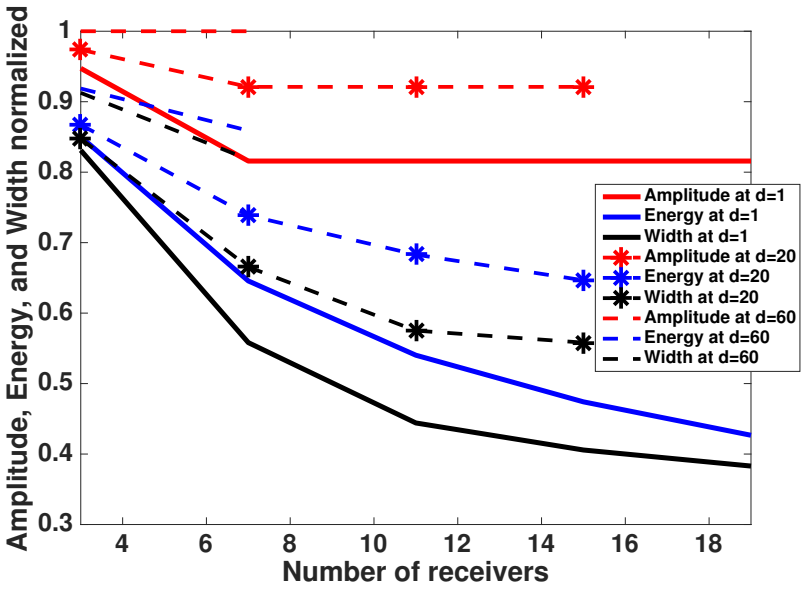

Figure 5.4: Pulse amplitude, width and energy at receiver one R_1 for different numbers of neighboring receivers where d equals to 1, 20, and 60 nm and D is fixed to 20 nm.

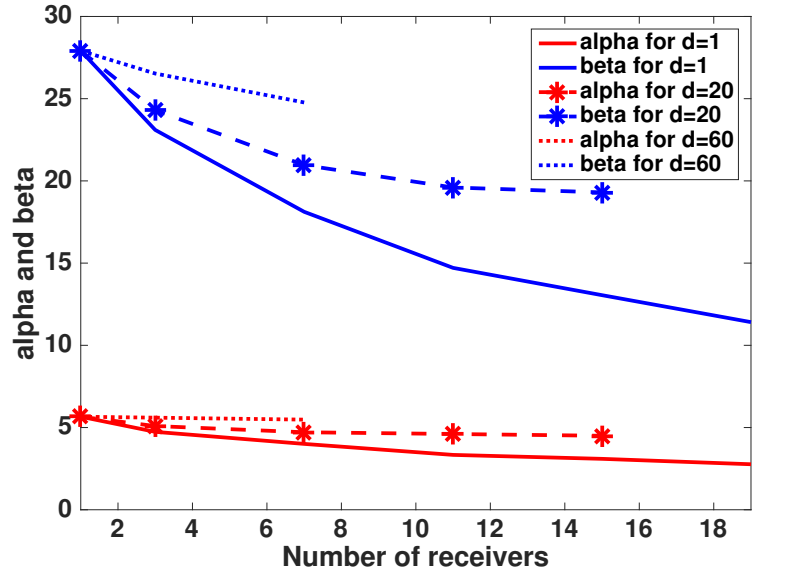

Figure 5.5: Linear model at receiver one R_1 for different numbers of neighboring receivers where d equals to 1, 20, and 60 nm and D is fixed to 20 nm.

amplitude of the impulse response at receiver one (R_1). However, in the case where d is equal to 60 nm the amplitude of the impulse response at receiver one R_1 will remain the same since the effect of neighboring receivers will diminish at this distance.

Accordingly, as d is smaller, the neighboring receivers are able to absorb more molecules in front of receiver one (R_1), hence showing a significant reduction on the pulse amplitude, pulse width and pulse energy. For fixed pulse amplitude, lower pulse energy and width imply lower pulse time and, hence, higher bit rates.

As it shown in Fig. 5.3 and 5.4, after the amplitude reaches it is maximum, the tail of the impulse response is varying as a polynomial decay when we increase the number of receivers. Fig. 5.5 shows the linear model at d equals to 1, 20, and 60 nm. First, we model the decay of the pulse by

$$\left(\frac{Q}{(t)}\right)^{\alpha} \tag{5.5}$$

where Q represents the number of molecules released and t is the time.

Then, we calculate these parameters as a logarithmic function

$$Y = \left(\frac{\beta}{(t)^{\alpha}}\right) \tag{5.6}$$

$$\log(Y) = \log(Q) - \alpha \log(t) \tag{5.7}$$

Finally, the linear model is calculated as

$$f(x) = p_1 x + p_2 \tag{5.8}$$

where α = - $p_1 10^{-4}$ and β = p_2

Therefore, by knowing the maximum reached amplitude, we can reconstruct the tail of the impulse response. Hence, by reconstructing the tails of the impulse response we calculated in section $5.1.2.3$ the achievable throughput and the BER reached at each specific case.

5.1.2.3 Achievable Throughput and BER

Fig. 5.6 displays the achievable throughput at receiver one (R_1) as a function of the number of receivers as well as a function of time slot (T_s). The achievable throughput is defined as the number of molecules that are successfully detected by the receiver node per unit of time. The time slot (T_s) is in nanoseconds. The number of receivers varies from three to nineteen where d equals to 1 nm. For d equals to 20 nm the number of receivers varies from three to fifteen,

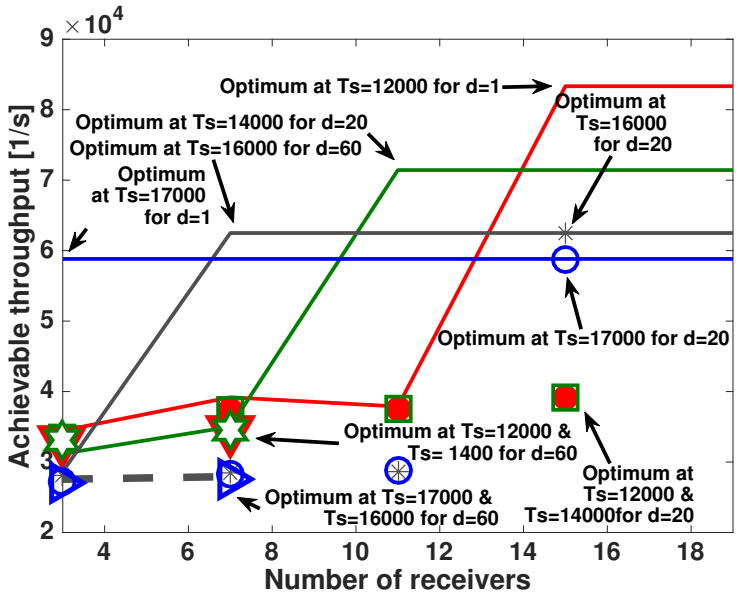

Figure 5.6: Achievable throughput as a function of number of receivers where d = 1, 20, and 60 nm. Number of receivers for d equals to 1 nm varies from 1 to 19. Number of receivers for d equals to 20 nm varies from 3 to 15. Number of receivers for d equals to 60 nm varies from 3 to 7.

however, for d equals to 60 nm the number of receivers varies from three to seven. First, the achievable throughput increases as the number of receivers increase till it reaches the optimum value for each T_s. This shows a good effect for neighboring absorbing receivers. However, no similar trend is obtained when we increase the number of receivers after the optimum values are reached, since the achievable throughput will remain the same, hence as the number of receivers increase the achievable throughput will be the same after reaching its maximum for each T_s. Second, as we can see when d is equal to 1 nm the achievable throughput reaches the maximum, since the effect of neighboring absorbing receivers at receiver one (R_1) is high at this distance d. However, no similar trend is shown when we increase d since the effect of neighboring receivers at receiver one (R_1) diminish. Therefore, as the number of neighboring receivers increase, the achievable throughput will be higher for the same T_s.

In Fig. 5.7 we illustrate the achievable throughput at receiver one (R_1) as a function of time slot (T_s) where d equals to 1 nm in Fig. 5.7 a), 20 nm in Fig. 5.7 b), and 60 nm in Fig. 4.7 c). These achievable throughputs are compared to the ideal achievable throughput where receiver one (R_1) resides alone without any neighboring receivers. First, in Fig. 5.7 a) and b) the result shows the positive influence of the neighboring receivers upon the achievable throughput. In the ideal case the optimum achievable throughput is approximately equal to 33380 bits/s however, it reaches approximately 83330 bits/s and 62500 bits/s in the case where we have fifteen

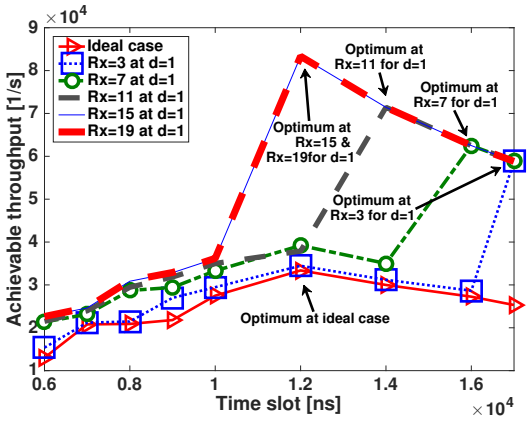

(a) d equals to 1 nm.

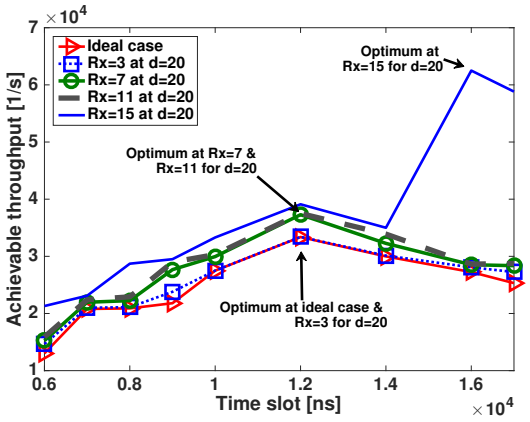

(b) d equals to 20 nm.

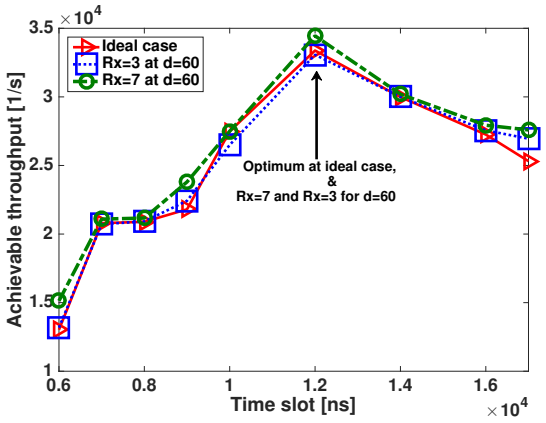

(c) d equals to 60 nm.

Figure 5.7: Achievable throughput as a function of T_s where d = 1, 20 and 60 nm. Number of receivers for d equals to 1 varies as 3, 7, 11, 15, and 19. For d equals to 20 nm the number of receivers is equal to 3, 7, 11, and 15. For d equals to 60 nm the number of receivers is equal to 3 and 7.

neighboring absorbing receivers and d equals to 1, and 20 nm respectively. However, in Fig. 5.7 c) the optimum achievable throughput is approximately the same as the ideal case. Hence, at this distance d the effect of neighboring receivers on receiver one (R_1) will become negligible. In addition, the optimum achievable throughput at seven absorbing receivers decreases from 62500 bits/s at d equals to 1 nm to 34550 bits/s at d equals to 60 nm. Therefore, as d is smaller, the influence of the neighboring receivers upon receiver one (R_1) will be stronger, which leads to a higher achievable throughput. Second, when we increase the number of T_s and after the optimum values are reached, the achievable throughput will be equal to the bit rate, hence as T_s increase the achievable throughput will decrease after reaching its maximum.

In Fig. 5.8 we show the BER as a function of Time slot (T_s) where d equals to 1 nm in Fig. 5.8 a), 20 nm in Fig. 5.8 b), and 60 nm in Fig. 5.8 c). These BER are compared to the ideal BER where (R_1) reside alone. First, the result reveals that as T_s and number of receivers increase the

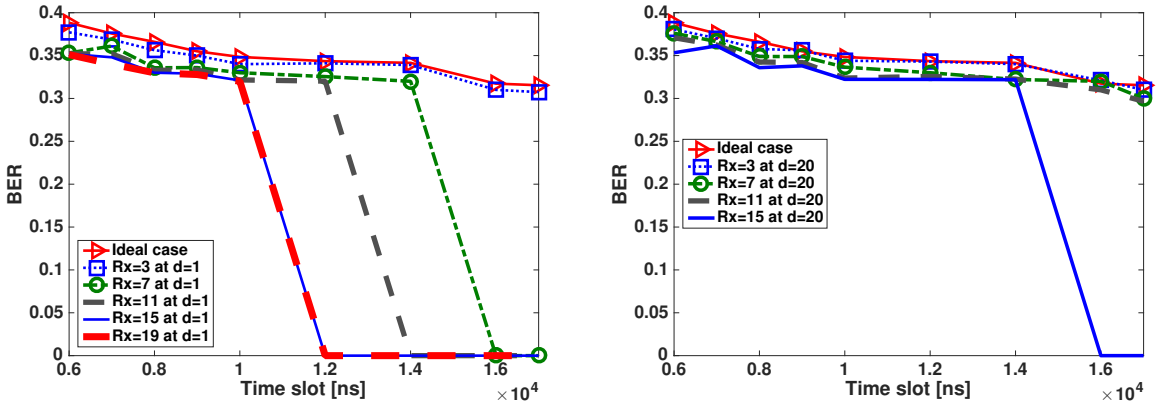

(a) d equals to 1 nm.

(b) d equals to 20 nm.

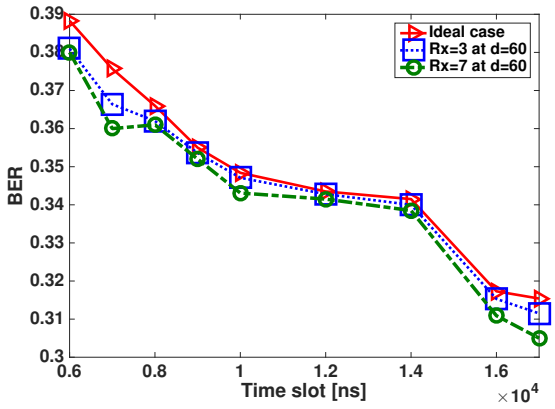

(c) d equals to 60 nm.

Figure 5.8: Bit Error Rate as a function of T_s where where d = 1, 20 and 60 nm. Number of receivers for d equals to 1 varies as 3, 7, 11, 15, and 19. For d equals to 20 nm the number of receivers is equal to 3, 7, 11, and 15. For d equals to 60 nm the number of receivers is equal to 3 and 7.

BER will decrease until it reaches zero. For example, in the case where we have fifteen receivers for d equals to 1 nm and T_s is larger than 12000 ns, the BER will be zero. Second, in Fig. 5.8 a) at fifteen absorbing receivers the BER reaches zero when T_s is larger than 12000 ns, however, in Fig. 5.8 b) the BER reaches zero at T_s larger than 16000 ns. Hence, as d is smaller the BER reaches zero at a smaller T_s. Moreover, in Fig. 5.8 c) we can see that even if we increase the number of receivers the BER will remain approximately the same as in the ideal case. Hence, at this distance d there is no effect of neighboring receivers on receiver one (R_1).

From the last two plots we see that as the tail of the impulse response goes to zero at a specific number of receivers and specific T_s, the BER will go to zero and the achievable throughput will reach its maximum. In such case, the effect of ISI in the system is canceled. Note that for a smaller d the tail of the impulse response will change steeper to zero and, hence, better achievable throughput is reached. However, as T_s increases the maximum achievable throughput

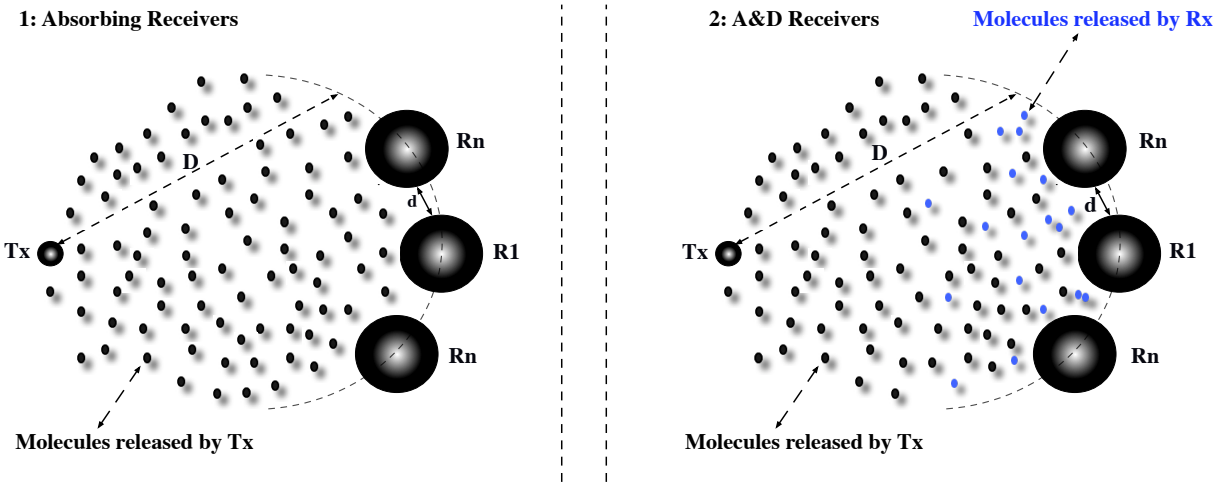

Figure 5.9: Considered Diffusion-based Molecular Communication (DMC) between: (1) SIMO with interfering neighboring absorbing spherical receivers, as well as (2) SIMO interfering neighboring A&D spherical receivers.

will decrease since we are increasing the symbol duration, which leads to inefficiency in terms of transmission rate.

5.2 Influence of Neighboring Adsorption and Desorption Receivers in a SIMO link

In this section, we model and propose a simulation framework of the Adsorption and Desorption (A&D) receiver in a Single Input Multiple Output (SIMO) DMC system that use a single molecular transmitter and multiple molecular receivers and comparing it to the SIMO absorbing receivers.

5.2.1 System Model

5.2.1.1 Emission and Diffusion

We consider a closed system in a fluid 3D environment where we have a single transmitter and multiple spherical receivers disposed on the same arc circumference while conserving a distance d between them as despite in Fig. 5.9. By having one transmitter and multiple spherical receivers this is analogous to SIMO configurations. The transmitter is a point source located at distance D from the closest point on the surface of the receivers with radius r.

We consider a pulse shape modulation, where the transmitter either releases one type of

molecules over a time period or remains silent. We assume that the emitted molecules are identical and indistinguishable from each other. The transmission of molecules through the medium occurs in time slots of equal duration; this is called the symbol duration and is denoted by T_s.

The environment is completely filled with a fluid and is discharged from flow currents. Therefore, the propagation in the environment solely depends on Brownian motion [40]; hence, the information encoded molecules which are emitted from the point transmitter diffuse through the medium where each molecule moves independently from the high concentration to the low concentration to carry the encoded information to the receivers. The flow of these molecules into the medium is governed by the Fick's law of diffusion given by equation (2.1).

5.2.1.2 Reception Process

In the reception process we use two types of spherical receivers. First, absorbing receivers as shown in Fig. 5.9 (1), where the receiver is a 3D sphere of radius r with fully absorbing boundaries. Therefore, every molecule that hits the surface of the receiver is absorbed by the receptors and removed from the communication environment through ligand-binding mechanisms [108]. Hence, the hitting rate of molecules f_{hit} is given by equation (5.2) and (5.3).

Second, A&D receivers where the receiver is a perfectly absorbing spherical receiver of radius r with a releasing rate, as illustrated in Fig. 5.9 (2). Hence, any molecules that hit the receptors of the receivers will be absorbed. However, the absorbed molecules can be released or they can remain absorbed. The releasing probability of molecules absorbed is derived in [110] where it is equal to

$$P_d = 1 - e^{-K_{off}\Delta t} \tag{5.9}$$

Where k_{off} is the desorption or releasing rate, and Δt is the simulation time step. Desorption rate k_{off} is naturally from $10^{-4}\ s^{-1}$ and $10^{4}\ s^{-1}$ [111].

For both types of receivers, the receivers are assumed to have the ability to count the number of absorbed molecules in any given time interval, in addition, all receptors on the surface of the receivers are identical and infinite where each molecule can be absorbed or released from any position on the surface, finally we ignore saturation; hence, the receivers do not show any restriction on the number of molecules absorbed by the receptors.

Moreover, the pseudo code to capture the SIMO A&D spherical receivers in N3Sim is given in Algorithm 1 where it considers the absorption and the releasing process for the signal reception. In the "for" loop after the receivers start to absorb molecules, if the desorption occurs start to compute the probability of desorption in each time step as shown in equation (5.9), afterwards, diffuse in each time step the number of molecules calculated following P_d in the environment, and finally, record the new number of absorbed molecules by the receivers.

Algorithm 1 A&D spherical receivers

```
for all the available absorbed molecules do
    if desorption arise then
        Calculate P_d                                   ▷ P_d is the releasing probability
        Diffuse the molecules that has been released in the environment
        Record the new number of molecules absorbed by the spherical receivers
    end if
end for
```

5.2.2 Performance Evaluation and Results

To perform a complete analysis of the SIMO fully absorbing spherical receivers and the SIMO A&D spherical receivers we implement the both cases in the java based simulator N3Sim.

Similarly to section 5.1, we assess the performance of the two SIMO systems by using neurotransmitters as the messenger molecules which diffuse in the chemical synaptic cleft to exchange information between neurons [39]. Hence, we adopt a set of parameters that define a virtual sample neuron used under simulation scenarios. Therefore, we use $GABA$ particles as the messenger molecule and, as the receiver, a device whose parameters are close to a $GABA_a$ receptor with a fixed radius r equal to 4 nm [109]. D represents the distance of the chemical synaptic cleft and it is equal to 20 nm [39]. In addition, we disposed the receivers on the same arc circumference. The number of receivers varies from three to nine where d equals 1 nm, 5 nm, and 20 nm, therefore, the effect of the absorbing and A&D spherical receivers on each others could be shown. The simulation time is set to 10 μs, with a time-step of 0.1 μs. The number of released molecules is fixed to 10000 molecules with a zero initial particles, and k_{off} is 40 s^{-1} [112].

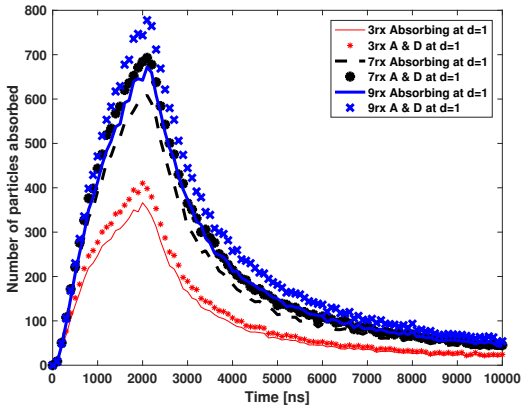

(a) d equals to 1 nm.

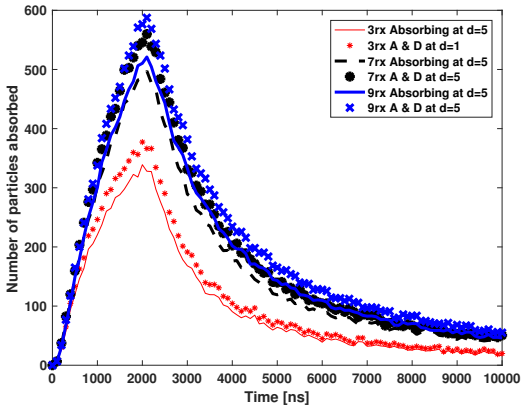

(b) d equals to 5 nm.

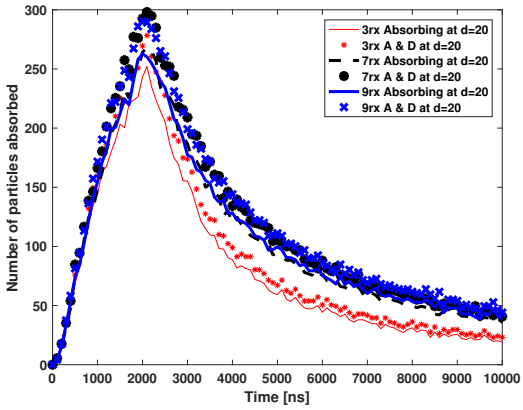

(c) d equals to 20 nm.

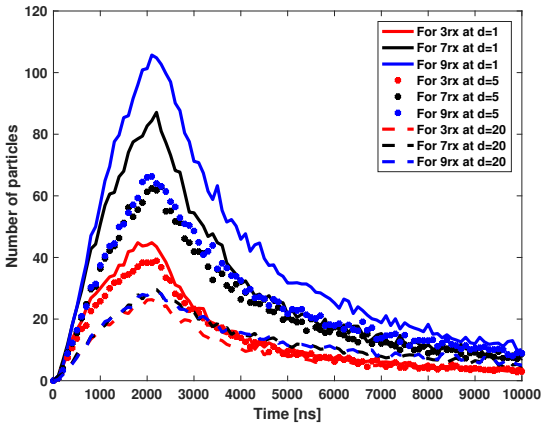

(d) Difference.

Figure 5.10: Set of impulse responses at SIMO absorbing receivers and SIMO A&D receivers for different numbers of receivers where d equals to 1, 5, and 20 nm and D is fixed to 20 nm with A&D pulse shape minus Absorbing pulse shape.

5.2.2.1 Impulse Response

To compare the impulse response of the two systems mentioned above, Fig. 5.10 displays the set of the impulse responses for SIMO absorbing and SIMO A&D receivers with various number of receivers where d takes different values as follow Fig. 5.10 a) d is equal to 1 nm, Fig. 5.10 b) d is equal to 5 nm, and finally, Fig. 5.10 c) d is equal to 20 nm. Furthermore, Fig. 5.10 d) shows the difference between the A&D pulse shapes and the absorbing pulse shapes for different values of d.

Fig. 5.10 a) and b) displays the influence of the neighboring A&D receivers upon the pulse-shape comparing it to the shape of the SIMO impulse responses. The maximum amplitude reached as well as the amplitude of the tail increase as the number of receivers increases in the case where we deploy A&D receivers. However, Fig. 5.10 c) shows the decrease in the maximum

amplitude reached and in the amplitude of the tail when we increase d, whereas we can see the difference between the pulse-shape of the A&D receivers and the absorbing receivers will be small. Moreover, Fig. 5.10 d) displays the new number of particles that have been absorbed by the receivers when we use A&D receivers. These new particles have been diffused in the environments by the receivers. As we can see the number of particles will increase as the number of receivers increase, however, as d increase the maximum number of particles will decrease. For example, in the case where we have nine receivers when d is equal to 1 nm the maximum number of absorbed particles is equal to 105 particles, nevertheless, the maximum number of absorbed particles will decrease dramatically to reach 28 particles where d is equal to 20 nm. Hence, in this particular case the maximum number of particles absorbed decreases around 73% while increasing d from 1 nm to 20 nm.

Hence, increasing the number of A&D receivers leads to an increase in the maximum amplitude reached as well as an increase on the tail of the pulse-shape comparing to the pulse-shape of absorbing receivers, nevertheless by increasing d the maximum amplitude reached and the amplitude of the tail regarding the A&D receivers will diminish, thereby approaching that to the SIMO absorbing receivers pulse-shape case since the effect of the neighboring A&D receiver on each other will degrade.

5.2.2.2 Pulse Amplitude, Pulse Energy, and Pulse Width

Fig. 5.11 presents the maximum amplitude, pulse width, and pulse energy for the SIMO absorbing receivers and SIMO A&D receivers while taking into consideration different distance d, as well as a different number of receivers. Therefore, Fig. 5.1 shows the impact of the neighboring A&D receivers as a function of amplitude, pulse energy, and pulse width on the impulse response comparing to the neighboring absorbing receivers. Accordingly, Fig. 5.11 a) shows the maximum amplitude reached, Fig. 5.11 b) appeals the pulse energy, and finally, Fig. 5.11 c) depicts the pulse width.

As we can see, first, there is a significant difference in the maximum amplitude between the case where we have absorbing receivers and A&D receivers while tweaking the number of receivers, and d. Mainly, for d equals to 1 nm, 5 nm, and 20 nm the difference between the maximum amplitude reached of the absorbing receivers and A&D receivers at nine receivers is respectively equal to 105 molecules, 66 molecules, and 28 molecules. Therefore, as d increases the effect of the neighboring A&D receivers on the maximum amplitude will diminish. This

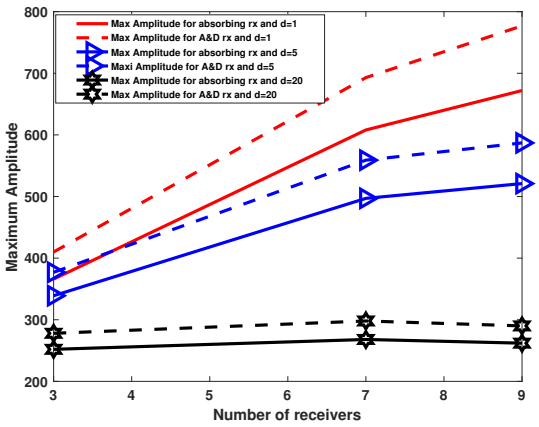

(a) Maximum Amplitude.

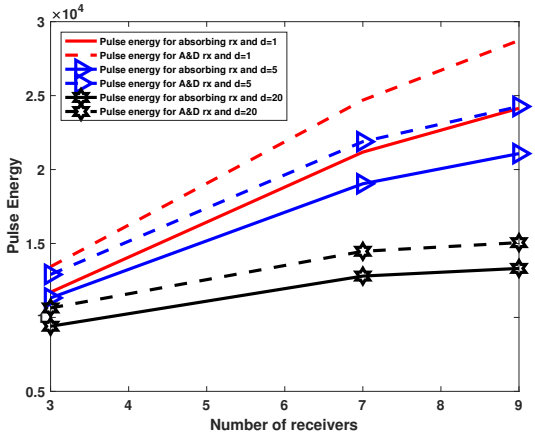

(b) Pulse Energy.

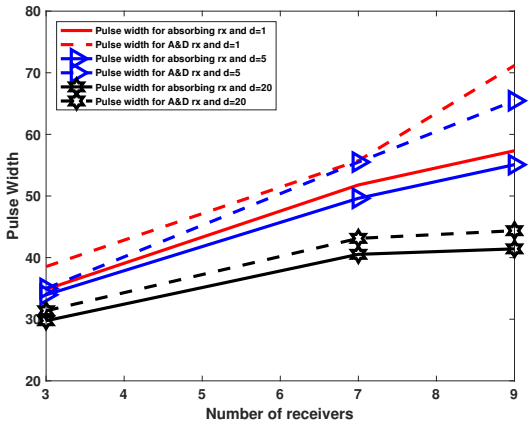

(c) Pulse Width.

Figure 5.11: Pulse amplitude, energy and width at SIMO absorbing receivers and SIMO A&D receivers for different numbers of receivers where d equals to 1, 5, and 20 nm and D is fixed to 20 nm.

is due to the small amount of molecules absorbed again by the A&D receivers receivers while using a higher value of d. Hence, as d is bigger, the maximum amplitude reached by the A&D receivers will be approximately equal to to the case where we deploy absorbing receivers.

Second, the pulse energy and the pulse width of the detected pulse shape for the two cases increase as the number of receivers increase. However, the difference between the neighboring A&D receivers and the absorbing neighboring receivers on the pulse energy as well as the pulse width is summarized as follow; as d increases the area found between the pulse energy and the pulse width of the two different receivers (absorbing receivers and A&D receivers) will decrease even if we increase the number of receivers.

In particular, for d equal to 1 nm the difference between the absorbing receivers and A&D receivers of the pulse energy increase approximately 17% and 20% respectively from seven to

nine receivers; however, at d equal to 20 nm the difference between the absorbing receivers and A&D receivers of the pulse energy will remain the same and it is approximately equal to 12%. Moreover, for d equals to 1 nm the difference between the absorbing receivers and A&D receivers of the pulse width increase approximately 8% and 24% respectively from seven to nine receivers; nonetheless, at d equals to 20 nm the difference between the absorbing receivers and A&D receivers of the pulse width will remain the same and it is approximately equal to 1%.

Finally, as d increases, the pulse energy and the pulse width does not show any significant change between the both different receivers even if we increase the number of receivers. Therefore, at this distance d the effect of neighboring A&D receivers on each other will diminish (the released molecules after absorption from a receiver will not be absorbed by the others receivers), hence, lower pulse energy and width will be reached which lead to a higher bit rates.

5.2.2.3 Achievable Throughput

Fig. 5.12 illustrates the achievable throughput of the SIMO absorbing receivers and of the SIMO A&D receivers as a function of a time slot (T_s) where d equals to 1 nm in Fig. 5.12 a), 5 nm in Fig. 5.12 b), and 20 nm in Fig. 5.12 c).

First, Fig. 5.12 a), b), and c) shows that for the both receivers used, the optimum achievable throughput is higher as we increase d. In particular, the difference between the optimum throughput reached at three absorbing and A&D receivers while d equals to 1 nm and 20 nm is around 15%. Moreover, not to mention that more molecules will be absorbed while we increase the number of receivers, hence, for each value of d the maximum achievable throughput decrease as the numbers of receivers increase.

Second, in Fig. 5.12 a), and b) the result shows the negative influence of the neighboring A&D receivers upon the achievable throughput comparing to neighboring absorbing receivers. Hence, when we deploy absorbing receivers the maximum achievable throughput reached is higher then the maximum achievable throughput reached by using A&D receivers. For example, for d equals to 1 nm the optimum achievable throughput at seven absorbing receivers is equal to 1.25×10^5 bits/s, yet, for seven A&D receivers the maximum achievable throughput is equal to 1.111×10^5 bits/s. However, as depicted in Fig. 5.12 c) the effect of neighboring A&D receivers diminishes as d increases, hence, the optimum achievable throughput for the both receivers deployed is the same even if we increase the number of receivers.

Finally, as the number of A&D receivers increase and d is small, the influence of these

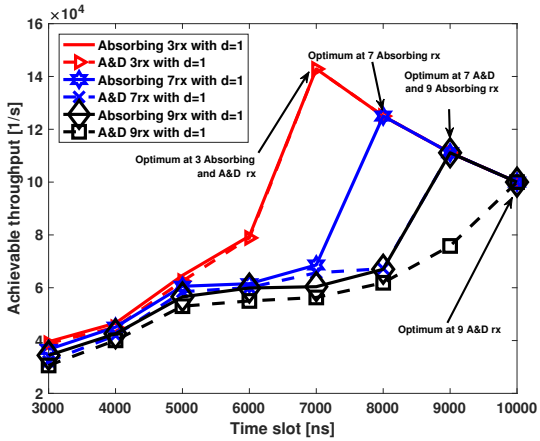

(a) d equals to 1 nm.

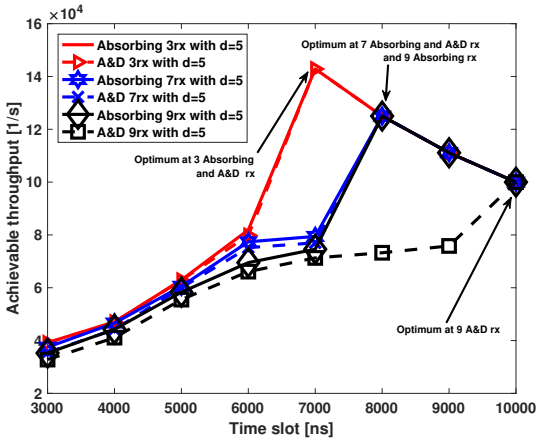

(b) d equals to 5 nm.

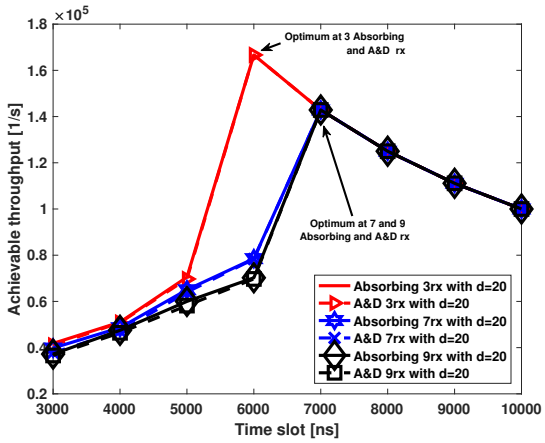

(c) d equals to 20 nm.

Figure 5.12: Achievable throughput as a function of Ts at SIMO absorbing receivers and SIMO A&D receivers for different number of receivers where d equal to 1, 5 and 20 nm.

receivers on each other increases, therefore, lower achievable throughput will be reached. Nevertheless, while we increase d the effect of neighboring A&D receivers diminishes, hence, the maximum achievable throughput reached is equal to the case where we deploy absorbing receivers.

5.3 Summary and Concluding Remarks

In section 5.1 a simplified MC synthetic scenario valuable for a design space exploration, yet representative of practical deployments where the position of each receiver is on the same arc circumference is studied. It shown that the optimal number of neighboring absorbing receivers and the optimal distance d between the receivers leads first to a steady state in the maximum amplitude of the impulse response and cancel the effect of ISI by reducing the amplitude of

the tail. Therefore, in such case lower BER as well as a higher achievable throughput will be reached.

However, in section 5.2, we studied the negative influence of a SIMO A&D neighboring receivers on the achievable throughput while comparing it to the case of the SIMO absorbing neighboring receivers. By modifying and using the particle-based simulators N3Sim, it shown that the effect of neighboring A&D receivers diminishes as we increase d, since after desorption and diffusion occur, the new absorbing molecules by the A&D receivers will be smaller as d increase. The optimal distance between the A&D receivers leads to a higher achievable throughput, hence, at this distance the achievable throughput of the A&D receivers will be equal to the achievable throughput of the SIMO absorbing receivers, consequently, the effect of ISI will decrease. Moreover, absorbing receivers, and A&D receivers can be used to model different types of artificial biological MC process to come up with new medical treatment. For example, in Parkinson's Disease (PD), or Alzheimer's Disease (AD) we can use an artificial neuron-to-neuron system, to compensate the degeneration of neurons, while deploying absorbing receivers. However, in the case of Huntington's Disease (HD), where a genetic mutation causes over-production of a neurotransmitter, we can use an artificial neuron-to-neuron system while deploying A&D receivers since a low achievable throughput is needed.

Chapter 6

Closed-loop Serotonin Control in Glutamatergic Synapses Through Diffusion-based Molecular Communication Characterization Aiming Alzheimer's Disease Treatment

This Chapter characterizes the effect of increasing the toxic Amyloid Beta ($A\beta eta$) on the excitatory glutamatergic synapses. In addition, this chapter presents a closed-loop control approach to control the concentration of serotonin doses depending on the number of $A\beta eta$ proteins residing and surrounding the synaptic cleft while taking advantage of using optogenetics technology.

Therefore, section 6.1 describes the cause of Alzheimer's Disease (AD), and the different technologies used to address brain disorders. In addition, section 6.2, 6.3, and 6.4 focus on understanding, modeling, and characterizing through simulation the DMC physical channel of the excitatory glutamatergic synapses between glutamate vesicles and AMPA receptors, and therefore quantifying the communication channel by altering the number of $A\beta eta$ which will impair the channel. Section 6.5 presents a complete sense-actuation closed-loop system to control the concentration of serotonin doses which is determined by the number of $A\beta eta$, while benefiting from the advantages of using optogenetics technology. Lastly, the summary and the concluding remarks are shown in section 6.6.

6.1 Cause of Alzheimer's Disease

Beside neurotransmitters, neurons also release a small peptide called Amyloid Beta ($A\beta eta$). $A\beta eta$ are formed when a protein called Amyloid Precursor Protein (APP) is sequentially split by two enzymes: Beta-secretase, and Gamma-secretase. Normally $A\beta eta$ is cleared away and metabolized by microglia.

Accumulation of $A\beta eta$ within the brain is the main event which initiates AD. $A\beta eta$ starts accumulating in the synapse. Thus, the synapse begins to accumulate plaques, which are deposits of a peptide called $A\beta eta$, and are insoluble. It takes at least 15 to 20 years of $A\beta eta$ accumulation before it reaches a tipping point. When it reaches the tipping point our microglia start to clean the synapse by themselves.

While drugs are being developed to target $A\beta eta$, it is unclear whether this method will eventually be successful in targeting the disease. Some studies have demonstrated that the activation of serotonin neurotransmitters will be beneficial in confronting AD [113].

Serotonin is produced in specialized neurons found mostly in the upper raphe nucleus and the caudal raphe nucleus located along the middle line of the brain stem. Since the axons of serotonin neurons reach almost every part of the nervous system and the spinal cord, serotonin neurons provide serotonin to the rest of the nervous system through serotonergic pathways. In addition, serotonin is synthesized from the amino acid tryptophan and is stored in small vesicles within the nerve terminal. When a serotonergic neuron is stimulated, serotonin is released into the synaptic cleft, where it binds with, and activates, serotonin receptors on the post-synaptic neuron. Finally, serotonin action is terminated via the disengaging of its molecules from the synaptic cleft through a protein called serotonin transporter.

Nowadays, to fight Alzheimer's disease the doctors are prescribing Selective Serotonin Re-uptake Inhibitors (SSRI) drugs. The drugs block the re-absorption of serotonin by the transmitter neurons which lead to increase in the levels of serotonin in the synaptic space which will reduce the production of $A\beta eta$ [113, 114].

However, at the present, three different technologies for addressing brain disorders are used. These technologies are as follows: pharmaceuticals which have been notably ineffective and manifest side effects, electrical simulation where electricity is used to target cell and cluster of cells, however in this process the electricity will go in all directions so all nearby cells will be affected, and finally, optogenetics which is an approach in which it is possible to locally activate with light a given cell of cell cluster without perturbing its neighbors.

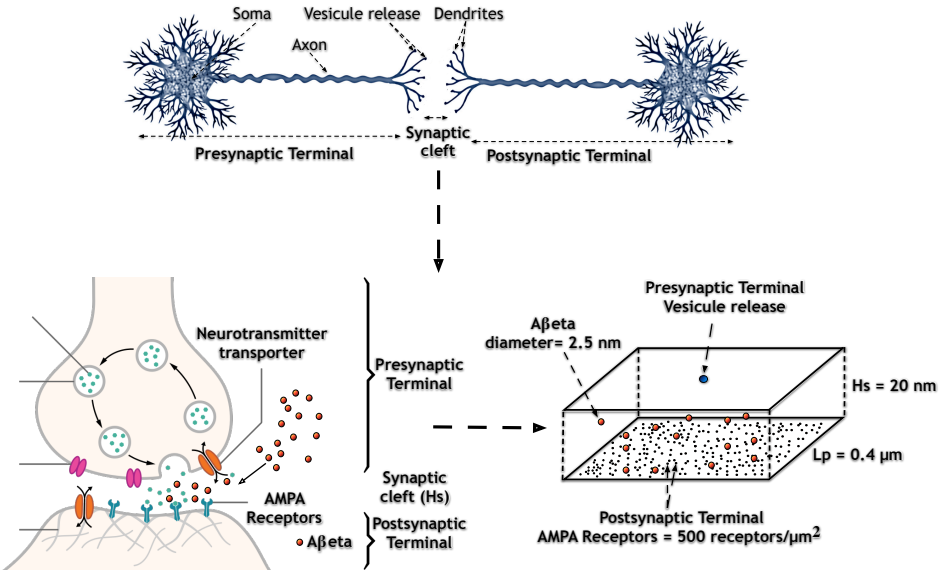

Figure 6.1: Biological structure and behavioural approximated model.

Optogenetics refers to the integration of optics and genetics to achieve gain or loss of function of well defined events with specific cells of living tissue [115]. Hence, in optogenetics, we can target just one neuron. Consequently, the target neuron is controllable now with light without affecting the neighbor neurons which are molecules that sense light and can convert the light into electrical signals. We target this neuron by using reagents which come from nature (as bacteria, plants). By knowing the DNA sequences of these reagents we produce the proteins which will be injected into a little virus and inserted it into the target cell to make it sensitive to, and controllable with, light. Therefore, in our work we consider the use of optogenetics technology since it allows us to be more specific and minimize the effect associated with the other two techniques.

6.2 Glutamatergic Synapses Between Glutamate Vesicles and AMPA Receptors Model

By way of specificity, to compare the accumulated molecules absorbed by AMPA receptors for different network topologies and to inspect the effect of $A\beta eta$ on the communication between neurons in the following sections, we have performed our study based on a simplified model of an excitatory glutamatergic synapses in which the vesicle release diffuses glutamate into the synapse and the AMPA receptors sense and collect these neurotransmitters. Hence, we model the synaptic cleft as a rectangular box with height H_s. For simplicity, as Fig. 6.1 shows, we

assumed that the shapes of neighboring cells were polyhedra, and we represented presynaptic cell membranes as a box-shaped structure that enclosed the pre- and post-synaptic elements [116]. Therefore, the top and the bottom planes of the box represent the presynaptic and postsynaptic membranes of the glutamatergic synapses, respectively, with fully absorbed AMPA receptors.

After vesicle release, the glutamate will diffuse freely into the synaptic cleft to reach the AMPA receptors where they bind. By cause of neglecting the interaction among the emitted molecules, and provided that there is no flux boundary conditions where the neurotransmitters are reflected into the synaptic cleft [40], then the distribution function of the neurotransmitters at any given time is represented by free diffusion with initial distribution taken as a sum of all reflection plus original source, and it is expressed as follows [117],

$$C_n(x,y,z,t) = \frac{Q}{(\sqrt{4\pi D_f t})^3} e^{\frac{(-x^2-y^2)}{4D_f t}} \left[2 \sum_{k=-\infty}^{\infty} e^{\frac{-(2-(2k+1)H_s)^2}{4D_f t}} \right] \tag{6.1}$$

where Q represents the number of molecules released, D_f denotes the diffusion coefficient, H_s the distance of the synaptic cleft, and t the time.

We performed our study by using N3Sim simulator. Moreover, Table I presents the set of parameters that we adopt to define a 3-dimensional (3D) virtual system composed of glutamatergic synapses between glutamate vesicles and AMPA receptors, with or without $A\beta eta$ used under simulation scenarios. The simulation time is set to 80 μs, with a time-step of 0.1 μs. The number of released molecules is equal to the number of glutamate in one vesicle which is fixed and equal to 3000 [118]. Additionally, the diffusion coefficient (D_f) in the glutamatergic synaptic cleft is fixed at 0.33 $\mu m^2/ms$ [119]. The number of AMPA receptors is fixed to eighty, and they are randomly deployed; accordingly, this corresponds to a receptor density of 500 receptors per μm^2 (80/L_p^2). Finally, The 3-D structure of $A\beta eta$ (1-42) in [120], shows that the diameter of the $A\beta eta$ sphere is equal to 2.5 nm. Lastly, the number of simulation performed for each case study is equal to 20 where the results presented are the average of these simulations.

6.3 Effect of Glutamatergic Neurons on Each Other

To compare the accumulated molecules absorbed by AMPA receptors for different network topologies, we implement the different cases in the java based simulator N3Sim. Hence, we

Table 6.1: Simulation Parameters

Name	Symbol	Number
Height of the synaptic cleft	H_s	20 nm [121]
Number of glutamate in 1 vesicle	Q	3000 [118]
Diffusion coefficient	D_f	0.33 $\mu m^2/ms$ [119]
Side length of the box	L_p	0.4 μm [116]
Receptors density	R_d	500-300/μm^2 [116]
Numbers of AMPA Receptors	N_{AMPA}	R_d x L_p^2
Sphere diameter of $A\beta eta$	$D_{A\beta eta}$	2.5 nm [120]
Numbers of simulation	N_s	20

implement three glutamatergic neurons with glutamate vesicles and AMPA receptors while maintaining a distance of d between them.

In Fig. 6.2 a), and b), we illustrate the accumulated and the total absorbed molecules by AMPA receptors for each neuron, where d equal to 0.5 μm, 1 μm, and 2 μm. As we can see in Fig. 6.2 a), the accumulated absorbed molecules for each neuron does not show any significant change even if we decrease the distance between the three neurons. Hence, the accumulated absorbed molecules for the three neurons with different distances between them is approximately the same of the accumulated molecules of one neuron. Similarly, in Fig. 6.2 b), a situation where we have one neuron and the total molecules absorbed is approximately equal to 2320 molecules is the ideal case. For d equal to 0.5 μm, and 2 μm the difference between the total molecules absorbed is approximately equal to 1 % for neuron one, 3.2 % for neuron two, and 3 % for neuron three. Hence, the total molecules absorbed will remain approximately the same for different distance d.

Moreover, Fig. 6.2 c) represents the accumulated absorbed molecules for the three neurons with d equal to 0.5 μm, 1 μm, and 2 μm, as well as the accumulated molecules of neuron one, times the number of neurons deployed (in our case the number of neurons used is equal to three). As we can see the accumulated absorbed molecules do not display any diversity even in the total amount of molecules absorbed. Therefore, the accumulated number of absorbed molecules can be derived through multiplying the number of neurons deployed by equation (5.1). Hence, the accumulated number of absorbed molecules can be well approximated as,

$$A_{(N)} = N \int_{-\infty}^{\infty} \int_{-\infty}^{\infty} \int_{-\infty}^{\infty} C_n(x, y, z, t) dx dy dz \tag{6.2}$$

where N is the number of neurons used.

Accordingly, in our future thorough analysis we will study the case of one neuron, since, as demonstrated, the effect of neurons on each other do not impact the total amount of molecules

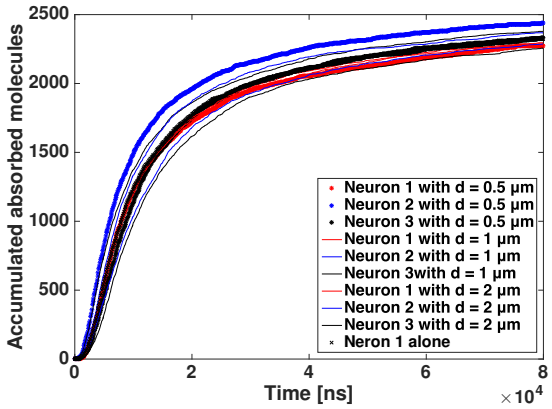

(a) Accumulated molecules for each neuron where d equals to 0.5 μm, 1 μm, and 2 μm.

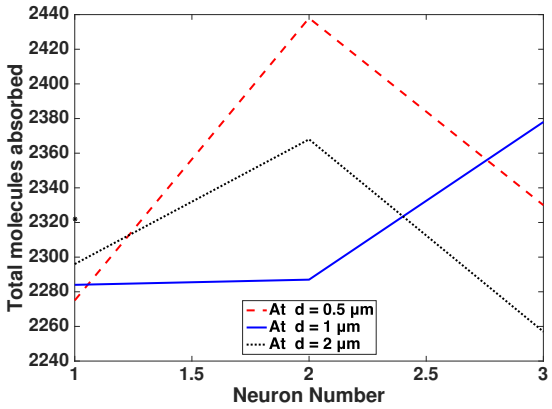

(b) Total molecules absorbed for each neuron where d equals to 0.5 μm, 1 μm, and 2 μm.

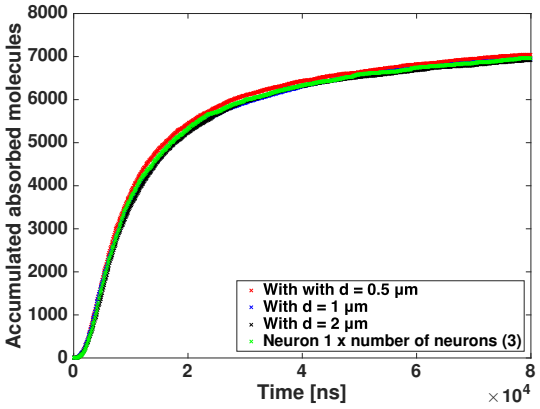

(c) Accumulated absorbed molecules for the three neurons with d equals to 0.5 μm, 1 μm, and 2 μm, and the accumulated molecules of neuron 1 times the number of neurons used.

Figure 6.2: Effect of glutamatergic neurons on each others.

absorbed.

6.4 Problem Statement: Accumulation of the Toxic Amyloid Beta Protein

Aggregation of $A\beta eta$ as toxic oligomers within the brain turn out to be the main reason behind Alzheimer's Disease (AD). To check the effect of the aggregation of $A\beta eta$ on the brain, we modeled a glutamatergic synaptic neuron with glutamate vesicle and AMPA receptors, coupled with $A\beta eta$ surrounding and adjacent to the synaptic cleft. Hence, Fig. 6.3 a) and b) shows the effect of $A\beta eta$ over the accumulated absorbed molecules by AMPA receptors, whereas $A\beta eta$ increases the total absorbed molecules by AMPA receptors decrease. Or, more precisely,

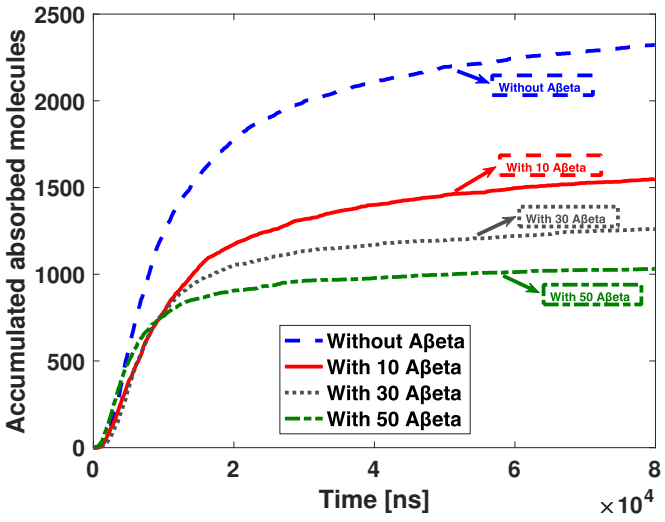

(a) Accumulated molecules absorbed by AMPA receptors with $A\beta eta$.

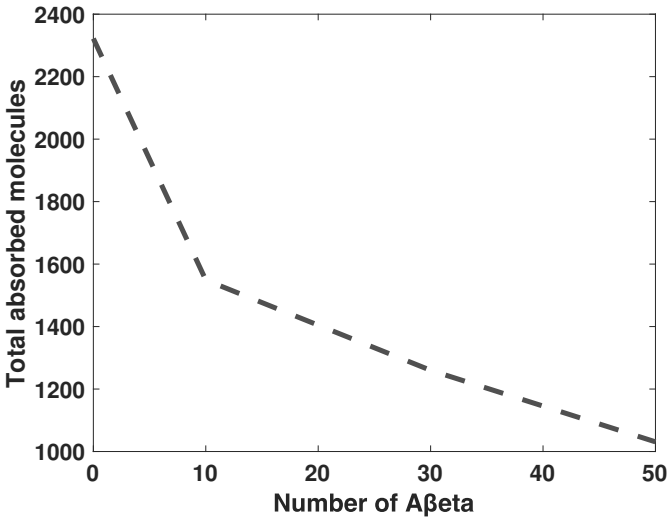

(b) Total absorbed molecules by AMPA receptors whith $A\beta eta$.

Figure 6.3: Effect of $A\beta eta$ on the physical channel.

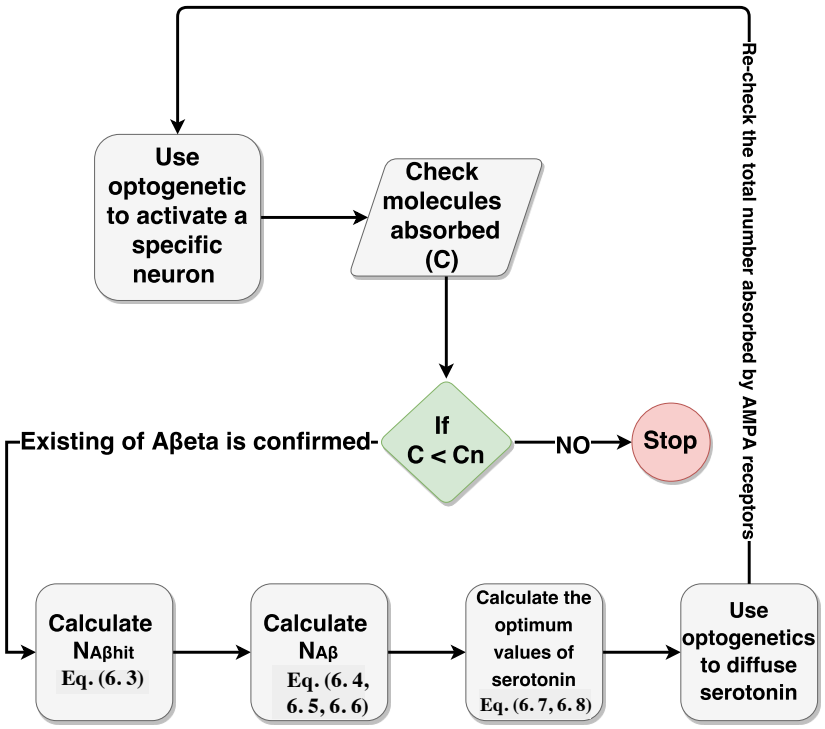

Figure 6.4: Loop control approach.

a decrease of roughly 56 % of the total absorbed molecules when $A\beta eta$ does not exist compared to fifty toxic $A\beta eta$ proteins occurring into the synaptic cleft. Note also that the characteristics in Fig. 6.3 b) show a monotonic behaviour thereby potentially allowing a stable quasi-static closed-loop operation. Thus, the accretion of the toxic $A\beta eta$ leads to a loss of communication between the pre- and postsynaptic neuron, since the diffused neurotransmitters will reach the AMPA receptors in small amounts compared to the normal case where there is no $A\beta eta$ in the synaptic cleft.

Unfortunately, it has been found that the activation of serotonergic neurotransmitters will decrease the number of the toxic $A\beta eta$ [114]. At the present time, the doctors prescribe Selective Serotonin Re-uptake Inhibitors (SSRI) drugs to block the re-absorption of serotonin and reduce the production of $A\beta eta$ [113, 114]. However, this method has been inadequate because it affects all the brain. Consequently, since the failure in communication between the the pre- and post-synaptic neuron allows an indirect measure of $A\beta eta$ concentration and the results show a monotonic behavior thereby in the following section we propose a new closed-loop system vision to regulate the concentration of serotonin doses depending on the number of $A\beta eta$ while benefiting from the advantages of using optogenetics technology.

6.5 Loop Control Approach and Results

For a proper understanding, and analyses of the system under different conditions, the proposed loop control approach for regulation of serotonin concentration is divided into eight steps as Fig. 6.4 shows. These steps are summarized as follows:

1. Use of optogenetics technology and checking the total number of molecules absorbed by AMPA receptors: First, we use the optogenetics technology to activate the specific neuron under investigation. After the activation of this neuron, we need to check the total number of molecules absorbed by AMPA receptors (C). If $C < C_n$, where C_n is the normal total number of molecules absorbed by AMPA receptors, the existence of $A\beta eta$ surrounding and adjacent to the synaptic cleft is confirmed; otherwise, no need to diffuse serotonin neurotransmitters. In the latter event, we check other neurons.

2. Calculate the expected number of molecules hitting $A\beta eta$: In case where $C < C_n$, we can calculate the expected number of molecules (glutamate) hitting the toxic $A\beta eta$ proteins ($N_{A\beta hit}$) as follows [122]:

$$N_{A\beta hit} = C_n - C \tag{6.3}$$

3. Compute the number of $A\beta eta$: In addition, the expected number of molecules hitting $A\beta eta$ ($N_{A\beta hit}$) in the interval [t_1;t_2] is given as follow [122],

$$\mathbb{E}[N_{A\beta hit}(t_1, t_2)] = QF_{hit}^{r_{A\beta}, N_{A\beta}} \tag{6.4}$$

where

$$F_{hit}^{r_{A\beta}, N_{A\beta}}(t_1, t_2) = F_{hit}^{r_{A\beta}, N_{A\beta}}(t_2) - F_{hit}^{r_{A\beta}, N_{A\beta}}(t_1) \tag{6.5}$$

and,

$$\begin{aligned} F_{hit}^{r_{A\beta}, N_{A\beta}}(t) = \frac{r_r}{r_v} \frac{r_{A\beta} N_{A\beta}}{r_{A\beta} N_{A\beta} + \pi r_r} (1 + erf[\frac{r_r - r_v}{\sqrt{4D_f t}}] \\ - exp[(r_v - r_r)(\frac{N_{A\beta} r_{A\beta} + \pi r_r}{\pi r_r^2}) \\ + D_f t (\frac{N_{A\beta} r_{A\beta} + \pi r_r}{\pi r_r^2})^2] \\ erfc \left[\frac{r_v - r_r + 2D_f t (\frac{N_{A\beta} r_{A\beta} + \pi r_r}{\pi r_r^2})}{\sqrt{4D_f t}} \right]) \end{aligned} \tag{6.6}$$

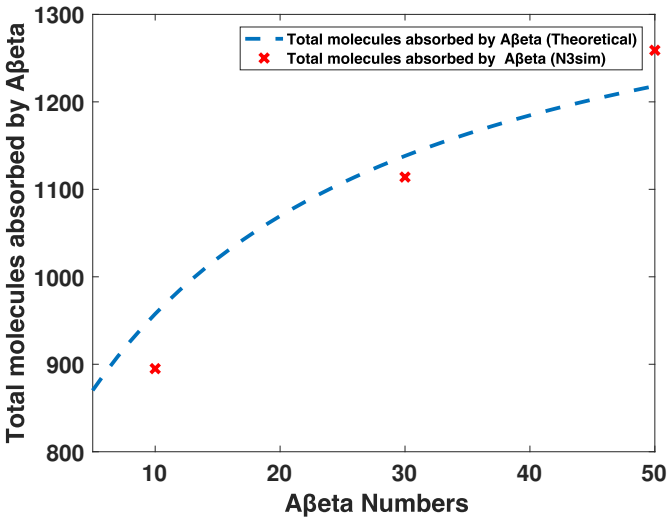

(a) Theoretical values vs N3Sim values.

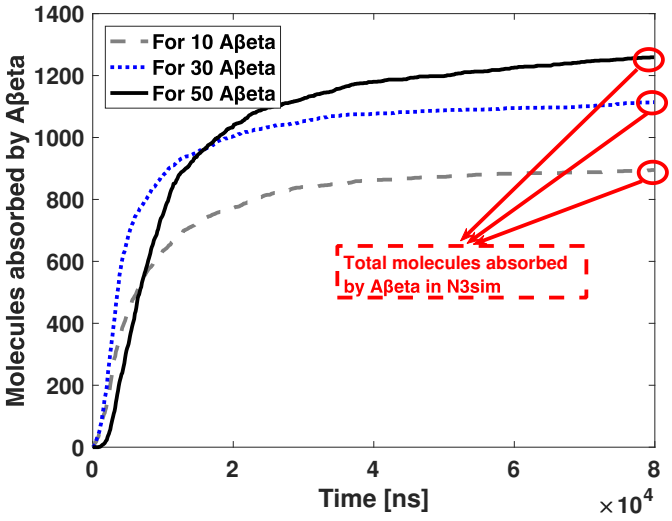

(b) N3Sim values.

Figure 6.5: Theoretical values and N3Sim values.

where $r_{A\beta}$ is the radius of $A\beta eta$, and r_r is the radius of sphere where $A\beta eta$ reside.

By knowing the $N_{A\beta hit}$, we are able to compute the number of $A\beta eta$ ($N_{A\beta}$) residing and surrounding the synaptic cleft from equation (6.4), (6.5), and (6.6). Precisely, we modeled a spherical receiver where $A\beta eta$ has a circular areas over a receiver surface. The receiver occupies the area of the synaptic cleft; however, $A\beta eta$ acts as a receptor on this receiver. The diffusive neurotransmitter is absorbed by the receiver only when it hits receptors.

To verify if the number of $A\beta eta$ ($N_{A\beta}$) can be derived from the expected number of molecules hitting $A\beta eta$ ($N_{A\beta hit}$), we modeled a glutamatergic synaptic neuron with eighty AMPA receptors, coupled with different concentrations of $A\beta eta$ in the synaptic

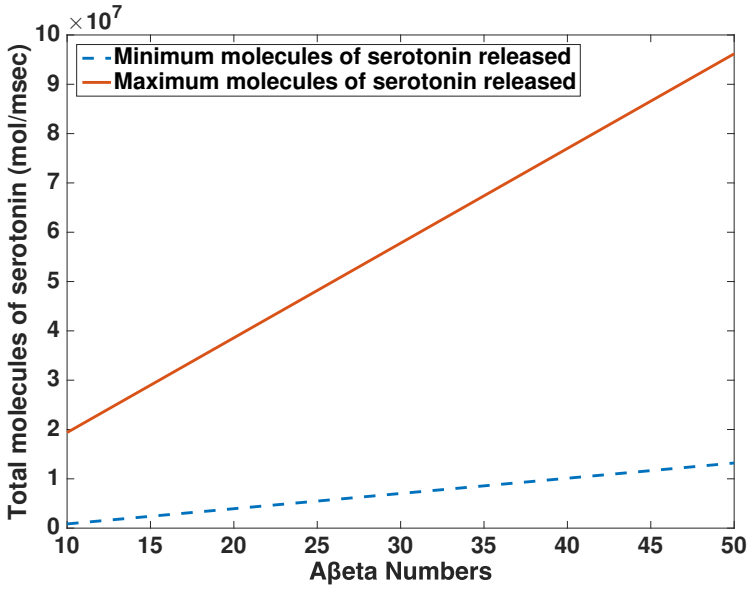

Figure 6.6: Minimum and maximum number of serotonin released.

cleft by using N3Sim. We then compared the results to the theoretical equation. Hence, Fig. 6.5 a), b) shows the theoretical values with N3Sim values of the total molecules absorbed by $A\beta eta$ for different numbers of $A\beta eta$. In more precise terms, for every thirty $A\beta eta$ the difference between the theoretical value and the experimental one is around 2 $\%$. Therefore, $N_{A\beta}$ can be derived from the expected number of molecules hitting $N_{A\beta hit}$.

4. Calculate the dose of serotonin that should be released: To calculate the optimum value of serotonin that should be released we optimize this value by calculating the minimum and the maximum serotonin molecules required. To calculate the minimum number of serotonin required, we assumed that $A\beta eta$ proteins occupy the closest point to the transmitter. However, to compute the maximum number of serotonin required we assumed that $A\beta eta$ proteins occupy the farthest distance from the transmitter. Hence, the optimum value of serotonin can be expressed as,

$$Q_{optmin} = 2\pi D_f C_{allowed} \sum_{1}^{N_{A\beta}} d_{min}(N_{A\beta}) \tag{6.7}$$

and,

$$Q_{optmax} = 2\pi D_f C_{allowed} \sum_{1}^{N_{A\beta}} d_{max}(N_{A\beta}) \tag{6.8}$$

where, $C_{allowed}$ is 10 mol/m^3 which equals to 10^{-5} mol/cm^3, $C_{allowed}$ is proved to produce significant apoptosis, and is considered as the threshold value [123], d_{min} = r_r, and d_{max} = $D_{A\beta eta}$.

Thus, in Fig. 6.6 we display the minimum and the maximum number of serotonin that should be released according to the amount of the toxic $A\beta eta$ proteins.

5. Use optogenetics technology to diffuse serotonin: To diffuse the appropriate number of serotonin, we use optogenetics technology to activate the specific neuron. After releasing the number of serotonin required, we need to re-check the number of molecules absorbed by AMPA receptors (C) and compare it to C_n, if If $C < C_n$ we need to repeat the steps mentioned above. If not, we stop and examine another neuron.

6.6 Summary and Concluding Remarks

The number of people affected with AD is expanding in a dramatic way. Drug treatments have not provided an effective solution since their effects diminish with time. It has been shown that serotonin doses can eliminate the toxic $A\beta eta$ proteins. Therefore, in this chapter, we first modeled the specific case of the excitatory glutamatergic synapses between glutamate vesicles and AMPA receptors, while taking into consideration the $A\beta eta$ accumulation surrounding and adjacent to the synaptic clef, and then we characterize the effect of increasing the number of $A\beta eta$ on this channel which shows that the accumulation of $A\beta eta$ proteins is an indicative of the channel loss. Hence, to fight the loss in the channel we proposed a closed-loop control approach to control the concentration of serotonin doses depending on the number of $A\beta eta$, while benefiting from the advantages of using optogenetics technology. The proposed approach can potentially guide to a novel solution for the treatment of AD, where a combination of nanotechnology, serotonin and optogenetics are used to reduce and eliminate the toxic $A\beta eta$ proteins.

Chapter 7

3D Model of Spermatozoa Movement in the Reproductive Female Tract

This Chapter proposes a mathematical model to describe the movement of spermatozoa in the reproductive female tract during the process of chemotaxis, from the standpoint of a molecular communication problem. The goal of modeling the movement of the spermatozoa in the reproductive female tract is to understand better the process, by quantitatively describing the communication problem from diffusion theory, as well as to describe better from simulation-based characterization in order to provide (design) guidelines for improvement oriented to come up with new treatment.

Hence, section 7.1 describes the spermatozoa movement in the reproductive female tract while taking into consideration the effect of chemo-attractant concentration in the medium. Section 7.2 shows the mathematical model used to track the movement of spermatozoa during the process of chemotaxis. Section 7.3 shows the effect of varying the appropriate metrics on the arrival time of the spermatozoa that reach the egg. Lastly, the summary and the concluding remarks are shown in section 7.4.

7.1 Spermatozoa Movement in the Reproductive Female Tract

As we discussed in section 2.2.3.1 the motion of the spermatozoa in the reproductive female tract relies on the chemo-attractant concentration released by the egg and it is shown in Fig. 2.6. When the spermatozoa sense that the surrounding concentration of chemo-attractant is increasing they

will keep swimming in a straight line for a longer time before they turn, since they are moving in the correct direction and approaching the egg. However, when the spermatozoa sense that the surrounding concentration of chemo-attractant is decreasing, turns and hyper-activation events take over, since they are moving away from the egg: hence, they pick a random direction by swimming in tight circles trying to replace the current one. In addition, the flow of the released chemo-attractant by the egg is governed by the Fick's second law of diffusion explained before in equation 2.1, where the chemo-attractant molecules diffuse freely in the medium from the regions with high concentration to the regions with lower concentration.

7.2 Modeling the Spermatozoa Movement During the Process of Chemotaxis

Section 7.2.1 and 7.2.2 present the mathematical model of the spermatozoa motion while taking into consideration the chemo-attractant concentration released by the egg. This model is inspired from [91] where it is developed in 3D with two types of spermatozoa movements, namely, the activated motility and the hyper-activated motility since the motion of the spermatozoa in the reproductive female tract relies on the chemo-attractant concentration released by the egg. In addition, in section 7.2.3 we model the chemo-attractant concentration in the medium by the Fick's second law of diffusion where the diffusion coefficient is moving in low Reynolds number fluids and can be modeled from Stokes–Einstein equation.

7.2.1 Activated Motility

The first type of spermatozoa movement is the activated motility, where the spermatozoa move in a more straight or quasi-linear trajectory. Hence, the activated motility can be modeled with a biased random walk while giving a heavier weight to the direction which the sperm has been moving in the past several steps, so that the sperm is more likely to move straight [91]. The position of sperm at time $t + \Delta t$ is given by [91],

$$p(t + \Delta t) = p(t) + \Delta t v_a b_i \tag{7.1}$$

where v_a is the velocity of activated motility and $b_i = (x_i, y_i, z_i)$ is a weighted random point on the unit sphere which represents the direction of the spermatozoa movement at step i.

b_i is chosen randomly in two steps. First, the average direction is tilted by an angle θ. Then the tilted direction is rotated by an angle γ with the average direction. The weight is calculated from the exponential distribution $w(\theta) = \lambda e^{-\lambda}\theta$ where $\theta\ \varepsilon$ (0,π). The angle γ is drawn uniformly from $\gamma\ \varepsilon$ (0,2π).

7.2.2 Hyper-activated Motility

The second type of spermatozoa movement is the hyper-activation. In this type the movement of spermatozoa at each time step is independent of other movements and the length of the movement is always the same since the time step is fixed. The position of sperm at time $t + \Delta t$ is given by [91],

$$p(t + \Delta t) = p(t) + \Delta t v_h d_i \tag{7.2}$$

where v_h is the velocity of hyper-activated motility and $d_i = (x_i, y_i, z_i)$ is the 3D vector which represents the direction of the spermatozoa movement at step i.

Note that the author in [91] selects a direction $d_i = (x_i, y_i, z_i)$ for the spermatozoa movement by using a previously derived algorithm in [124]. The algorithm can be summarized as follows,

1. Select u uniformly from [-1,1].
2. Select θ uniformly from (0, 2π).
3. Characterize d_i as: $x_i = \sqrt{1-u^2}\cos\theta$, $y_i = \sqrt{1-u^2}\sin\theta$, and $z_i = u$

Adding equation 7.1 and 7.2 can lead us to the full model of spermatozoa position which can be expressed as follows,

$$p(t) = p(0) + \Delta t \left[v_a \sum_i b_i s_i + v_h \sum_i d_i (1 - s_i) \right] \tag{7.3}$$

where s_i will be equal to 1 when the spermatozoa sense an increase of chemo-attractant concentration in the medium. However, s_i will be equal to 0 when the spermatozoa sense a decrease of chemo-attractant concentration in the medium. Note that in activated motility the spermatozoa carry out straight swimming with occasional hyper-activation events and turns [125, 126]. However, in the hyper-activated motility the spermatozoa swim in tight circles rather than a straight line.

7.2.3 Chemo-attractant Concentration

For simplicity, in [91] the author considers that the chemo-attractant concentration increases as it is closer to the egg. Hence, the chemo-attractant concentration is fixed for the period of the simulation and it is calculated as follows,

$$C(t) = \frac{1}{|| \, p(t) - E_c \, ||} \tag{7.4}$$

where, $p(t)$ is the position of the sperm at time t and E_c is the location of the center of the egg, and $\| \, . \, \|$ denotes the euclidean norm.

Since the flow of the chemo-attractant concentration in the medium is governed by the Fick's second law of diffusion, accordingly in our enhanced model the chemo-attractant concentration at any position in the medium is calculated as follows,

$$C\left(d,t\right) = \frac{M}{\left(4\pi D_f \, t\right)^{3/2}} e^{-d^2/4D_f \, t} \tag{7.5}$$

where M represents the number of chemo-attractant released, d is the distance between the transmitter and the egg, and t the time, and D_f denotes the diffusion coefficient.

In addition, the diffusion coefficient (D_f) of the chemo-attractant is moving in low Reynolds number fluids and can be calculated from Stokes–Einstein equation as [127],

$$D_f = \frac{K_B T}{6\pi\eta r_c} \tag{7.6}$$

where k_B is the Boltzmann constant, T is the temperature in Kelvin (K), η represents the viscosity of the medium calculated in Pa.s, and r_c denotes the radius of the chemo-attractant.

In section 7.3 we consider the movement of the spermatozoa in the reproductive female tract as a molecular communication problem, hence, we study the effect of varying the dose of spermatozoa, altering the viscosity of the medium, and varying the dose of chemo-attractant concentration upon the arrival time of the spermatozoa that reach the egg as an aggregated communication metrics.

7.3 Results

We performed our study by using MATLAB software [92] to implement a behavioral model of the system based on the modelling assumptions of the previous sections. We deploy one

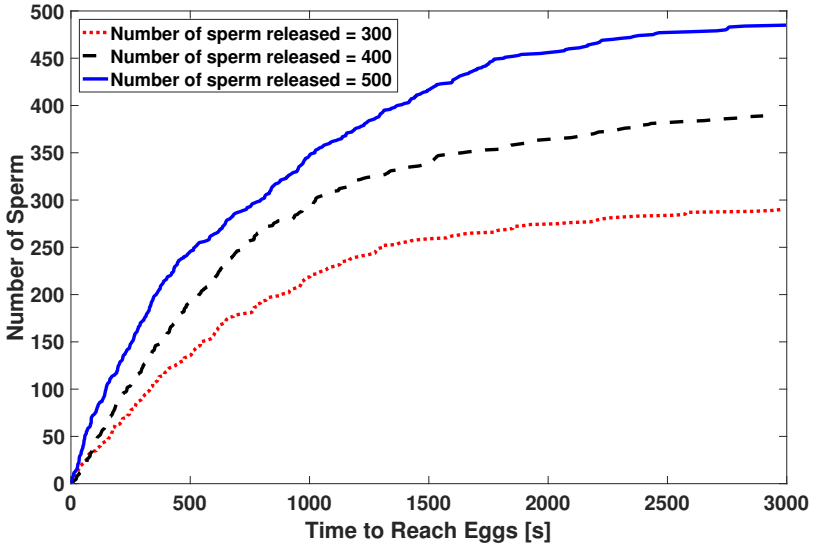

Figure 7.1: Arrival times of spermatozoa that reached the egg while altering the number of spermatozoa released.

transmitter that releases spermatozoa and one receiver which represent the egg. The distance between the transmitter and the receiver is fixed to 5 μm, while the diameter of the egg is fixed to 100 μm [128], both of them biologically representative values. r_c is fixed to 1 μm. v_h and v_a is equal to 82 and 46 μm per seconds respectively [129]. The temperature is fixed at 27 degree Celsius. The simulation time is set to 3000 seconds.

7.3.1 Altering the dose of Spermatozoa

First we consider the dose of spermatozoa as an evaluation design value. Hence, to check the effect of altering the number of spermatozoa released on the number of spermatozoa received by the egg we fixed the chemo-attractant concentration to 100 molecules, and we fixed the viscosity of the medium to 0.01 Pa.s.

Fig. 7.1 shows the arrival times of spermatozoa that reached the egg while altering the number of spermatozoa released. The number of spermatozoa released is equal to 300, 400, and 500. It is observed that the number of spermatozoa reach the egg faster as the number of spermatozoa released increase. In particular, at 500 seconds the number of spermatozoa that reached the egg is equal to 245 when 500 spermatozoa are released, however it is equal to 127 when 300 spermatozoa are released. Hence, when the number of spermatozoa increase in the medium the probability of spermatozoa that reach the egg increase. Lastly, it is obviously noticed that a higher number of spermatozoa will be detected by the egg when a higher number

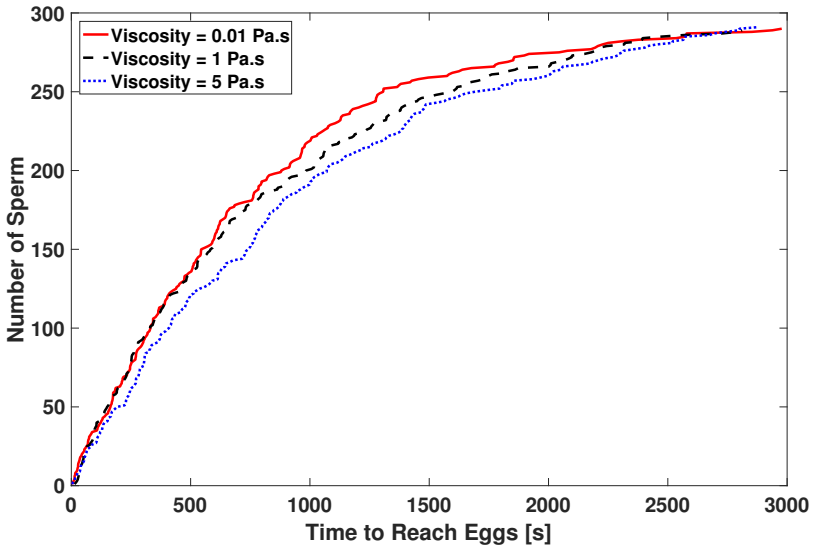

Figure 7.2: Arrival times of spermatozoa that reached the egg while altering the viscosity of the medium.

of spermatozoa are released in the medium, while this section quantitatively characterizes up to what extent.

7.3.2 Altering the Viscosity of the Medium

Next, we consider altering the viscosity of the medium as design variable. Therefore, to analyze the effect of adjusting the viscosity of the medium on the number of spermatozoa received by the egg we defined the number of spermatozoa released to 300, and we fixed the chemo-attractant concentration to 100 molecules.

Fig. 7.2 displays the arrival times of spermatozoa that reached the egg while altering the viscosity of the medium. The viscosity of the medium is equal to 0.1 Pa.s, 1 Pa.s, and 5 Pa.s. In these two plots we noticed that when the medium is more viscous the spermatozoa reach the egg faster. In particular, at 1000 seconds the number of spermatozoa that reached the egg is equal to 220 when the viscosity is equal to 0.1 Pa.s, however it is equal to 190 when the viscosity is equal to 5 Pa.s.

The definition of viscosity is the measure of a fluid's resistance to flow. It describes the internal friction of a moving fluid. Therefore, a fluid with large viscosity resists motion because its molecular makeup gives it a lot of internal friction. However, a fluid with low viscosity flows easily because its molecular makeup results in very little friction when it is in motion. Ultimately, this definition evidently describes the results that we obtained.

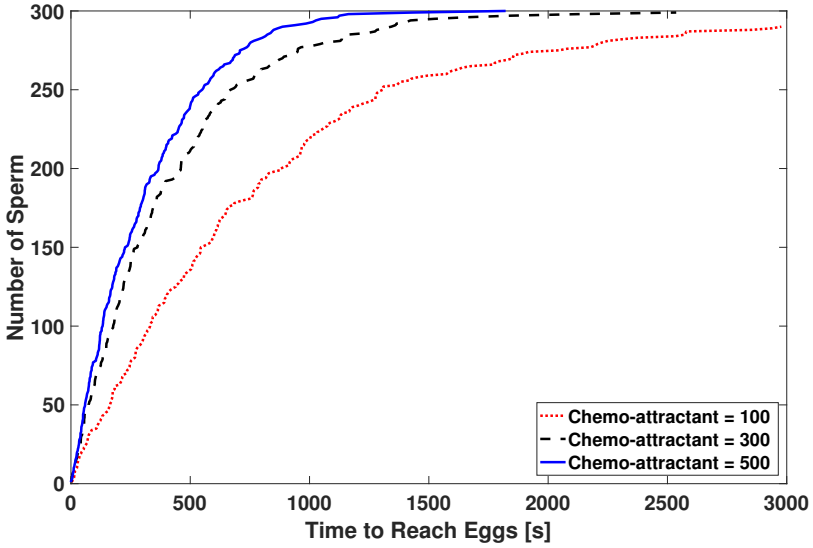

Figure 7.3: Arrival times of spermatozoa that reached the egg while altering the chemo-attractant concentration released.

7.3.3 Altering the dose of Chemo-attractant Concentration

Lastly, we show the dose of chemo-attractant concentration released by the egg under study. To analyze the effect of varying the dose of chemo-attractant concentration on the number of spermatozoa received by the egg we fixed the number of spermatozoa released to 300, and we fixed the viscosity of the medium to 0.01 Pa.s.

Fig. 7.3 displays the arrival times of spermatozoa that reached the egg while altering the chemo-attractant concentration released. The chemo-attractant concentration released in the medium is equal to 100 molecules, 300 molecules, and 500 molecules. As we can see the number of spermatozoa reaches the egg faster as the number of chemo-attractant released increases. In particular, it took around 500 seconds for 135 spermatozoa to reach the egg when the number of chemo-attractant is equal to 100 molecules, however, when we increased the number of chemo-attractant to 500 molecules it took around 500 seconds for 240 spermatozoa to reach the egg. In addition, 100% of the spermatozoa released reached the egg in 30 minutes when the number of chemo-attractant is equal to 500 molecules. However, 96% of the spermatozoa released reached the egg in 50 minutes when we reduced the number of chemo-attractant to 100 molecules.

From the last three plots we can conclude that the effect of chemo-attractant concentration on the arrival time of the spermatozoa is the more adequate and reliable one. Following our analysis we can deduce that the chemotaxis process plays an important aspect to deal with the fertility

problems. Hence, it would be viable to develop a treatment for infertility based on this method. In addition, this chapter pursued to quantitatively characterize this process by incorporating diffusion molecular communication aspects in the system.

7.4 Summary and Concluding Remarks

In this chapter, we proposed a mathematical model to describe the movement of the spermatozoa in the reproductive female tract during the process of chemotaxis where we considered it as a molecular communication problem. Therefore, we showed the effect of varying the appropriate design variables on the arrival time of the spermatozoa that reach the egg. First we considered changing the dose of spermatozoa as design variable where we found that the number of spermatozoa reached the egg faster as the number of spermatozoa released increase. Then, we considered altering the viscosity of the medium as design variable where we found the spermatozoa reach the egg faster when the medium is more viscous. Moreover, we considered varying the dose of the chemo-attractant concentration as evaluation metric where we deduce that the number of spermatozoa reaches the egg faster as the number of chemo-attractant released increases. Lastly, it has been found that the chemotaxis process plays an important aspect to deal with the fertility problems.

Chapter 8

Conclusion

The focus of this Ph.D. thesis is on Diffusion-based Molecular Communication (DMC), where the propagation of biological molecules between a transmitter and a receiver is realized through free diffusion in a fluid medium and characterized and modeled as a communication process. First, the choice of investigating the neuronal physical layer (layer 1) is motivated by the fact that there is no specific research that has been conducted to derive the appropriate performance metrics imposed by a point-to-point neuron neighboring absorbing receivers communication link, as well as by the Single Input Multiple Output (SIMO) networks. Secondly, the choice of investigating the physical channel of a DMC between glutamate vesicles and AMPA receptors is motivated by the numbers of affected people on neurodegenerative diseases which are estimated to increase dramatically and the fact that there are no efficient treatments to treat these neurodegenerative diseases. Thirdly, the choice of building a mathematical model to track the movement of spermatozoa during the process of chemotaxis is motivated by proposing new treatments which are more reliable, and less expensive than the existing one. The main contributions included in each chapter of this Ph.D. thesis are summarized in the following.

Chapter 4 targets the MolCom Markup Language (MolComML), as an enabler of more scalable multi-platform description language to exchange simulation setups for molecular communication setups and systems. In particular, the main contributions are as follows:

1. We define and identify the main objectives of the MolComML.

2. We introduce the architecture of the MolComML, with a special focus on its main elements and peculiarities that allow describing molecular communications systems.

3. We validate the N3Sim simulator by comparing it to the BiNS2 simulator through a

benchmark comparison, showing that the results of both simulators are similar to the theoretical assumptions.

4. We evaluate the performance of the neuron MC systems by using two different simulation packages, namely N3Sim and BiNS2, configured by using the MolComML, in order to demonstrate both its portability and the possibility of combining different platforms for creating complex simulation tools.

Chapter 5 is devoted to neuronal physical layer (layer 1) of a DMC . In particular, the main contributions are as follows:

1. In the Point-to-Point neuron neighboring absorbing receivers communication link:

    a) We analyze the influence of neighboring absorbing receivers on the maximum amplitude and pulse energy of the impulse response. This is carried out by investigating the impact of three scalars as design variables (distance from the transmitter, and the distance between the receivers, and their radius) on the impulse response.

    b) We investigate the impact of the neighboring absorbing receivers on the tail of the impulse response, oriented to model and characterize the Inter-Symbol Interference (ISI) of this system. We evaluate the system and derive the adequate metrics performance.

2. In the SIMO networks:

    a) We model the synaptic SIMO channel with absorbing receivers.

    b) We model the synaptic SIMO channel with Adsorption and Desorption (A&D) receivers.

    c) We study how these two systems will influence the pulse amplitude, width, energy, and tail, with the objective of deriving optimum design guidelines.

    d) We model the ISI of the two systems while deriving and comparing the achievable throughput of each system.

    e) We check how the number of receivers and the distance between the receivers will affect the performance of the two systems, thereby exploring scalability trends.

Through the results from the Point-to-Point neuron neighboring absorbing receivers communication link we learn that the optimal number of neighboring absorbing receivers and the

optimal distance between the receivers leads first to a steady state in the maximum amplitude of the impulse response and cancel the effect of ISI by reducing the amplitude of the tail. Therefore, in such case lower Bit Error Rate (BER) as well as a higher achievable throughput will be reached. In addition, from SIMO networks we learn that the optimal distance between the A&D receivers leads to a higher achievable throughput, hence, at this distance the achievable throughput of the A&D receivers will be equal to the achievable throughput of the SIMO absorbing receivers, consequently, the effect of ISI will decrease. Moreover, we found that absorbing receivers, and A&D receivers can be used to model different types of artificial biological MC process to come up with new medical treatment. In Parkinson's Disease (PD), or Alzheimer's Disease (AD) we deploy absorbing receivers. However, in the case of Huntington's Disease (HD) we use A&D receivers.

Chapter 6 focus on the physical channel of a DMC between glutamate vesicles and AMPA receptors, in the context of characterizing MC aspects in Alzheimer's disease. In particular, the main contributions are as follows:

1. We characterize the physical channel of a DMC between glutamate vesicles and AMPA receptors.

2. We analyze the effect of glutamatergic neurons on each other.

3. We investigate the effect of increasing the number of the toxic Amyloid Beta on this channel.

4. We introduce and propose a complete sense-actuation closed-loop system which leverages such characterization to infer the toxic Amyloid Beta concentration for fighting AD while using serotonin which, as is widely accepted, can reduce the production of Amyloid Beta proteins.

Through the results of the physical channel of a DMC between glutamate vesicles and AMPA receptors we learn that the proposed approach can potentially guide to a novel solution for the treatment of Alzheimer's Disease (AD), where a combination of nanotechnology, serotonin and optogenetics are used to reduce and eliminate the toxic $A\beta eta$ proteins through a fine-grain calibration of dose enabled by embedding the MC process in the closed-loop system.

Chapter 7 focus on building a mathematical model to track the movement of spermatozoa during the process of chemotaxis. In particular, the main contributions are as follows:

1. We build a mathematical model to track the movement of spermatozoa during the process of chemotaxis by using MATLAB software.

2. We understand, and describe better through simulation the biological process, particularly by incorporating MC diffusion aspects.

3. We model and characterize the system by quantifying the communication problem. Hence, we investigate the effect of varying the dose of spermatozoa released, modifying the viscosity of the medium, and releasing higher concentration of chemo-attractant on the channel.

Through the results it has been found that the chemotaxis process play an important aspect to deal with the fertility problems.

Finally, the results in this Ph.D. thesis ultimately are aimed to provide to synthetic biology design-oriented guidelines. In addition, this Ph.D. thesis presents new solutions for treating diseases which establish a new vision of dealing with them, as well as serve as guidelines for the medical committee, through an interdisciplinary approach bridging engineering techniques, particularly communication systems engineering one, into biological systems incorporating diffusion Molecular Communications (MC) processes, aiming eventual medical treatment.

Bibliography

[1] I. F. Akildiz, F. Brunetti, and C. Blazquez. Nanonetworks: A new communication paradigm. *Elsevier Computer Networks*, 52(12):2260–2279, August 2008.

[2] T. Suda, M. Moore, T. Nakano R. Egashira, and A. Enomoto. Exploratory research on molecular communication between nanomachines. *Proceedings Genetic and Evolutionary Computation Conference*, June 2005.

[3] I. Llatser, A. C. Aparicio, and M. Pierobon. Detection techniques for diffusion-based molecular communication. *IEEE Selected Areas Communication*, 31(12):726–734, December 2013.

[4] I. Llatser, E. Alarcón, and M. Pierobon. Diffusion-based channel characterization in molecular nanonetworks. *IEEE Conference on Computer Communications Workshops*, pages 467–472, 2011.

[5] I. Llatser, C. Kremers, D. N. Chigrin, J. Jornet M. C. Lemme, A. C. Aparicio, and E. Alarcón. Exploring the physical channel of diffusion-based molecular communication by simulation. *IEEE Global Telecommunications Conference (GLOBECOM)*, pages 1–5, December 2011.

[6] I. F. Akyildiz and F. Fekri. Monaco: fundamentals of molecular nano- communication networks. *IEEE Wireless Communications*, 19(5):12–18, 2012.

[7] T. Nakano A. W. Eckford and T. Haraguchi. Molecular communication. *Cambridge University Press*, 2013.

[8] I. Llatser, S. Abadal, A. M. Sugranes, A. C. Aparicio, and E. Alarcón. Graphene-enabled wireless networks-on-chip. *International Black Sea Conference on Communications and Networking (BlackSeaCom)*, pages 69–73, October 2013.

[9] I. Llatser, C. Kremers, A. C. Aparicio, J. M. Jornet, E. Alarcón, and D. N.Chigrin. Graphene-based nano-patch antenna for terahertz radiation. *IEEE International Black Sea Conference on Communications and Networking (BlackSeaCom)*, 10(4):353–358, October 2012.

[10] I. Llatser, C. Kremers, D. N. Chigrin, J. Jornet M. C. Lemme, A. C. Aparicio, and E. Alarcón. Radiation characteristics of tunable graphennas in the terahertz band. *Radioengineering*, 21(4):946–953, December 2012.

[11] S. Abadal, S. E. Hosseininejad, A. C. Aparicio, and E. Alarcón. Graphene-based terahertz antennas for area-constrained applications. *IEEE International Conference on Telecommunications and Signal Processing (TSP)*, pages 817–820, October 2017.

[12] S. Abadal, E. Alarcón, M. C. Lemme, M. Nemirovsky, and A. C. Aparicio. Graphene-enabled wireless communication for massive multicore architectures. *IEEE Communications Magazine*, 51(11):137–143, November 2013.

[13] S. Abadal, I. Llatser, A. Mestres, H. Lee, E. Alarcón, and A. C. Aparicio. Time-domain analysis of graphene-based miniaturized antennas for ultra-short-range impulse radio communications. *IEEE Transactions on Communications*, 63(4):1470–1482, April 2015.

[14] I. F. Akyildiz and J. M. Jornet. Electromagnetic wireless nanosensor networks. *Elsevier Nano Communication Networks*, 1:3–19, May 2010.

[15] J. M. Jornet and I. F. Akyildiz. Graphene-based nano-antennas for electromagnetic nanocommunications in the terahertz band. *International Conference in Transparent Optical Network*, July 2012.

[16] I. F. Akyildiz, J. M. Jornet, and M. Pierobon. Propagation models for nanocommunication networks. *IEEE Proceedings European Conference on Antennas and Propagation*, pages 1–5, April 2010.

[17] J. M. Jornet and I. F. Akyildiz. Graphene-based plasmonic nano-antenna for terahertz band communication in nanonetworks. *IEEE Journal on Selected Areas in Communications*, 31(12):685–694, December 2013.

[18] J. M. Jornet and I. F. Akyildiz. Channel modeling and capacity analysis for electromagnetic wireless nanonetworks in the terahertz band. *IEEE Transactions on Wireless Communications*, 10(10):3211–3221, October 2011.

[19] N. Farsad, H. B. Yilmaz, A. W. Eckford, C. B. Chae, and W. Guo. A comprehensive survey of recent advancements in molecular communication. *IEEE Communications Surveys & Tutorials*, 18(3):1887–1919, February 2016.

[20] S. Hiyama and Y. Moritani. Molecular communication: Harnessing biochemical materials to engineer biomimetic communication systems. *Elsevier Nano Communication Networks*, 1(1):20–30, March 2010.

[21] S. Hiyama, T. Inoue, T. Shima, Y. Moritani, T. Suda, and K. Sutoh. Autonomous loading, transport, and unloading of specified cargoes by using dna hybridization and biological motor-based motility. *Small*, 4(4):410–415, March 2008.

[22] M. Kuscu and O. B. Akan. Maximum likelihood detection with ligand receptors for diffusion-based molecular communications in internet of bio-nano things. *IEEE Transactions on NanoBioscience*, 17(1):44–54, January 2018.

[23] J. Wang, B. Yin, and M. Peng. Diffusion based molecular communication: principle, key technologies, and challenges. *China Communications*, 14(2):1–18, March 2017.

[24] S. Balasubramaniama, N.T. Boyle, A. Della-Chiesa, F. Walsha, A. Mardinoglue, D. Botvicha, and A. Prina-Melloc. Development of artificial neuronal networks for molecular communication. *Elsevier Nano Communication Networks*, 2(2):150–160, June 2011.

[25] J. M. Jornet, J.C. Pujol, and J.S. Paret. Phlame: A physical layer aware mac protocol for electromagnetic nanonetworks in the terahertz band. *Elsevier Nano Communication Networks*, 3(1):74–81, January 2012.

[26] C.E. Koksal, E. Ekici, and S. Rajan. Design and analysis of systems based on rf receivers with multiple carbon nanotube antennas. *Elsevier Nano Communication Networks*, 1(3):160–172, October 2010.

[27] Y. Chahibi, I. F. Akyildiz, and I. Balasingham. Propagation modeling and analysis of molecular motors in molecular communication. *IEEE Transactions on NanoBioscience*, 16(8):917–927, October 2016.

[28] M. T. Barros. Ca2+ signaling-based molecular communication systems: Design and future research directions. *Elsevier Nano Communication Networks*, 11:103–113, March 2017.

[29] M. Gregori and I. F. Akyildiz. A new nanonetwork architecture using flagellated bacteria and catalytic nanomotors. *IEEE Journal on Selected Areas in Communications*, 28(4):612–619, May 2010.

[30] B. D. Unluturk and I. F. Akyildiz. An end-to-end model of plant pheromone channel for long range molecular communication. *China Communications*, 16(1):11–20, November 2016.

[31] L. I. Golbe, M. H. Mark, and J. I. Sage. Parkinson's disease handbook. *American Parkinson Disease Association*, 2014.

[32] Alzheimer's Association. 2017 alzheimer's disease facts and figures. *Alzheimers Dement*, 13:325–373, 2017.

[33] M. Prince, A. Comas-Herrera, M. Knapp, M. Guerchet, and M. Karagiannidou. World alzheimer report 2016. *Alzheimer's Disease International (ADI), London*, September 2016.

[34] J. M. Lepkowski, W. D. Mosher, K. E. Davis, R. M. Groves, and J. Van Hoewyk. The 2006-2010 national survey of family growth: Sample design and analysis of a continuous survey. *National Center for Health Statistics. Vital Health Stat*, 2(150), June 2010.

[35] W. M. Mercer. Infertility as a covered benefit. 1997.

[36] R. Cajal. Histology of nervous system of man and vertebrates. *Oxford University Press*, 1995.

[37] E. Balevi and O. B. Akan. A physical channel model for nanoscale neuro-spike communications. *IEEE s on Communications*, 61(3):1178–1187, March 2013.

[38] G. Stuart, J. Schiller, and B. Sakmann. Action potential initiation and propagation in rat neocortical pyramidal neurons. *Journal of Physiology*, 505(3):617–632, 1997.

[39] E. R. Kandel, J. H. Schwartz, and T. Jessell. Principles of neural science. *McGraw-Hill, New York, ed. 4*, 2000.

[40] I. Karatzas and S. E. Shreve. *Brownian Motion and Stochastic Calculus*. Springer, 1991.

[41] W. H. Bossert and E. O. Wilson. The analysis of olfactory communication among animals. *Theoretical biology*, 5(3):443–469, November 1963.

[42] W. Gerstner and W. M. Kistler. Spiking neuron models: Single neurons, populations, plasticity. *Cambridge University Press*, 2002.

[43] Z. F. Mainen and T. J. Sejnowski. Reliability of spike timing in neocortical neurons. *Science*, 268(5216):61503–1506, June 1995.

[44] S. Ishijima, S. Oshio, and H. Mohri. Flagellar movement of human spermatozoa. *Gamete Research*, 13(3):185–197, March 1986.

[45] W. C. Hamlett and T. J. Koob. Female reproductive system. in sharks, skates, and rays: The biology of elasmobranch fishes. *Johns Hopkins University Press, Baltimore, MD*, pages 398–443, 1999.

[46] M. Williams, C. J. Hill, I. Scudamore, B. Dunphy, I. D. Cooke, and C. L. R. Barratt. Physiology: Sperm numbers and distribution within the human fallopian tube around ovulation. *Human Reproduction*, 8(12):2019–2026, December 1993.

[47] M. Eisenbach and I. T. Kaspa. Do human eggs attract spermatozoa? *Human Reproduction*, 21(3):203–210, March 1999.

[48] M. Eisenbach and L. C. Giojalas. Sperm guidance in mammals—an unpaved road to the egg. *Nature Reviews Molecular Cell Biology*, 7(12):276–285, April 2006.

[49] L. Gnessi, A. Fabbri, L. Silvestroni, C. Moretti, F. Fraioli, C. B. Pert, and A. Isidori. Evidence for the presence of specific receptors for nformyl chemotactic peptides on

human spermatozoa. *The Journal of Clinical Endocrinology & Metabolism*, 63(4):841–846, October 1986.

[50] L. M. Ballesteros, N. M. Delgado, A. Rosado, C. Correa, and O. H. Perez. Binding of chemotactic peptide to the outer surface and to whole human spermatozoa with different affinity states. *Gamete Research*, 20(2):233–239, June 1988.

[51] D. Ralt, M. Manor, A. C. Dayag, I. T. Kaspa, I. B. Shlomo, A. Makler, I. Yuli, J. Dor, S. Blumberg, S. Mashiach, and M. Eisenbach. Chemotaxis and chemokinesis of human spermatozoa to follicular factors. *Biology of Reproduction*, 50(4):774–785, April 1994.

[52] B. S. Jaiswal, I. T. Kaspa, J. Dor, S. M., and M. Eisenbach. Human sperm chemotaxis: is progesterone a chemoattractant? *Biology of Reproduction*, 60(6):1314–1319, June 1999.

[53] M. Yoshida, M. Murata, K. Inaba, and M. Morisawa. A chemoattractant for ascidian spermatozoa is a sulfated steroid. *Proceedings of the National Academy of Sciences of the United States of America*, 99(23):14831–14836, November 2002.

[54] U. B. Kaupp, J. Solzin, E. Hildebrand, J. E. Brown, A. Helbig, V. Hagen, M. Beyermann, F. Pampaloni, and I. Weyand. The signal flow and motor response controling chemotaxis of sea urchin sperm. *Nature Cell Biology*, 5:109–117, January 2003.

[55] J. Solzin, A. Helbig, Q. Van, J. E. Brown, E. Hildebrand, I. Weyand, and U. B. Kaupp. Revisiting the role of h+ in chemotactic signaling of sperm. *Journal of General Physiology*, 124:115–124, July 2004.

[56] T. Strunker, N. Goodwin, C. Brenker, N. D. Kashikar, I. Weyand, R. Seifert, and U. B. Kaupp. The catsper channel mediates progesterone-induced ca2+ influx in human sperm. *Nature*, 471:382–386, March 2011.

[57] P. V. Lishko, I. L. Botchkina, and Y. Kirichok. Progesterone activates the principal ca2+ channel of human sperm. *Nature*, 471:387–391, March 2011.

[58] L. Armon and M. Eisenbach. Behavioral mechanism during human sperm chemotaxis: Involvement of hyperactivation. *PLoS One*, 6(12):e28359, December 2011.

[59] L. Robertson, D. P. Wolf, and J. S. Tash. Temporal changes in motility parameters related to acrosomal status: identification and characterization of populations of hyperactivated human sperm. *Biology of reproduction*, 39:797–805, August 1988.

[60] D. Malak and O. B. Akan. Molecular communication nanonetworks inside human body. *Elsevier Nano Communication Networks*, 3(6):19–35, March 2012.

[61] A. Guney, B. Atakan, and O. B. Akan. Mobile ad hoc nanonetworks with collision-based molecular communication. *IEEE Transaction on Mobile Computing*, 11(3):353–366, March 2012.

[62] L. Gallucio, S. Pallazzo, and G. E. Santagati. Modeling signal propagation in nanomachime-to-neuron communication. *Elsevier Nano Communication Networks*, 2:213–222, October 2011.

[63] M. Veletic, P. A. Floorand, and I. Balasingham. From nano-scale neural excitability to long term synaptic modification. *ACM The First Annual International Conference on Nanoscale Computing and Communication*, (22), 2014.

[64] D. Malak, M. Kocaoglu, and O. B. Akan. Communication theoretic analysis of the synaptic channel for cortical neurons. *Elsevier Nano Communication Networks*, 4(3):131–141, September 2013.

[65] Q. Liu, P. He, K. Yang, and S. Leng. Inter-symbol interference analysis of synaptic channel in molecular communications. *IEEE International Conference on Communications (ICC)*, pages 4424–4429, June 2014.

[66] K. V. Srinivas, A. W. Eckford, and R. S. Adve. Molecular communication in fluid media: The additive inverse gaussian noise channel. *IEEE Inf. Theory*, 58:4678–4679, July 2012.

[67] H. B. Yilmaz, A. C. Heren, T. Tugcu, and C. B. Chae. Three-dimensional channel characteristics for molecular communications with an absorbing receiver. *IEEE Commun. Lett.*, 18:929–932, June 2014.

[68] M. Pierobon and I. F. Akyildiz. Capacity of a diffusion-based molecular communication system with channel memory and molecular noise. *IEEE Inf. Theory*, 59:942–954, February 2013.

[69] A. Noel, K. Cheung, and R. Schober. Improving receiver performance of diffusive molecular communication with enzymes. *IEEE Transactions on NanoBioscience*, 13:31–43, MARCH 2014.

[70] S. Kadloor and R. Adve. A framework to study the molecular communication system. *Proceedings IEEE ICCCN*, pages 1–6, August 2009.

[71] A. Einolghozati, M. Sardari, A. Beirami, and F. Fekri. Capacity of discrete molecular diffusion channels. *Proceedings 2009 IEEE ISIT*, pages 723–727, August 2011.

[72] S. Kadloor, R. R. Adve, and A. W. Eckford. Molecular communication using brownian motion with drift. *IEEE Transactions on NanoBioscience*, 11:89–99, June 2012.

[73] K. V. Srinivas, A. W. Eckford, and R. S. Adve. Molecular communication in fluid media: The additive inverse gaussian noise channel. *IEEE Inf. Theory*, 58:4678–4692, July 2012.

[74] T. Nakano, Y. Okaie, and A. V. Vasilakos. Throughput and efficiency of molecular communication between nanomachine. *IEEE WCNC*, pages 704–708, April 2012.

[75] L. S. Meng, P. C. Yeh, K. C. Chen, and I. F. Akyildiz. Mimo communications based on molecular diffusion. *Proceedings IEEE GLOBECOM*, pages 5602–5607, December 2012.

[76] M. Pierobon and I. F. Akyildiz. Inter symbol and co-channel interference in diffusion-based molecular communication. *Proceedings IEEE ICC MONACOM*, pages 6126–6131, June 2012.

[77] M. S. Leeson and M. D. Higgins. Forward error correction for molecular communications. *Nano Commun. Net.*, pages 161–167, September 2012.

[78] H. B. Yilmaz and C. Chae. Simulation study of molecular communication systems with an absorbing receiver: Modulation and isi mitigation techniques. *Simul. Model. Pract. Theory*, 49:136–150, December 2014.

[79] B. Tepekule, A E. Pusane, C. B. Chae H. Birkan Yilmaz, and Tuna Tugcu. Isi mitigation techniques in molecular communication. *IEEE transactions on molecular*, pages 2332–7804, June 2015.

[80] M. U. Mahfuz, D. Makrakis, and H. T. Mouftah. Performance analysis of convolutional coding techniques in diffusion-based concentration-encoded pam molecular communication systems. *Springer Bio-NanoSci.*, 3(3):270–284, September 2013.

[81] P. J. Shih, C. H. Lee, P. C. Yeh, and K. C. Chen. Channel codes for reliability enhancement in molecular communication. *IEEE J. Sel. Areas Communication*, 31(12):857–867, December 2013.

[82] Y. J. Cho, H. B. Yilmaz, W. Guo, and C. B. Chae. Effective inter-symbol interference mitigation with a limited amount of enzymes in molecular communications. *Wiley Transaction Emerging Telecommunication*, September 2016.

[83] H. B. Yilmaz, Y. J. Cho, W. Guo, and C. B. Chae. Interference reduction via enzyme deployment for molecular communication. *IET Electron. Lett.*, 52(13):1094–1096, June 2016.

[84] M. T. Barros and S. Dey. Feed-forward and feedback control in astrocytes for ca2+-based molecular communications nanonetworks. *bioRxiv*, August 2017.

[85] N. I. Fisher, T. Lewis, and B. J. J. Embleton. Statistics analysis of spherical data. *Cambridge University Press*, 1987.

[86] B. D. Unluturk and I. F. Akyildiz. Random walk models in biology. *China Communications*, 5:813–834, August 2008.

[87] M. Uttieri, D. Cianelli, Strickler J. R. Strickler, and E. Zambianchi. On the relationship between fractal dimension and encounters in three-dimensional trajectories. *Journal Theoretical Biology*, 247(3):480–491, March 2007.

[88] B. M. Friedrich and F. Julicher. Chemotaxis of sperm cells. *National Acad Sciences*, 104(33):13256–13261, August 2007.

[89] M. Uttieri, D. Cianelli, Strickler J. R. Strickler, and E. Zambianchi. Strategies for sperm chemotaxis in the siphonophores and ascidians: A numerical simulation study. *Biol Bul*, 206:95–102, April 2004.

[90] L. Alvarez, L. Dai, B. M. Friedrich, N. D. Kashikar, I. Gregor, R. Pascal, and U. B. Kaupp. The rate of change in ca2+ concentration controls sperm chemotaxis. *Journal of Cell Biology*, 96(5):653–663, March 2012.

[91] Y. Zhang. 3-dimensional model and simulations of sperm movement. *Worcester Polytechnic Institute*, April 2013.

[92] S. Attaway. Matlab: A practical introduction to programming and problem solving. *Elsevier, Inc., Waltham, MA, USA, and Kidlington, Oxford, United Kingdom*, 2012.

[93] I. Llatser, D. Demiray, A. C. Aparicio, D. T. Altilar, and Alarcón. N3sim: Simulation framework for diffusion-based molecular communication nanonetworks. *Simulation Modelling Practice and Theory*, 42:210–222, March 2014.

[94] N. Garralda, I. Llatser, A. C. Aparicio, and M. Pierobon. Simulation-based evaluation of the diffusion-based physical channel in molecular nanonetworks. *IEEE Conference on Computer Communications Workshops (INFOCOM WKSHPS)*, pages 443–448, April 2011.

[95] L. Felicettia, M. Femminella, and G. Reali. A simulation tool for nanoscale biological networks. *Elsevier Nano Communication Networks*, 3(1):2–18, March 2012.

[96] S. Balasubramaniam and P. Lio. Multi-hop conjugation based bacteria nanonetworks. *IEEE Transactions on NanoBioscience*, 12(1):47–59, March 2013.

[97] G. Wei, P. Bogdan, and R. Marculescu. Efficient modeling and simulation of bacteria-based nanonetworks with bnsim. *IEEE Journal on Selected Areas in Communications*, 31(12):868–878, December 2013.

[98] Y. Chahibi, M. Pierobon, S. O. Song, and I. F. Akyildiz. A molecular communication system model for particulate drug delivery systems. *IEEE Transactions on Biomedical Engineering*, 60(12):3468–3483, December 2013.

[99] M. T. Barros, S. Balasubramaniam, and B. Jennings. Comparative end-to-end analysis of ca2+-signaling-based molecular communication in biological tissues. *IEEE Transactions on Communications*, 63(12):5128–5142, December 2015.

[100] E. Gul, B. Atakan, and O. B. Akan. NanoNS: A nanoscale network simulator framework for molecular communications. *Elsevier Nano Communication Networks*, 1(2):138–156, June 2010.

[101] S. F. Bush, J. L. Paluh, G. Piro, V. Rao, R V. Prasad, and A. Eckford. Defining communication at the bottom. *IEEE s on Molecular, Biological and Multi-Scale Communications*, 1(1):90–96, March 2015.

[102] A. Akkaya, G. Genc, and T. Tugcu. HLA based architecture for molecular communication simulation. *Simulation Modelling Practice and Theory*, 42(0):163–177, March 2014.

[103] E. Alarcón, R. G. Cid-Fuentes, A. Davy, L. Felicetti, , M. Femminella, P. Lio, G. Reali, and J. Solé-Pareta. Molcomml: The molecular communication markup language. *in Proc. of the 3rd ACM International Conference on Nanoscale Computing and Communication (NANOCOM),New York, USA*, (6):1–16, 2016.

[104] L. Felicettia, S. S.Assaf, M. Femminella, G. Reali, E. Alarcón, and J. Solé-Pareta. The molecular communications markup language (molcomml). *Elsevier Nano Communication Networks*, 16(6246):12–25, June 2018.

[105] S. Abadal, I. Llatser, A. Mestres, H. Lee, E. Alarcón, and A. C. Aparicio. Xml, bioinformatics and data integration. *Bioinformatics*, 17(2):115–125, February 2001.

[106] W3c. w3c's math home page. available via the world wide web at. `http://www.w3.org/Math/`.

[107] L. Felicetti, M. Femminella, G. Reali, T. Nakano, and A. V. Vasilakos. Tcp-like molecular communications. *IEEE Journal on Selected Areas in Communications*, 32(12):2354–2367, December 2014.

[108] J. Rospars, V. K rivan, and P. Lánský. Perireceptor and receptor events in olfaction. comparison of concentration and flux detectors: a modeling study. *Chem. Senses*, 5(3):293–311, June 2000.

[109] P. S. Miller and A. R. Aricescu. Crystal structure of a human $gaba_a$ receptor. *Nature*, pages 270–275, August 2014.

[110] S. S. Andrews. Accurate particle-based simulation of adsorption, desorption, and partial transmission. *Phys Biol*, 6(4), November 2009.

[111] C. Tom and M. R. D'Ordogna. Multistage adsorption of diffusing macromolecules and viruses. *Chemical Physics*, 127(10):2013–2018, 2007.

[112] D. K. Lee, D. J. Albershardt, and R. S. Cantor. Exploring the mechanism of general anesthesia: Kinetic analysis of gabaa receptor electrophysiology. *Biophysical*, 108:1081–1093, March 2015.

[113] J. R. Cirritoa, B. M. Disabatod, J. L. Restivoa, D. K. Vergesa, W. D. Goebela, A. Sathyana, D. Hayrehd, G. D'Angelob, T. Benzingerb nd H. Yoona, J. Kima, J. C. Morrisa, M. A. Mintunb, and Y. I. Shelinea. Serotonin signaling is associated with lower amyloid-β levels and plaques in transgenic mice and humans. *Proceedings of the National Academy of Sciences of the United States of America*, 108(36):14968–14973, August 2011.

[114] S. Claeysen, J. Bockaert, and P. Giannoni. Serotonin: A new hope in alzheimer's disease? *ACS Chemical Neuroscience*, 6(7):940–943, May 2015.

[115] K. Deisseroth. Optogenetics. *Nature Methods*, 8(1):26–29, January 2011.

[116] J. Montes, J. M. Peña, J. DeFelipe, and O. Herreras A. Merchan-Perez. The influence of synaptic size on ampa receptor activation: A monte carlo model. *PloS one*, 10(6):e0130924, June 2015.

[117] T. Khan, B. A. Bilgin, and O. B. Akan. Diffusion-based model for synaptic molecular communication channel. *IEEE Transactions on NanoBioscience*, 16(4):299–308, June 2017.

[118] D. A. Rusakov, L. P. Savtchenko, K. Zheng, and J. M. Henley. Shaping the synaptic signal: molecular mobility inside and outside the cleft. *Trends in neurosciences, Elsevier Current Trends*, 34(7):359–369, July 2011.

[119] T. A. Nielsen, D. A. DiGregorio, and R. A. Silver. Modulation of glutamate mobility reveals the mechanism underlying slow-rising ampar epscs and the diffusion coefficient in the synaptic cleft. *Neuron*, 42(5):757–771, June 2014.

[120] T. Lr̈ihrs, C. Ritter, A. C. Aparicio, M. Adrian, D. Riek-Loher, B. Bohrmann, H. Döbeli, D. Schubert, and R. Riek. 3d structure of alzheimer's amyloid-β(1-42) fibrils. *Proceedings of the National Academy of Sciences of the United States of America*, 102(48):17342–17347, November 2005.

[121] L. P. Savtchenko and D. A. Rusakov. The optimal height of the synaptic cleft. *Proceedings of the National Academy of Sciences of the United States of America*, 104(6):1823–1828, December 2006.

[122] Ali Akkaya, H B. Yilmaz, C. B. Chae, and T. Tugcu. Effect of receptor density and size on signal reception in molecular communication via diffusion with an absorbing receiver. *IEEE Communications Letters*, 19(2):155–158, February 2015.

[123] L. Tang, A. L. van de Ven, V. Andasari, V. Cristini, K. C. Li, and X. Zhou. Computational modeling of 3d tumor growth and angiogenesis for chemotherapy evaluation. *PloS one*, 9(1):e83962, January 2014.

[124] J. M. Cook. Technical notes and short papers: Rational formulae for the production of a spherically symmetric probability distribution. *Math. Tables Aids Computer*, 11:81–82, 1957.

[125] R. L. Miller. Chemotaxis of the spermatozoa ciona intestinalis. *Nature*, 254:244–245, March 1975.

[126] U. B. Kaupp, N. D. Kashikar, and I Weyand. Mechanisms of sperm chemotaxis. *Annual Review of Physiology*, 70:93–117, March 2008.

[127] A. Einstein. A new determination of the molecular dimensions. *Ann Phys*, 19:289–306, 1906.

[128] M. Eisenbach and I. Tur-Kaspa. Do human eggs attract spermatozoa? *Bioessays*, 21(3):203–210, March 1999.

[129] Y. Hirano, H. Shibahara, K. Shimada, S. Yamanaka, T. Suzuki, S. Takamizawa, M. Motoyama, and M. Suzuki. Accuracy of sperm velocity assessment using the sperm quality analyzer v. *Reproductive Medicine and Biology*, 2:151–157, 2003.

List of Figures

Acronyms

$A\beta eta$	Amyloid Beta.
3D	3-dimensional.
A&D	Adsorption and Desorption.
AD	Alzheimer's Disease.
ADI	Alzheimer's Disease International.
APP	Amyloid Precursor Protein.
BER	Bit Error Rate.
DMC	Diffusion-based Molecular Communication.
ISI	Inter-Symbol Interference.
IUI	Intrauterine insemination.
IVF	In Vitro Fertilization.
MC	Molecular Communications.
MIMO	Multiple Input Multiple Output.
MISO	Multiple Input Single Output.
MolComML	MolCom Markup Language.
N3cat	NaNoNetworking Center in Catalunya.

NINDS	National Institute of Neurological Disorders and Stroke.
PD	Parkinson's Disease.
SIMO	Single Input Multiple Output.
SIMO	Single Input Single Output.

Appendix A

Example of the MolComML Configuration File

```
<?xml version="1.0" encoding="UTF-8"?>
<molcomml version="1.0">
   <model name="Platelet\_TCell\_Communication" description="...">
      <listOfConfigurationParameters>
         <param name="T" value="310" unit="K" description="temp" />
      </listOfConfigurationParameters>
      <listOfUnits>
         <unit name="nm" scale="-9" />
      </listOfUnits>

   <listOfNetworkElements>
      <NetworkElement name="platelet" type="transmitter/receiver">
         <size name="radius" unit="nm" value="1000" />
         <signal type="cd40l" direction="out" />
         <signal type="trombin" direction="in" />
         <motion type="none" />
      </NetworkElement>
   </listOfNetworkElements>

   <listOfCommunicationInterface>
```

```
    <CommunicationInterface name="platR" type="element">
       <status type="enabled" />
       <direction input="no" output="yes" />
       <signal type="cd40l" direction="out" time="4" unit="s"
       affinity="none" />
    </CommunicationInterface>
</listOfCommunicationInterface>

<listOfProtocolStacks>
    <protocolStack name="Adaptive\_Mol\_Delivery" maxLevel="5">
       <layer level="1" type="Physical">
          <rule>
             <signal type="cd40l" direction="forward"></signal>
             <signal type="IL-4" direction="feedback"></signal>
          </rule>
       </layer>
       <layer level="2" type="Link">
          <rule>
             <signal type="cd40l" direction="forward">
                <controlMessage name="start" format="1011" />
                <synchronization name="syncAlgorithm" />
             </signal>
             <signal type="IL-4" direction="feedback">
                <dataMessage name="upload" format="burst"
                payload="none"/>
                <rateControl name="TCP\_Like\_Algorithm" />
             </signal>
          </rule>
       </layer>
    </protocolStack>
</listOfProtocolStacks>
```

```
    <listOfCompartments>
       <externalChannel name="diffusion">
          <Compartment name="box" parent="none">
             <shape type="cube" />
          <gate name="gate1" />
          <channel name="diffusion" />
          </Compartment>
       </externalChannel>
    </listOfCompartments>


    <listOfChannels>
       <channel name="diffusion" >
          <mathRule name="diffusion" path="./mathEquations">
          </mathRule>
       </channel>
    </listOfChannels>

    <networkTopology>
       <disposedNetworkElement name="tx1" type="platelet" >
          <compartment name="tube" />
          <position name="coords" x="100" y="200" z="100" unit="um" />
          <protocolStack type="Adaptive\_Mol\_Delivery" />
       </disposedNetworkElement>
    </networkTopology>
    </model>
</molcomml>
```

Appendix B

SIMO MC Scenarios in N3Sim Simulator

First, the only prerequisite to install the jar file N3Sim.cfg and the configuration file N3Sim.cfg is Java JRE 1.6. These files can be found at the NaNoNetworking Center in Catalunya (N3cat) web site (http://www.n3cat.upc.edu).

In the configuration file, we can classify and organize the parameters as follows: Simulation parameters, space parameters, emitter parameters, and finally receivers parameters.

For the simulation parameters we can specify the name of the folder where the result files will be stored, the value of the particle displacements due to Brownian motion (default set to 1), the collision among the emitted particles (if set to false the emitted particles are assumed to be transparent to each other and never collide), the total time of the simulation as well as the duration of each time step.

In the space parameter we can define for example if the system is bounded or unbounded (for the bounded system a rectangular bounded space is simulated where you need to specify his coordinates X and Y), the diffusion coefficient, and the radius of the emitted particles.

In the emitter parameters we can indicate the number of transmitters, the transmitter's radius, the transmitter's location (horizontal and vertical location), the release particles time with their initial speed, the number of particles released by the transmitter at every time step, and the type of the transmitter (Type one where the transmitters emits a fixed number of particles at every time step, type two where the transmitter emits particles following rectangular waveform, type three where the transmitter emits particles following a white noise waveform, type four where the transmitters reads the waveform of the signal to be emitted from a text file, and finally type five

where the transmitters is the same as transmitter type four but in a 3-dimensional (3D) simulation space).

For the receiver parameters we can indicate the number of receivers, the receiver's radius, the receiver's location (horizontal and vertical location), the receiver's name, and the receivers type (Type one where the detection area of the receiver is a square, type two where the detection area of the receiver is a circle, type three where the detection volume of the receiver is a sphere).

Note that the units of the parameters are nanometers (nm) and nanoseconds (ns).

SIMO stands for Single Input Multiple Output (SIMO) where we have single transmission node and multiple reception nodes from the same information sink. Hence, to simulate a SIMO Molecular Communications (MC) scenarios used in this paper for SISO with adjacent absorbing receivers we need to specify in the configuration file mentioned above the following parameters:

1. The number of transmitters: Set to one.
2. The location of the transmitter and its radius.
3. The start time and the end time of releasing particles.
4. The type of transmitters.
5. The number of released particles.
6. The number of receivers: Set to two or higher.
7. The name of each receivers.
8. The location of the receivers: The receivers should maintain the same distance from the transmitters so the receivers are disposed on the same arc circumference.
9. The type of receivers.
10. The radii of the receivers.
11. The distance between the transmitter and the receivers.
12. The distance between the receivers.

After editing the values of the parameters in the downloaded configuration file (N3Sim.cfg) in order to have a specific SIMO Molecular Communications (MC) scenario, we need to write the following console command to start the simulation process:

- java -jar N3Sim-0.7.jar myConfigFile.cfg

Finally, when the simulation is ended, we can find a file under the name of *receiver_name.csv* for each receiver in the simulation. The output of these files can be divided into two columns, the first column contains the time steps in nanoseconds, and the second one represents the number of particles measured by the receiver at the each time step

Appendix C

Derived Publications

C.1 Journal publications

- S. S. Assaf, J. Solé-Pareta, and E. Alarcón, "Closed-loop Serotonin Control in Glutamatergic Synapses Through Diffusion-based Molecular Communication Characterization Aiming Alzheimer's Disease Treatment", Under submission to *IEEE Transactions on NanoBioScience*.

- L. Felicetti, S. S. Assaf, M. Femminella, G. Reali, E. Alarcón, and J. Solé-Pareta, "The Molecular Communications Markup Language (MolComML)", in *Nano Communication Networks (Elsevier)*, Volume 16, June 2018, Pages 12-25. (10.1016/j.nancom.2018.03.001)

- S. S. Assaf, S. Salehi, R. G. Cid-Fuentes, J. Solé-Pareta, and E. Alarcón, "Influence of neighboring absorbing receivers upon the inter-symbol interference in a Diffusion-based Molecular Communication system", in *Nano Communication Networks (Elsevier)*, Volume 14, December 2017, Pages 40–47. (10.1016/j.nancom.2017.05.001)

- S. Salehi, N. S. Moayedian, S. S. Assaf, R. G. Cid-Fuentes, J. Solé-Pareta, and E. Alarcón, "Releasing rate optimization in a single and multiple transmitter local drug delivery system with limited resources", in *Nano Communication Networks (Elsevier)*, Volume 11, March 2017, Pages 114–122. (10.1016/j.nancom.2017.03.001)

C.2 Conference publications

- S. S. Assaf, J. Solé-Pareta, and E. Alarcón, "Characterizing Glutamatergic Synapse of a Diffusion-based Molecular Communication Channel to Measure $A\beta eta$ Oriented to

Alzheimer's Disease", 3rd Workshop on Molecular Communications, Ghent, Belgium, April 4-6, 2018.

- S. S. Assaf, S. Salehi, R. G. Cid-Fuentes, J. Solé-Pareta, and E. Alarcón, "Characterizing the Physical Influence of Neighboring Absorbing Receivers in Molecular Communication", in Proc. of the ACM International Conference on Nanoscale Computing and Communication (NANOCOM), New York, USA, 2016. (10.1145/2967446.2967474)

- S. Salehi, S. S. Assaf, N. S. Moayedian, R. G. Cid-Fuentes, J. Solé-Pareta, and E. Alarcón, "Optimal Deployment of Multiple Transmitter Drug Delivery System: A Spatial Sampling Theorem Approach", in Proc. of the ACM International Conference on Nanoscale Computing and Communication (NANOCOM), New York, USA, 2016. (10.1145/2967446.2967473)

C.3 Acknowledgment

This work started under the framework of the EU CIRCLE project (Ref.: H2020-CSA-665564), and it has been partially funded by the Spanish Ministry of Economy and Competitiveness under contract TEC2017-90034-C2-1-R (ALLIANCE project) that receives funding from FEDER.